Improved Bio-inspired Artificial Gecko Adhesive by Using Hierarchical Fibrillar Structures

by

Yasong Li

M.A.Sc, Simon Fraser University, 2009

B.Eng., South China Agricultural University, 2006

Thesis Submitted in Partial Fulfillment of the
Requirements for the Degree of
Doctor of Philosophy

in the
School of Engineering Science
Faculty of Applied Sciences

SIMON FRASER UNIVERSITY

Fall 2014

Approval

Name: **Yasong Li**

Degree: **Doctor of Philosophy**

Title: ***Improved Bio-inspired Artificial Gecko Adhesive by Using Hierarchical Fibrillar Structures***

Examining Committee: **Chair:** Marinko Sarunic
Associate Professor

Carlo Menon
Senior Supervisor
Associate Professor, PEng

Byron D. Gates
Supervisor
Associate Professor
Department of Chemistry

Ash M. Parameswaran
Supervisor
Professor, PEng

Bonnie L. Gray
Internal Examiner
Associate Professor

Karen Cheung
External Examiner
Associate Professor
Department of Electrical and Computer Engineering
The University of British Columbia

Date Defended/Approved: December 3rd, 2014

Partial Copyright Licence

Abstract

Geckos are well known for being rapid climbers that have long existed in nature. The reversible and reusable adhesive on their feet intrigues scientists to explore a bio-mimetic adhesive, which inherits the adhesion properties of the gecko's adhesives. Recent advances in electron microscopy reveal the secret of gecko's climbing ability: there are hierarchical fibrillar structures branching from the skin of their climbing feet. Sizes of these hierarchical fibrils range from micrometer to nanometer. These fibrils are arranged to closely resemble a tree, and these tree like structures form a fibril forest on the skin of the climbing feet. Nano-fibrils in close proximity with the contacting surfaces interact with the substrate through intermolecular forces. Slender micro-fibrils extend the nano-fibrils, which are located at their open ends, to reach recesses of the contacting surfaces. The special arrangement of the fibrillar arrays enables quick attachment and detachment of the feet from surfaces of different materials and varying roughness.

Inspired by the gecko's adhesive, artificial fibrillar adhesives have been sought developing for more than a decade. Early attempts were focused on making use of the intermolecular interaction by nano-fibrillar arrays. These artificial fibrillar adhesives have achieved great performance on flat surfaces but not as good when they were used on relatively rough surfaces. Recent attempts of preparing a hierarchical fibrillar structure, which contains fibrils in different length scales, have rare success on improving adhesion performance. Evidence of extra compliancy provided by the hierarchical structure is also not clear. This thesis provides evidence that there is a correlation between structure compliancy and adhesion performance of a hierarchical fibrillar adhesive. Improved compliancy and adhesion forces are observed on a hierarchical fibrillar structure with achievements of several milestones, which include developing methods for preparing and characterizing hierarchical fibrillar structures. Experimental results also reveal the interaction of fibrillar arrays with the contacting surfaces. Information obtained is valuable for future development and application of such artificial fibrillar adhesive.

Keywords: Gecko adhesive; hierarchical dry adhesive; nano-fibrils fabrication; replica molding; scanning probe microscopy; enhanced compliancy

To My Family

To the Exploration of Knowledge

To the Enchanted Universe

Acknowledgements

I would like to dedicate sincere appreciation to my senior supervisor, Dr. Carlo Menon, who provided the opportunity for me to work on this project. The freedom of exploration and your patient guidance supported through the duration of my PhD studies.

I would also extend my acknowledgements for my other supervisor, Dr. Byron D. Gates, who provided valuable suggestions and information on my research. Thank you for providing the opportunity to work with your group and sharing your precious experience. I am also grateful to have the support of Dr. Ash Parameswaran, who gave me valuable lesson on critical thinking, and your efforts put into running the engineering clean room.

This thesis would not be possible without the helps from my colleagues, staffs in the engineering department and the 4D LABS. Special thanks are given to Gary Houghton and Raj Pabla, who help setup devices and handling purchasing; Dr. Dan Sameoto who gave the initial clean room lesson for micro-fabrication; all staffs in 4D LABS nano-fabrication for valuable discussion and device training; Dr. Li Yang and Dr. Xin Zhang for SEM imaging training; Cheng Zhang for AFM force measurement training; Jason Bemis from Asylum Research who wrote the code of AFM cantilever manipulation, Him-Wai Ng for silane deposition training. Acknowledgements are also extend to Simon Fraser University who provided such an open education environment that allow me to learn from all departments.

This work was supported in part by Natural Sciences and Engineering Research Council of Canada and Simon Fraser University. Fabrication and characterization made use of 4D LABS shared facilities supported by the Canada Foundation for Innovation, British Columbia Knowledge Development Fund, Western Economic Diversification Canada, and Simon Fraser University.

Table of Contents

List of Figures

Chapter 1.

Introduction

Adhesive is a common type of medium that joins two objects together. Without physically intruding into the structure of the objects, adhered joints may not be able to withstand loads as high as a mechanical fastening. Convenience of minor modifications on the objects, however, continuously propels the development of adhesives aimed at different applications. In this thesis, development of a new type of adhesive is presented. This adhesive is inspired by geckos, the most representative animals that can rapidly climb on various surfaces without leaving residues. Advancement of electron microscopy helped to discover the secret of their climbing feet. On gecko's feet, there are millions of fibrils branching from micro-size to nano-size and structured into the shape similar to trees [1]. Numerous slender nano-fibrils collectively produce high adhesion forces with a substrate through intermolecular interactions. The special nano-structures intrigue scientists and engineers to study and utilize the unique properties of the gecko inspired adhesive. This thesis is one of the outcomes in this field of studies.

1.1. Motivation

Traditional adhesives include glues and tapes. Typical glues need a period of time to form a secure bond between two objects. This period of time is usually referred to as "cure time" [2]. As rapid as chemical reactive glues, which produce molecular cross-linking inside the substance and adhesion on surfaces of both objects, cure time can be minimized to be about 1 minute [2]. Upon curing of the bond, the adhesive joint is usually not easily broken under certain loads as it is the criteria of the glue being designed. On the other hand, tapes, or pressure sensitive adhesives, can form bonds in a shorter time, depending on the pressure applied. Most types of the tapes are designed to be reversible, which allows the detachment of the tapes by peeling it from the substrate. Once the tape has been used, its performance drastically drops compared to its initial condition. This performance drop is caused by picking up contaminations from the adhered surfaces and damage of the tacky material on the tapes. For some of the applications, such as the sticking mechanism on climbing robots, rapidly forming and detaching secure bonds from climbing surfaces using reversible and reusable adhesives is essential for their functionality. These applications urge the development of a new type of adhesive different from the traditional ones. Mother Nature has provided some elegant solutions in various creatures.

Inspired by burrs of burdock, Velcro was invented as a rapid fastening mechanism, which is reversible and reusable [3]. This well-known fastener contains two pieces of fabric with micro-structures. One piece contains flexible micro-hooks and the other one contains micro-loops in a random fashion. Upon applied pressure, the two pieces attach to each other by mechanical interlocking. The fastener's ability to bear pure normal or shear forces is much better than the combination of the two types of forces. Velcro is easily unfastened when either piece of the fabric is peeled from the other one. Although this bio-inspired fastener provides feasibility of a fast reversible and reusable attaching mechanism, application of Velcro-like fastener is subject to the same challenges of traditional adhesives. The fabric pieces of Velcro need to be secured on the surfaces of intended fastening objects, which requires the use of glue, tape or sewing.

Gecko adhesives, on the other hand, adhere to almost all surfaces regardless of the surface roughness and composite materials [1]. Surfaces independent of the gecko adhesive rely on the hierarchical micro- to nano-sizes fibrillar structures. Fibrils having different length scales branch from the gecko's feet, with the nano-size fibrils forming millions of contact points with the contacting substrates (Figure 1.1a). Each of these contacts are formed by van der Waals interactions, the intermolecular attractive force that results in a firm grip between the geckos' feet and the contact surfaces. The shape of these nano-fibrils provides flexibility to conform to different substrates. Without using chemical secretion, there is almost no residue left behind after the gecko adhesive detaches from the surfaces. A simply drag of the gecko's feet gently engages the fibrillar adhesive with the contact surfaces. The bonds stay firm as long as the shear forces continuously apply to the contacting substrates. A peel angle of ~30 degrees initiated from the end of the gecko's toes is generally used for a rapid release of the gecko adhesive. The unique attaching and releasing mechanism of the gecko's adhesive enables the creature to walk freely without being bound to the rules of gravity.

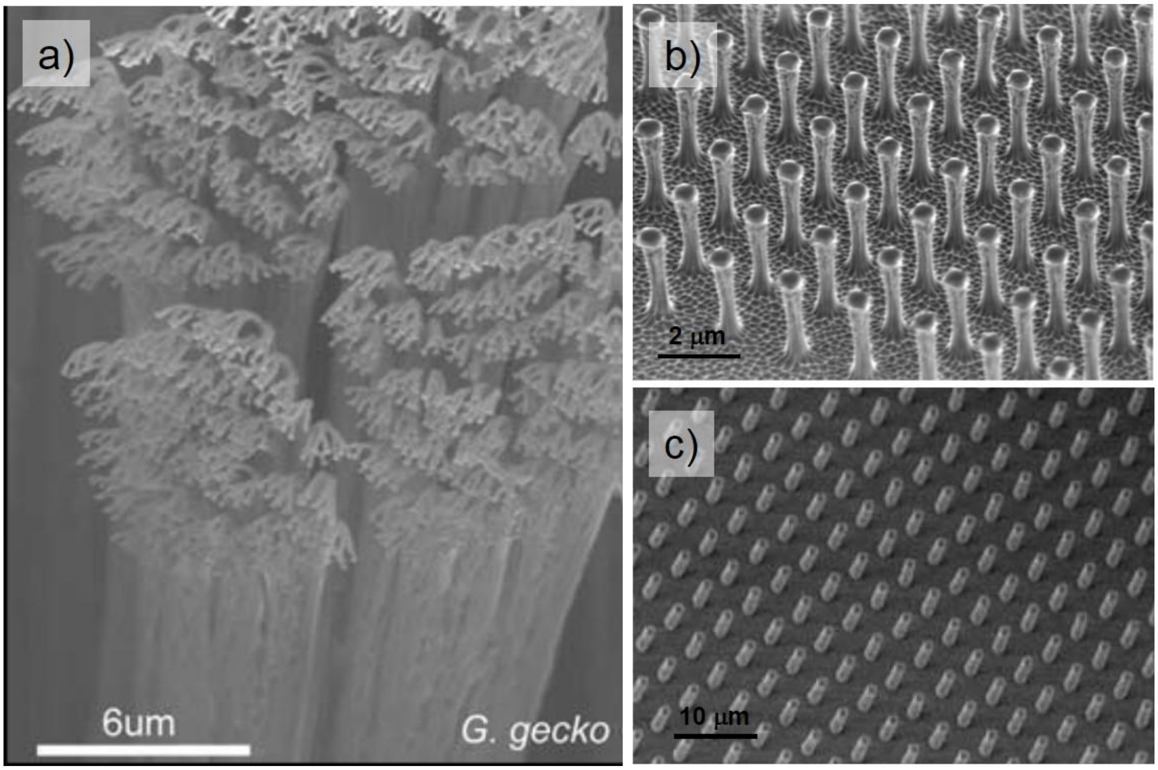

Figure 1.1. Scanning electron microscope images of gecko adhesive and gecko inspired fibrillar adhesive. a) Setae of Gecko gecko [4]. b) Arrays of nano-fibrils in artificial fibrillar adhesive [5]. c) Arrays of micro-fibrils in artificial fibrillar adhesive [4]. All images are taken with tilted stage. Reproduction of the published images complies with copyright protection in Canada.

All the above-mentioned desired properties of gecko adhesives have attracted broad interest for their scientific and industrial applications. Artificial gecko adhesives, which are prepared in laboratories, replicate partially the shape of the gecko adhesive and have achieved a compatible adhesion ability. Progressive understanding of the working mechanism of gecko adhesives is continuously help overcoming the limitations of these artificial adhesives. Studies conducted in this thesis intend to further improve our knowledge and the performance of existing artificial gecko adhesives. Characterization methods are also developed to reveal the adhesion properties mimicking how geckos use their adhesives. Hierarchical fibrillar structures are specifically of interest to promote adhesion by providing extra compliancy with the contact substrate.

Early artificial gecko adhesives contained micro- or nano-size fibrils arranged as upright arrays on a substrate [4-6]. Figure 1.1 shows two examples of these artificial adhesives. Improvements were made later by changing the shape of fibrils by adding a mushroom cap at the open end of each fibril (Figure 1.2) [7-8]. These single layer fibrillar structures provide insights into the contacts forming through van der Waals forces with microscopic flat surfaces. However, these artificial adhesives cannot form firm contacts on microscopically rough surfaces as well as the flat ones. The reason behind this phenomenon is that the single layer fibrillar structures do not have enough compliancy that most of the fibrils cannot extend to reach and interact with the rough surfaces (Figure 1.3). In nature, the soft skin on the gecko's feet conform to rough surfaces and rely on the hierarchical fibrils to stretch deep inside the cleavage of the rough surfaces [1]. Inspired by this concept, creating hierarchical artificial fibrillar adhesive appears to be another route for improving adhesion performance [9-11].

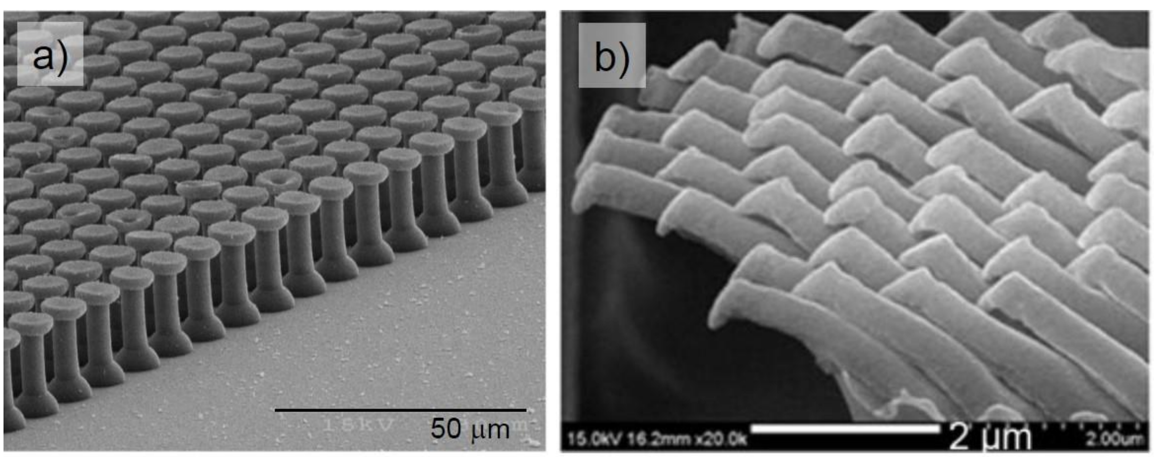

Figure 1.2. Scanning electron microscope images of artificial fibrillar adhesive having mushroom shape fibrils. a) Micro-mushroom fibrils in artificial fibrillar adhesive [7]. b) Nano-mushroom fibrils in artificial fibrillar adhesive [8]. Reproduction of the published images complies with copyright protection in Canada.

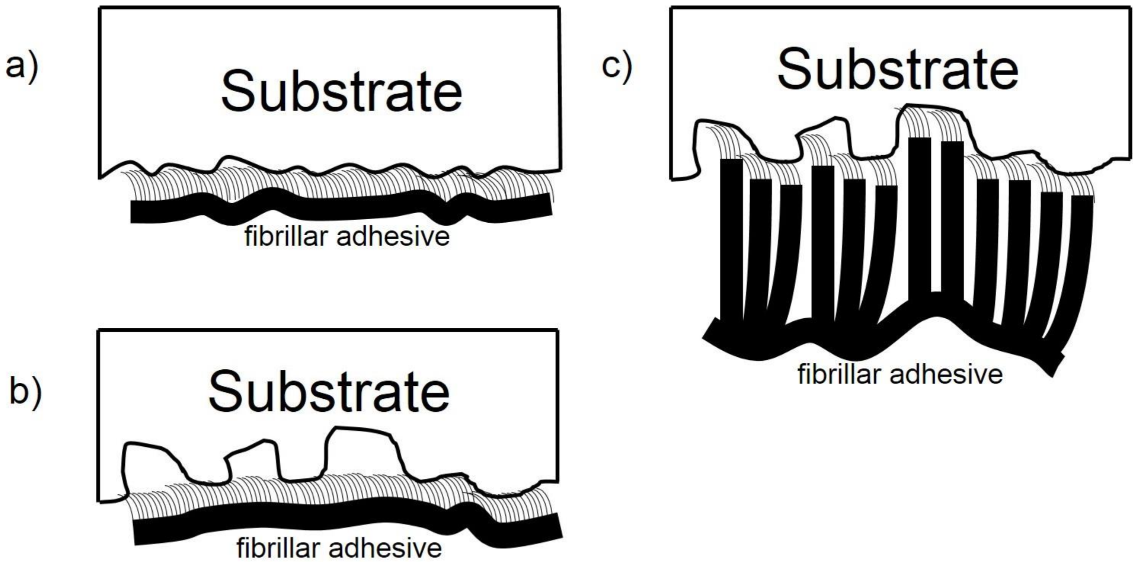

Figure 1.3. Schematics showing compliancy effect of fibrillar adhesives. a) the single level fibrillar adhesive adhered to relatively flat substrate with most small fibrils in contact with the substrate; b) single level fibrillar adhesive adhered to relatively rough substrate with limited fibrils in contact to the substrate; c) dual level fibrillar adhesive adhered to relatively rough substrate with most of the small fibrils in contact with the substrate.

Adhesion characterization methods are also evolving along with the fabrication of the fibrillar adhesives. Adhesion and friction forces are measured in most of the fabricated artificial adhesives. Adhesion measurements focus on recording the highest force when the test substrate is pulling off the adhesive, usually in a vertical direction. Friction measurements focus on recording the highest force when the test substrate has a displacement along the same axis as the artificial adhesive. Figure 1.4 depicts the differences between the two types of measurements. Geckos usually apply a dragging movement to finish the attachment process when they are climbing [1]. This dragging movement has been proved to help fibrils reach their optimized position and create better contact with the contact surfaces. Inspired by this phenomenon, applying such dragging movement during the tests of artificial adhesive can provide deeper insights on utilizing the artificial adhesives.

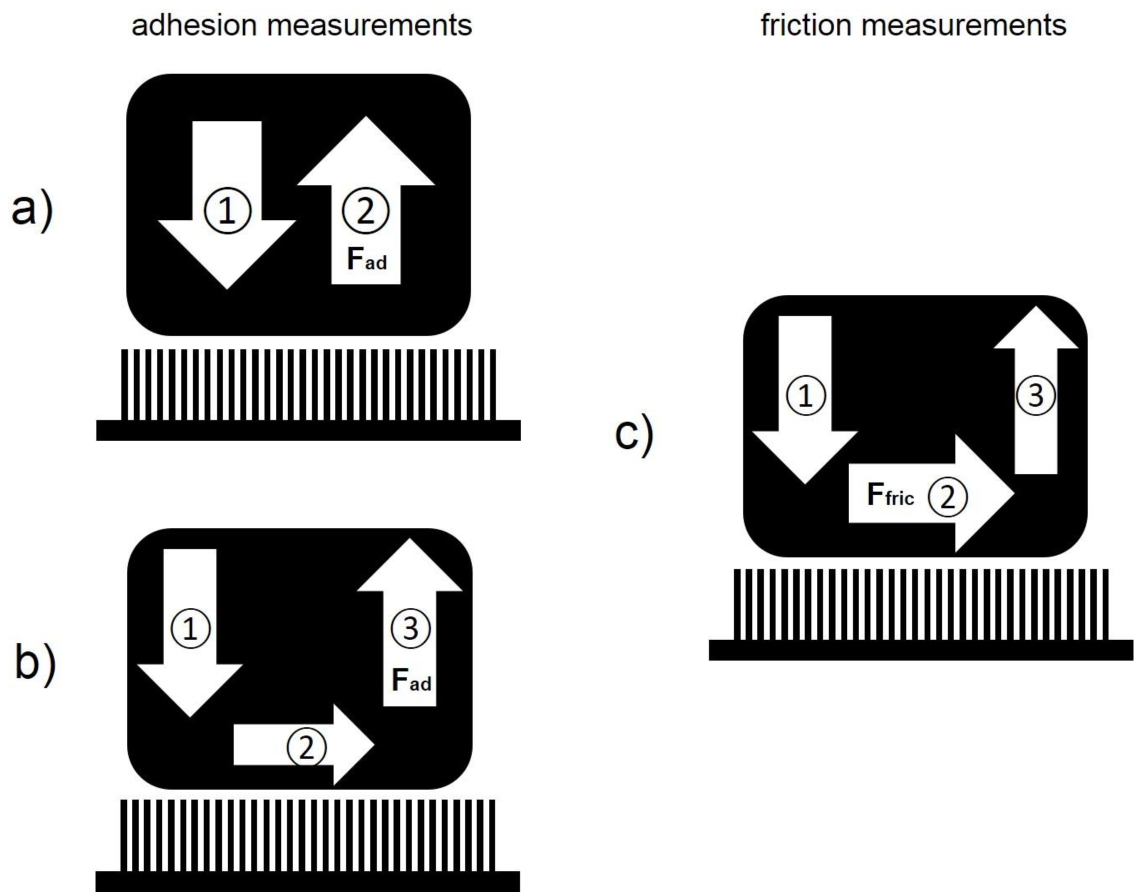

Figure 1.4. Schematics of comparing measurement methods on fibrillar adhesives. The big block represents the contact substrate usually connected to a force sensor. a) Adhesion measurement of pull up force. The contact substrate lowers down to the fibrillar arrays vertically and then pulls up vertically. F_{ad} represents the adhesion force measured. b) Adhesion measurement with an extra shearing step in between lowering down and pulling up to separate the contacting substrates. Adhesion force (F_{ad}) is measured at step 3. c) Friction measurement designed to obtain information on the shear forces at step 2. F_{fric} represents the friction force measured.

1.2. Objectives

Based on the aforementioned background studies, which will be elaborated in Chapter 2, five objectives are proposed in this thesis: OBJECTIVE 5 is the final goal of the entire thesis with OBJECTIVE 1 through 4 as necessary milestones.

OBJECTIVE 1: to prove that hierarchical fibrillar adhesive (containing micro- and millimeter size fibrils) performs better on adhesion forces than the single layer fibrillar adhesive. Achievement of this hypothesis consolidates the foundation of improving adhesion via fabricating hierarchical fibrillar structures.

OBJECTIVE 2: to demonstrate the ability of preparing nano-size fibrillar arrays using desired materials. Achievement of this goal is a necessary step towards OBJECTIVE 5.

OBJECTIVE 3: to prove that the dragging movement, which is applied before detachment of the two substrates, can improve the adhesion force. Achievement of this hypothesis sets up another foundation of understanding fibril-substrate interaction.

OBJECTIVE 4: to demonstrate that there is a set of optimized parameters in the measurements involving dragging movements. Achievement of this goal provides the necessary study of optimal parameters which are used in the characterization of artificial adhesives with dragging movements.

OBJECTIVE 5: to prove that the hierarchical fibrillar adhesive (containing nano- and micro-size fibrils) can produce a higher adhesion force than the single layer fibrillar adhesive by providing extra compliancy. Achievement of this hypothesis makes use of the results in the previous objectives. Improvement of the adhesion force should be accomplished by preparing hierarchical fibrillar structures. With the proper test method, the hierarchical fibrillar adhesives should provide better compliancy and adhesion forces with the flat substrate.

1.3. Thesis layout

The following chapters of this thesis will be arranged as follows. Rationale for the connection among each chapter is also discussed.

Chapter 2 provides a detailed literature review on the BACKGROUND of artificial gecko adhesives. Both backgrounds of the preparation and characterization of artificial gecko adhesives are discussed.

Chapter 3 describes the fabrication of hierarchical fibrillar arrays and the adhesion measurements to demonstrate the achievement of OBJECTIVE 1. Fibrils in micro-size and millimeter size were combined to form a structure similar to the gecko adhesive. Adhesion performances were assessed through a customized adhesion force platform. Experimental results prove that hierarchical fibrillar structures improved the adhesion performance of artificial adhesives. The hierarchical adhesive optimized the anisotropic property which enables the adhesive to grip the substrate in one pulling direction but release easily from a different pulling direction. This phenomenon showed that there is a need to explore fibril-substrate interaction by a force measurement setup with the ability of studying anisotropic properties, which is investigated in Chapter 5 and 6.

Chapter 4 describes a low cost and high yield fabrication of nano-size fibrillar arrays with versatile material choices. This chapter demonstrates the realization of OBJECTIVE 2. A replica molding method is presented to break the limitation of fabricating upstanding nano-fibrils using various materials. By choosing a proper construction material, adhesion forces were increased compared to a fibrillar adhesive having very similar topography but made of a different material. Successful preparation of nano-fibrils using a desired material led to the successful preparation of hierarchical fibrillar structure which is demonstrated in Chapter 7.

Chapter 5 illustrates the importance of the shear movement applied after the fibril-surface engagement. This chapter demonstrates the achievement of OBJECTIVE 3. Inspired by the results obtained in Chapter 3 and considering the fibril size in Chapter 4, a technique based on a scanning probe microscopy was developed to assess the uniformity of nano-fibrillar adhesives and investigate the fibril-surface interactions. Measured adhesion forces increased due to the shear movement after the flat substrate was pressed against the fibrillar arrays. Experimental results inferred that the fibrillar structure has a better performance when it is dragged on the contact substrate before pulling up. This characterization method is adapted in later tests of a hierarchical fibrillar structure in Chapter 7.

Chapter 6 investigates the optimal parameters used in the shear induced adhesion measurement method as described in Chapter 5. This chapter demonstrates the successful achievement of OBJECTIVE 4. The characterization method introduced in Chapter 5 provides various possibilities for manipulating the interaction between fibrillar arrays and the flat substrate. Based on the dynamics of interactions, the substrate drag distance, drag velocity and substrate retract (or pull-up) velocity are investigated. Statistical analysis of experimental results revealed the relationship between adhesion forces and these parameters. Measured forces over time visualize the nanoscopic interactions, which are not observable with a typical test setup. Results are utilized in Chapter 7 for characterization of a hierarchical fibrillar adhesive.

Chapter 7 describes the fabrication of a hierarchical fibrillar adhesive containing micro- and nano-size fibrils based on the methods developed in Chapter 4. Characterization of this adhesive was based on the method developed in Chapter 5 and 6. This chapter makes use of all the useful results in previous chapters and provides evidence of achieving the ultimate goal of this thesis (OBJECTIVE 5): improve adhesion and the compliancy of the fibrillar adhesives by using hierarchical structures. Combination of the micro- and nano-scale fibrils gives enhanced adhesion, which provided future direction for developing this type of reusable and reversible adhesive. The enhanced adhesion has proven to be a result of extra compliancy provided by the supporting micro-fibrils.

Chapter 8 concludes the study with a discussion of future work.

1.4. Contributions

This thesis presents the evidence that hierarchical fibrillar structure provide extra compliancy to improve adhesion forces. The outcomes of the research conducted in this thesis explore the route for improving adhesion performance using hierarchical structures, which in part contributed to the research in the scientific society of artificial fibrillar adhesive studies.

Chapter 3 to Chapter 7 are composed of five individual manuscripts, 3 of which were published as journal articles and 2 of which were currently submitted to peer-review journals. Each chapter, which consists of a paper or manuscript, represents the realization of each objective described in Sections 1.2 and 1.3. In this section, a list of publications corresponding to each chapter is presented. Co-authorship is also claimed in this section. All the following publications are results obtained exclusively in the duration of my PhD degree studies.

Chapter 3: Yasong Li, Dan Sameoto and Carlo Menon, “Enhanced Compliant Adhesive Design and Fabrication with Dual-Level Hierarchical Structure” published in *Journal of Bionic Engineering*, **2010**, *vol. 7*, 228-234. Dan Sameoto and Carlo Menon provided ideas and edited the manuscript. Yasong Li conducted the experiments and wrote the manuscript.

Chapter 4: Yasong Li, Him Wai Ng, Byron D. Gates and Carlo Menon, “Material versatility using replica molding for large-scale fabrication of high aspect-ratio, high density arrays of nano-pillars” published in *Nanotechnology*, **2014**, *vol. 25*, 285303. Byron D. Gates and Carlo Menon provided suggestions and guidance and edited the manuscript. Yasong Li and Him Wai Ng conducted the experiments. Yasong Li planned and executed the experiments and wrote the manuscript.

Chapter 5: Yasong Li, Cheng Zhang, James H.-W. Zhou, Carlo Menon and Byron D. Gates, “Measuring Shear-Induced Adhesion of Gecko-Inspired Fibrillar Arrays Using Scanning Probe Techniques” published in *Macromolecular Reaction Engineering,* **2013**, *vol. 7*, 638-645. Carlo Menon and Byron D. Gates provided idea and guidance and edited the manuscript. Yasong Li, Cheng Zhang, James H.-W. Zhou planned and conducted the experiments. Yasong Li processed the data and wrote the manuscript.

Chapter 6: Yasong Li, James H.-W. Zhou, Cheng Zhang, Carlo Menon and Byron D. Gates, “Harnessing Tunable Scanning Probe Techniques to Measure Shear Enhanced Adhesion of Gecko-inspired Fibrillar Arrays” submitted to ACS Applied

Materials & Interfaces. Carlo Menon and Byron D. Gates provided ideas, guidance and edited the manuscript. Yasong Li, James H.-W. Zhou and Cheng Zhang planned and conducted the experiments. Yasong Li processed the data and wrote the manuscript.

Chapter 7: Yasong Li, Byron D. Gates and Carlo Menon, “Improved adhesion and compliancy of hierarchical fibrillar adhesives” submitted to Advanced Functional Materials. Byron D. Gates and Carlo Menon provided guidance and edited the manuscript. Yasong Li planned and executed the experiments and wrote the manuscript.

1.5. References

[1] K. Autumn, *MRS Bull.* **2007**, *32*, 473-478.

[2] W. C. Wake, *Synthetic adhesives and Sealants*, Chichester: Wiley, **1987**.

[3] N. M. Pugno, *Appl. Phys. Lett.* **2007**, *90*, 121918.

[4] N. J. Glassmaker, A. Jagota, C.-Y. Hui and J. Kim, *J. R. Soc. Interface* **2004**, *1*, 23-33.

[5] A. K. Geim, S. V. Dubonos, I. V. Grigorieva, K. S. Novoselov, A. A. Zhukov, S. Y. Shapoval, *Nature Materials* **2003**, *2*, 461–463.

[6] C. Majidi, R.E. Groff, K. Autumn, S. Baek, B.Bush, N. Gravish, R. Maboudian, Y. Maeno, B. Schubert, M. Wilkinson, and R.S. Fearing, *Phys. Rev. Lett.* **2006**, *97*, 076103.

[7] S. Kim and M. Sitti, *Appl. Phys. Lett.* **2006**, *89*, 261911.

[8] H. E. Jeong, J.-K. Lee, H. N. Kim, S. H. Moon, and K. Y. Suh, *Proc. Nat. Acad. Sci.* **2009**, *106*, 5639–5644.

[9] M. P. Murphy, S. Kim, M. Sitti, *ACS Appl. Mater. Interfaces* **2009**, *4*, 849-855.

[10] M. Roehrig, M. Thiel, M. Worgull, H. Hoelscher, *Small* **2012**, *8*, 3009-3015.

[11] D. Y. Lee, D. H. Lee, S. G. Lee, K. Cho, *Soft Matter* **2012**, *8*, 4905-4910.

Chapter 2.

Literature Review

Gecko adhesives have been studied for more than a decade in order to reveal the remarkable climbing ability of geckos. The nano-structures on gecko's climbing feet rely on van der Waals interactions to realize their rapid climbing. Several other animals are also discovered to have similar nano-structures on their feet. Inspired by these climbing animals, artificial fibrillar adhesives are prepared in laboratories to mimic the reversible and reusable properties of the fibrillar adhesives. Numerous attempts have been made to achieve certain properties of the adhesive similar to their natural counterpart, but none of the current artificial adhesives possess all of the properties of the animal fibrillar adhesive. In this chapter, the development of the fibrillar adhesive is illustrated. Current state of the art artificial fibrillar adhesives are also discussed. Discussion of past research leads to the conclusion of the goal of this thesis: improve fibrillar adhesive by using hierarchical structure.

2.1. Inspiration from nature

Humans have been amazed since ancient time that climbing animals such as geckos and spiders possess extraordinary ability to adapt to different climbing surfaces. Aristotle, who might have the first written record of geckos' climbing ability, described the creature as having the "superior ability to climb and cling", "even with the head downwards" [1]. Although geckos' feet have long been studied, the secret of gecko climbing was discovered about a decade ago, thanks to the advancement made on electron microscopy [2]. However, arguments have been made about whether these nano-structures adhere to surfaces relying on van der Waals interaction or other effect such as ionic electrostatic attractions and capillary interactions [3-5]. The dispute was finalized by a series of investigations [6]. It is believed that geckos' fibrillar adhesives rely mainly on the contribution of van der Waals forces and a combination with capillary forces. Van der Waals interactions then became the most important feature that represents fibrillar adhesives.

2.1.1. Van der Waals forces in fibrillar adhesive

In 2000, measuring adhesion forces of a single gecko foot-hair (Figure 2.1) brought attention to the nano-structures on gecko's feet [2]. The experiments provided evidence to support, though indirectly, the hypothesis that nano-fibrils on geckos' feet function through van der Waals interactions with the contacting substrate [7-8]. Data obtained using a micro-electromechanical sensor (MEMS) eliminated the possibility of suction, friction, microinterlocking and electrostatic attraction. Experimental results of a follow up research [9] gave simple evidence to eliminate the contribution of capillary effects on the adhesion of geckos' fibrillar adhesive. Later some other researchers challenged this theory with evidence of adhesion increase when raising room humidity [4,10-11]. The most recent study about humidity effects on gecko's fibrillar adhesives had demonstrated a new theory that the mechanical property of the structure material (β-keratin) changed with respect to the humidity [12-13]. To summarize, van der Waals interaction dominated among all the possible attraction forces effecting adhesion forces generated by a gecko's foot.

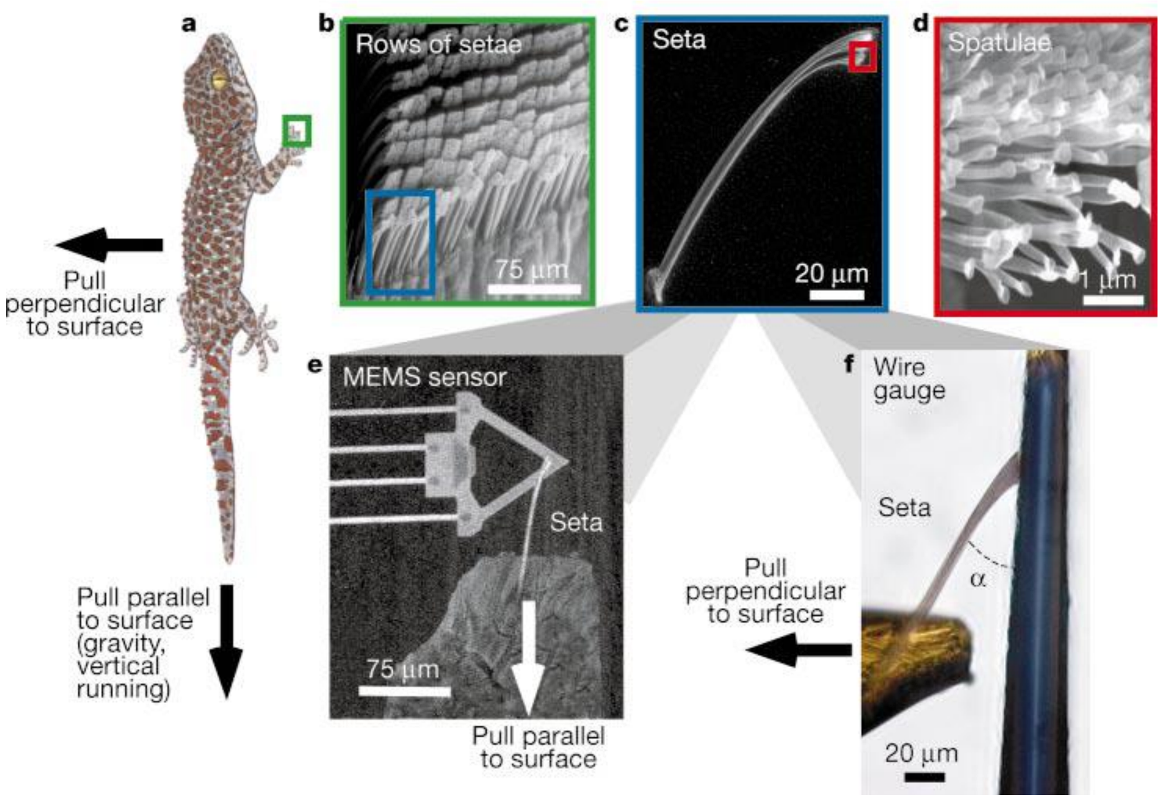

Figure 2.1. Adhesion measurements on a single seta from gecko's feet [2]. Each colored border image denoted the magnified view in the previous image. a) Schematic of the forces applied by the climbing gecko on a vertical wall; b) SEM image of setae found on a gecko's foot; c) SEM image of a single seta pulled from a gecko's foot; d) SEM image of spatulae branching on the open ends of a seta; e) SEM image of the measurement setup. A microelectromechanical sensor with a seta attached can manipulate the seta to interact with a surface. f) A seta attached to a wire gauge which is able to measured force perpendicular to the wire plane. Permission is obtained from the publisher for reproduction of this image.

The gecko is not the only animal that relies on nano-fibrils to climb different surfaces. Spiders, who are also excellent climbers, have fibrillar feet with nano-structures (Figure 2.2) found on their cuticles [14]. Adhesion forces were also measured which were comparable to the gecko's fibrillar adhesive [15-16]. The experimental results did not focus on ruling out the possibility of capillary effects and other possible forces. Compared to beetles which rely on fluid secretion to climb, adhesion provided by the spider's feet greatly exceeds (more than an order of magnitude) the performance of beetles' [17].

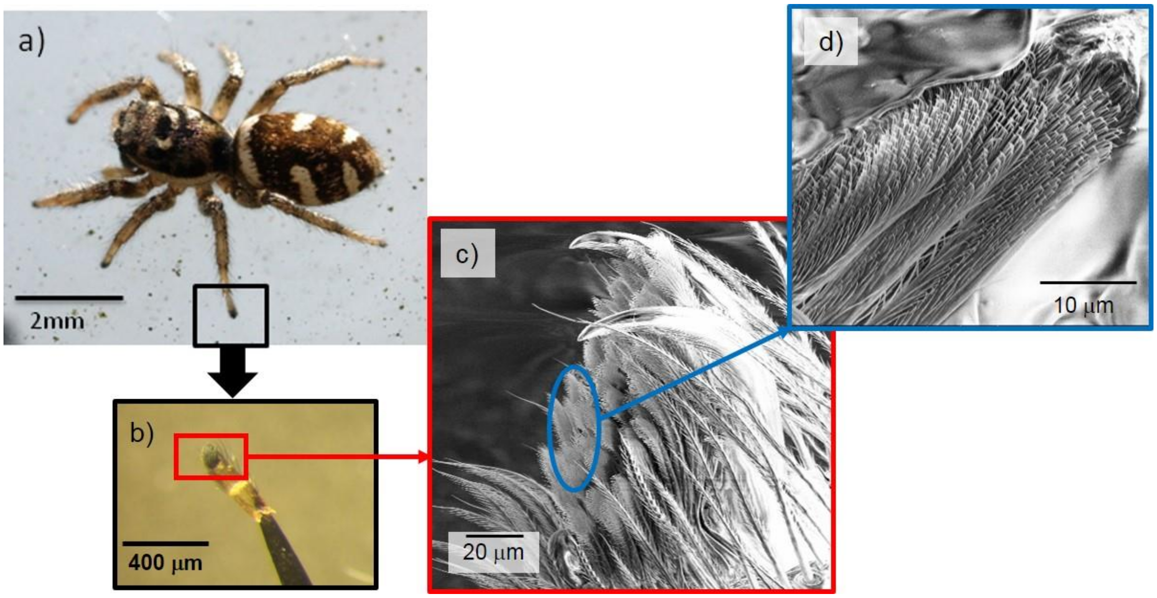

Figure 2.2. Climbing mechanism of a jumping spider. Each colored border image represents the magnified view in the corresponding area of the previous image. a) a zebra spider (Salticus Scenicus); b) optical microscope image of a section of spider leg; c) SEM image of the open end of the spider leg; d) SEM image of three setae pulled from the spider leg.

All discoveries of nano-structures on animals' feet encouraged the conclusion that the short range van der Waals interactions play an important role for these climbing animals. The short range forces require the fibrils to be in close proximity to the climbing surfaces, which is realized by the hierarchical fibrillar structure.

2.1.2. Hierarchical structure in fibrillar adhesive

In the gecko's adhesive, there are various lengths of fibrils which each has their own name and function (Figure 2.1) [6]. The nano-fibrils, which are the end effectors making contact with the climbing substrate, are called spatulae. They are named for their wider ends which look similar to a cooking spatula. These spatulae bundle on top of a larger fibril, which has a larger diameter than the spatulae. The larger fibrils are called seta, with its plural form of setae. The setae are spread out on thin films with one edge attached to the skin of the gecko's toe. Numerous of these thin films are arranged in rows and form the structure called lamellar. Rows of lamellar form the adhesive system on each toe, which is composed of soft materials and flexible joints. This hierarchical structure well defines the adhesive system in gecko adhesives, which allows as many nano-fibrils to reach corners of a contact substrate and create short range interactions. The composite materials of geckos' adhesive and spiders' adhesives are keratin [6] and chitin [15] respectively, which have a relatively high elastic modulus (~1.6 GPa [18] and ~150 GPa [19], respectively) in bulk material. However, the effective elastic modulus of gecko's setal arrays is reduced to ~100 kPa because of the movable fibrillar structure [20-22]. The effective elastic modulus was calculated by treating each of the fibrils as an independent spring [20]. The calculated values are validated by experiments [22]. Experimental results also indicated that the effective elastic modulus of gecko setal arrays are close to but have not yet reach the upper limit of the Dahlquist criterion for tack, which is defined by the empirical observation of elasticity of pressure sensitive adhesives [23]. Pressure sensitive adhesives, e.g. office tape, are a type of representative adhesive for tacky adhesion. Reduction of elastic modulus of hierarchical fibrillar structure results in better compliancy of the gecko's adhesive with rough surfaces.

Several studies have simulated the adhesion forces of the geckos' adhesive on surfaces with different roughness [24-26], but seldom studies been performed on validating the simulation results. Huber et al. [27] demonstrated a simple experimental result of geckos' adhesive complying with surfaces of different roughness. Both separated seta and living geckos were tested on surfaces with root mean squared (RMS) roughness ranging from 90 to 3000 nm. Adhesion forces of a single seta were relatively high in either very low or high asperities. The high adhesion force on rough surfaces provided evidence that the hairy structure can conform to rough surfaces to create as strong as an adhesion comparable to the adhesion force with atomically flat surfaces. Similar results are obtained in studies provided by Gillies et al. using a customized force platform to measure interaction forces of geckos climbing on vertical surfaces with different asperities [28]. Close observation of the lamellar structure conforming to different surface roughness (wave surfaces with different amplitude ranging from 0.5 to 2 mm) enabled the visualization of changing contact area, which resulted in a variation of adhesion forces. The compliancy of fibrils and the superior adhesion of the geckos' adhesive are realized by a dragging movement in a certain direction [29]. This direction is determined by the special curvature of the setal arrays on the gecko's feet. The hierarchical fibrillar structures reach the best performance when this dragging movement is applied when the animal is climbing [2,6]. Interactions between fibrillar arrays and climbing substrates are investigated on separated setal arrays and climbing animals [16, 30-33], which will be reviewed in the next section.

2.1.3. Fibril-substrate interaction of climbing animal

Both geckos and spiders use special movements to engage their adhesives with climbing substrates [16,31-33]. By closely examining the geometry of the gecko's setal arrays, the curvature of these fibrillar structures have proven to be advantageous structure: the setal arrays are best attached to a surface at ~30 degrees between the approaching setal shaft and the contacting substrate, and are simply detached from a surface at an angle larger than 30 degrees between the setal shaft and the contacting substrate, referred to as a movement of "peel" [2,6]. The anisotropic attachment and detachment mechanism enables the gecko to climb with stable patterns regardless of the climbing speed [34]. A similar mechanism can be found on spiders' extremities: the brushes of fibrils at the end of the climbing feet are pulled toward the body to form numerous contacts, but pushed away from the body to easily detach the adhesives [16,30]. These experimental results inspired further investigation of the relationship between friction and adhesion of these natural adhesives [29,31,33]. Autumn et al. introduced a characterization method inspired by these animal's climbing movements to investigate the coupling of friction and adhesion forces [35]. This method is widely referred to as the Load-Drag-Pull (LDP) method (Figure 2.3) which, by its name, vividly illustrates the test procedure: i) the fibrillar adhesive and the testing substrates are first brought into contact by vertically compressing one towards the other, which is referred to as the "load" step; ii) the two substrates are then sheared (a lateral displacement in one direction with the compression force staying constant), which mimics the ways the animals "drag" their feet with respect to the contact substrate; iii) the two substrates are at last separated by pulling the substrate vertically away from the other one, which is referred to as the "pull" step. This method demonstrates the usefulness of characterizing fibrillar adhesives [36-38]. The extra "dragging" movement, in comparison to traditional "Indentation" [36] or "Push-Pull" [39] method, is believed to provide pre-tension inside the spatula when it is adhered to a substrate [40]. This pre-tension exposes the side-wall of the fibrils and allows more contact area to be created between the two substrates with constant compressing force applied. The increase of contact area results in increased adhesion forces [36]. The LDP experiments are widely applied in the studies that investigate interactions between fibrillar arrays and testing substrate which will be detailed in the next section.

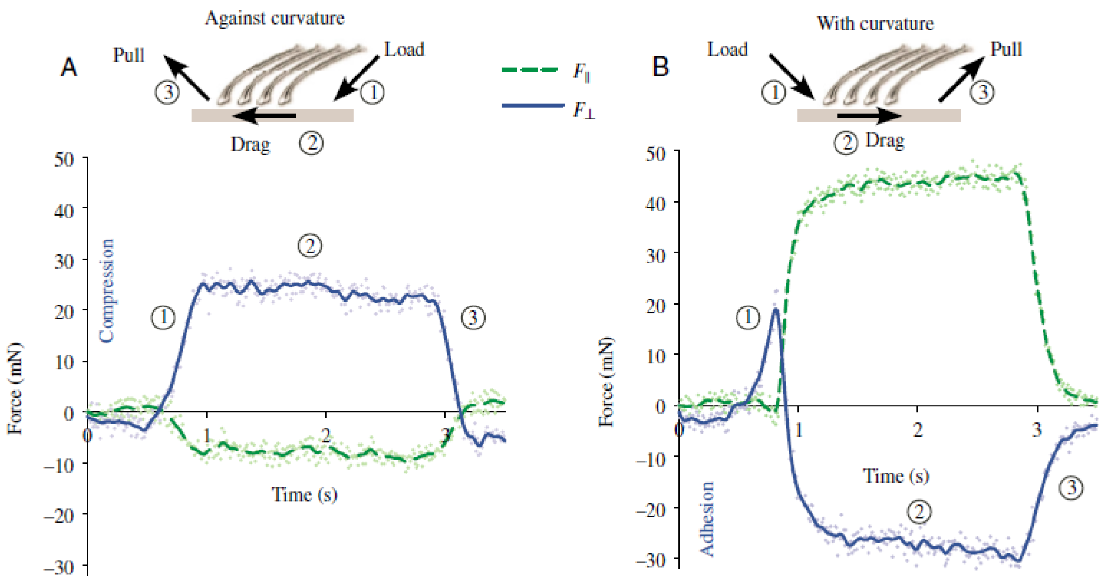

Figure 2.3. Schematics and force-time responses of Load-Drag-Pull (LDP) measurement method [35]. Blue solid trace represents the force perpendicular to the contacting surfaces. Green dashed trace represents the force parallel to the contacting surfaces. a) A LDP measurement performed against the curvature of the setal shaft. b) A LDP measurement performed with the same direction of the curvature of setal shaft. Permission is obtained from the publisher for reproduction of this image.

2.2. Current fabrication and characterization technologies of artificial fibrillar adhesive

Artificial fibrillar adhesives were prepared in laboratories soon after the discovery of van der Waals interactions as the main contribution to gecko's adhesives [41]. Early attempts were focused on preparing fibrillar arrays of a single length scale [42-44]. The preparation of nano-scale fibrils was the goal of early studies, aiming at creating numerous van der Waals attraction forces with the contacting substrates mimicking the gecko's fibrillar feet [42-44]. However, these simple fibrillar structures reached a plateau of adhesion performance after exploration of different fibril shapes and materials [45-48]. Hierarchical artificial fibrillar adhesives became available at this time with the advancement of fabrication technologies [49-52]. Characterization methods also evolved with the progress of studying the climbing behaviour of animals. Measuring the adhesion or friction between fibrillar surfaces and the contact substrates were the general methods of comparing the performances of artificial and the natural fibrillar adhesives [42-51]. Discovery of coupling friction and adhesion, during a shear movement at the time when the two substrates are completely in contact, inspired the development of a better characterization method, the LDP method as described in the previous section, mimics the way that geckos use their adhesives [36-40]. Preparation and characterization of artificial fibrillar adhesives are not well standardized by any research group; therefore results from different researchers are difficult to compare and systematically categorize. Based on the development history of artificial fibrillar adhesives, the following literature review will give a general comparison of the topography and adhesion performance in two categories of structures: single level adhesives, which contain only one length-scale of fibrils, and hierarchical fibrillar adhesives, which contain brush-like hierarchical fibrils of different length-scales. Representative artificial fibrillar adhesives are discussed in the following section to demonstrate the advancements of fibrillar adhesives in this field.

2.2.1. Artificial adhesive containing single length-scale fibrils

In order to mimic the use of van der Waals interaction in the natural fibrillar adhesives, fibrillar arrays with a diameter in the range of sub-micrometer scale were prepared by molding various polymers from nano-needle indentations and nano-porous filters [41]. The lack of control over the fibril's aspect ratio resulted in the fibril collapsing or stubby fibrillar arrays, which did not demonstrate any of the advantageous properties of fibrillar adhesives [41]. Preparation of single level adhesives has evolved from these early trials since: micrometer size of polymeric fibrillar arrays have demonstrated extraordinary friction and adhesion properties [46-47,53-56] which outperformed the nano-fibrillar adhesives. Although nano-scale fibrils continue to be investigated and improved from early fabrication methods [45,57-59], various micro-fibrils have demonstrated excellent adhesion and friction with flat substrates, such as silicon wafers

[53] and glass substrates [54]. In the research on preparing artificial micrometer size fibrillar adhesives, polyurethane fibrils with spatula tips (Figure 2.4a) have demonstrated more than 7 times higher adhesion forces than the flat substrate made by the same polymer material [55]. The adhesion pressure was measured to be 18 N/cm^2, which was much higher than the Tokay Gecko's (10 N/cm^2). In this research, adhesion measurements were performed using a load cell with a glass hemisphere (diameter of 6 mm) as the substrate interacting with the fibrillar arrays. The hemisphere was controlled by lowering it down vertically until it made contact with the fibrillar arrays, and then to pull up vertically to measure the detachment force. The use of the hemisphere is believed to avoid non-uniform contact forming between two planar substrates, i.e. "alignment error" as the authors suggested [55]. It is also believed that the spatula tips, or mushroom cap shape of the fibrils, have drastically improved the adhesion performances. However, it is suspected that these micro-mushrooms mainly rely on suction cup or vacuum effects rather than making use of van der Waals forces [60-61]. Other researchers (Figure 2.4b and c) have demonstrated similar shapes of micro-fibrils with comparable adhesion force measured [56,62-63].

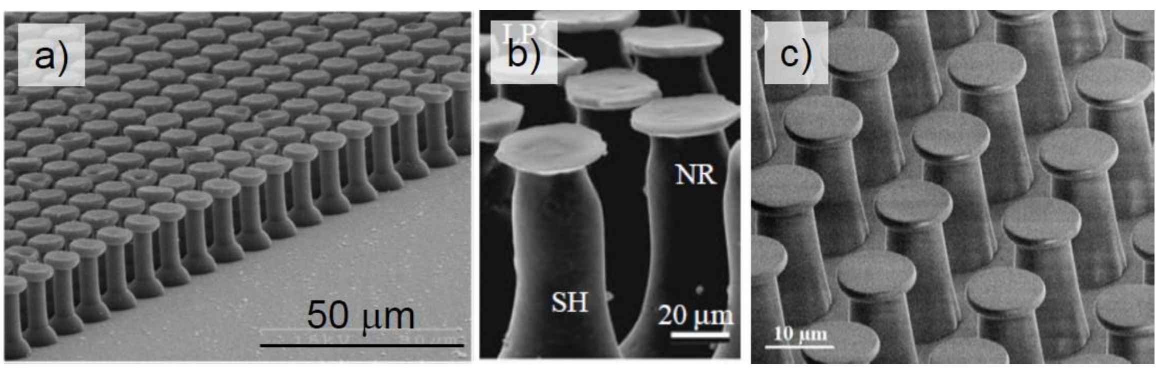

Figure 2.4. **Examples of micro-scale mushroom shape fibrillar adhesives. a) Polyurethane (PU) micro-fibrillar arrays with fibril diameter of 4.5 μm, tip diameter of 9 μm and length of 20 μm [55]. b) Polyvinylsiloxane (PVS) micro-fibrillar arrays with fibril diameter of 35 μm (middle shaft) and length of 100 μm [56]. c) polydimethylsiloxane (PDMS) micro-fibrillar arrays with fibril diameter of 6 μm and length of 10.5 μm [62]. Reproduction of the published images complies with copyright protection in Canada.**

Advancing technologies redirect the attention from single level adhesives research back to preparing nano-size fibrillar arrays, which have a closer shape resemblance to the gecko's adhesive [57-59]. Polyurethane acrylate (PUA) nano-fibrillar arrays (Figure 2.5a) were prepared and tested for adhesion and frictional forces [64]. By using electron beam irradiation, the polymeric hairs could be bent in certain directions and used as anisotropic directional adhesives. Further tuning of their customized polymeric material allowed the fibrillar arrays to realize different effective modulus. Although the adhesion of these fibrils did not show improvements by using electron beam bending, the frictional forces measured demonstrated the usefulness of anisotropic fibrillar arrays. An adhesive patch of 1 x 1 cm^2 could bear a shear load of more than 1 kilogram on an indium tin oxide (ITO) coated glass substrate. Another research (Figure 2.5b) demonstrated shear-induced adhesion of polypropylene nano-fibrils (diameter of ~300 nm) with improved adhesion and friction proportional to the sliding distance [36]. The measurements of these nano-fibrils were performed using load cells and LDP procedures. However, polypropylene nano-structures deformed under repeated dragging measurements, which resulted in adhesion and friction reduction after ~100 measurement cycles. The disadvantages of polymeric materials has driven the researchers to explore other possible materials such as carbon nano-tubes (CNT) [59,65].

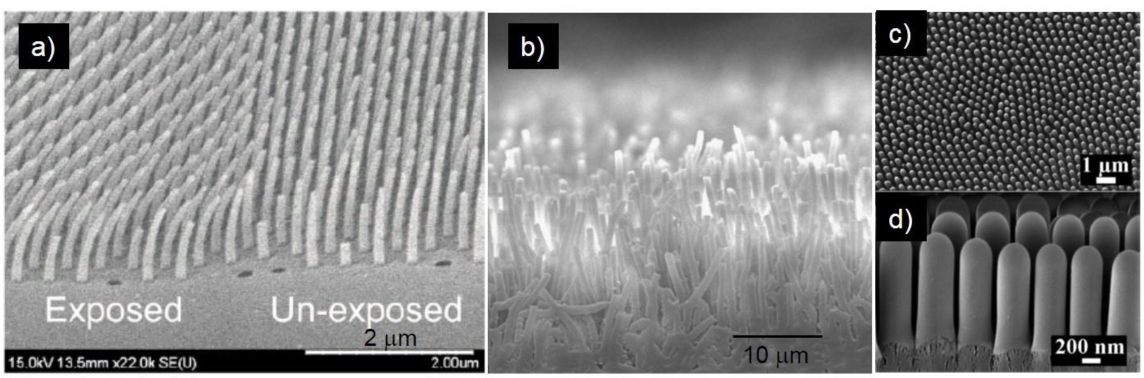

Figure 2.5. Examples of nano-fibrillar adhesives. a) Polyurethane acrylate (PUA) nano-fibrillar arrays [64]. Half of the fibrils on the left were exposed to electron beam irradiation, which resulted in tilted fibrils. b) Polypropylene (PP) nano-fibrillar arrays with fibril diameter of 600 nm and length of 18 μm [57]. c) and d) Top-view and side-view of Polystyrene (PS) nano-fibrillar adhesive, with fibril diameter of ~330 nm and length of ~1.5 μm [58]. Reproduction of the published images complies with copyright protection in Canada.

With a smaller dimension than the polymeric fibrils, carbon nanotube (CNT) arrays were prepared [59] and bundled into blocks to mimic the setae structure of the gecko's adhesive [65]. Although improvement could be observed from these CNT adhesives, the interactions between the contact substrate and the CNT forests were not reversible. This type of adhesive is not reusable and fabrication of these structures is also expensive. Other inorganic materials explored include silicon carbide [66] and hybrid germanium-parylene nanowires [67]. This nanowire forest demonstrated excellent shear loading resistance but the problem of irreversible damage persists.

Exploration of single level fibrillar adhesives has demonstrated superior adhesion and friction properties when they are interacting with flat surfaces. However, these adhesives did not yet surpass the gecko's fibrillar adhesives on rough surfaces [68]. Hierarchical fibrillar structures in the gecko's adhesive provide a possible solution for this problem.

2.2.2. Artificial adhesive containing hierarchical fibrillar structures

Geckos rely on the hierarchical fibrillar structure to adapt to surfaces of different roughness [2-6]. Taking this bio-inspiration, one of the earliest hierarchical fibrillar structures simply combined two length-scales of stubby fibrils with different aspect ratios on the bottom supporting fibrils [69] (Figure 2.6a). Adhesion forces measured were much lower than the single level adhesive, since the space between fibrils reduced the potential contact area between the adhesive and the contacting substrate. The adhesion measurements with varying preloads should have provided information of structure compliancy, but the trend of enhanced compliancy was not obvious from the results.

Variations of hierarchical structures have flourished ever since, trying to reproduce the structure of the gecko's hierarchical fibrillar structure [70-82]. The hierarchical mushroom shape fibrils (Figure 2.6b) were fabricated and tested with indentation (or push-pull) procedures, showing improvement of adhesion when the preload force was larger than 100 nN [70]. Adhesion was measured through an indentation setup with a load cell attached to a 12 mm diameter of glass hemisphere tips as the interaction substrate. Another hierarchical adhesive (Figure 2.6c) with spatula tips and a tilted fibril arrangement [50] were prepared which demonstrated enhanced frictional properties for use as a pick and place device. The test substrates were glass and silicon surfaces with nano-patterns. Only friction was investigated. This research showed an increase of frictional response when the roughness of the test substrate increased to the dimension of the fibril’s diameter, which indicated that mechanical interlocking might also contributed aside from van der Waals interactions. Some hierarchical fibrillar structures demonstrated a close resemblance to the shapes of the gecko’s adhesive (Figure 2.6 d-e), the improvement of adhesion was however limited [71-73], or only focused on testing the frictional response [74]. Fibrillar structure damage was still a problem for the polymeric materials (Figure 2.7a) [74] and CNT (Figure 2.7b) [52]. Characterization methods in recent studies have moved on to using a hemisphere and making use of scanning probe microscopy to automatically collect large amounts of data on the adhesive properties of artificial adhesives [71-73].

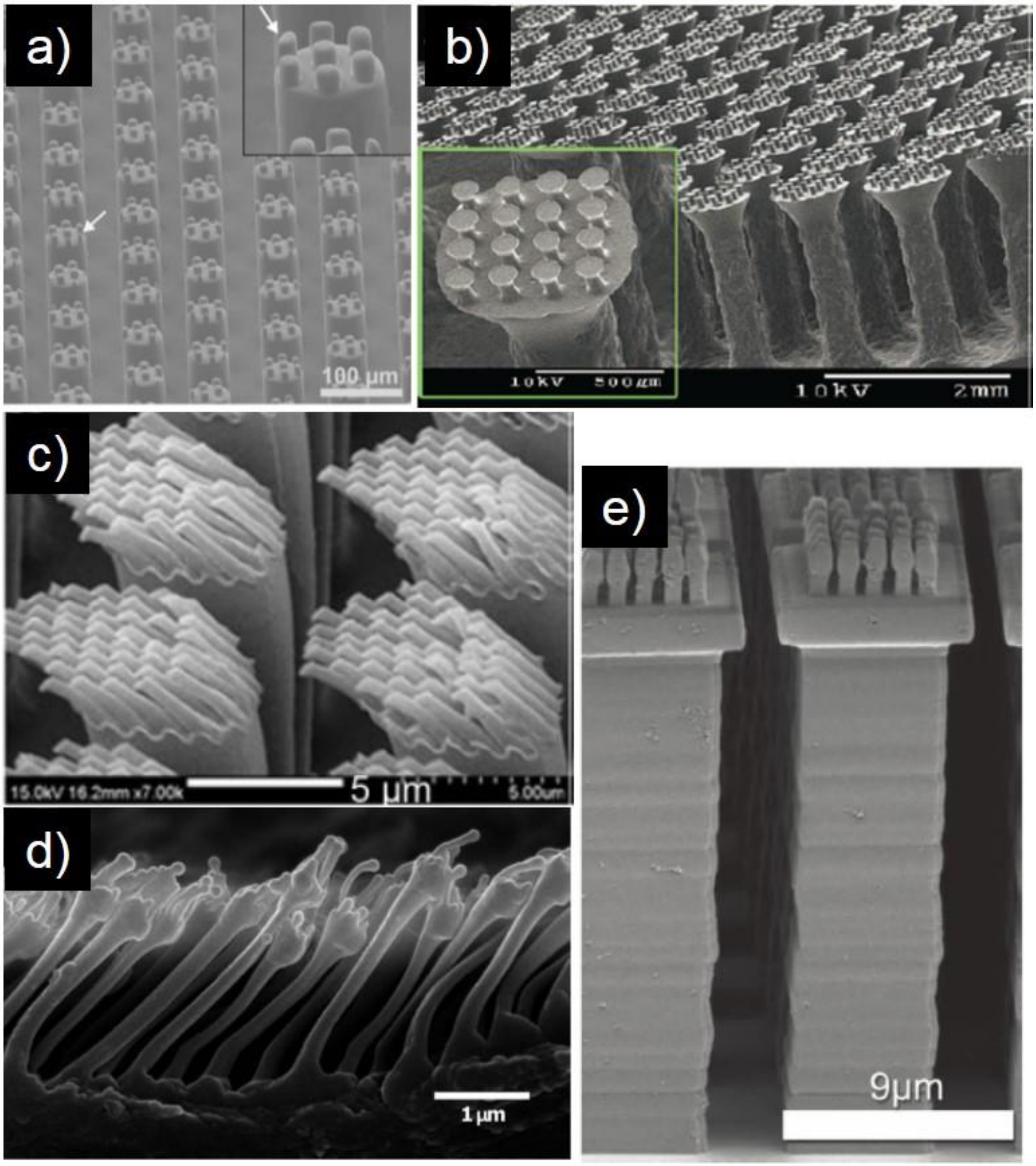

Figure 2.6. **SEM images of example hierarchical fibrillar adhesives. a) Simple PDMS hierarchical fibrillar arrays molded from SU-8 mold [69]. b) PU hierarchical fibrillar arrays prepared by molding method [70]. Inset is a magnified view of the top of a large fibril. c) PUA hierarchical fibrillar adhesive with nano-size fibrils tilted in an angle [50]. d) PS hierarchical nano-fibrillar arrays prepared by hot-pulling from an aluminum oxide template [71]. e) Polymeric hierarchical fibrillar arrays prepared by direct laser writing on a photoresist layer [72]. Reproduction of the published images complies with copyright protection in Canada.**

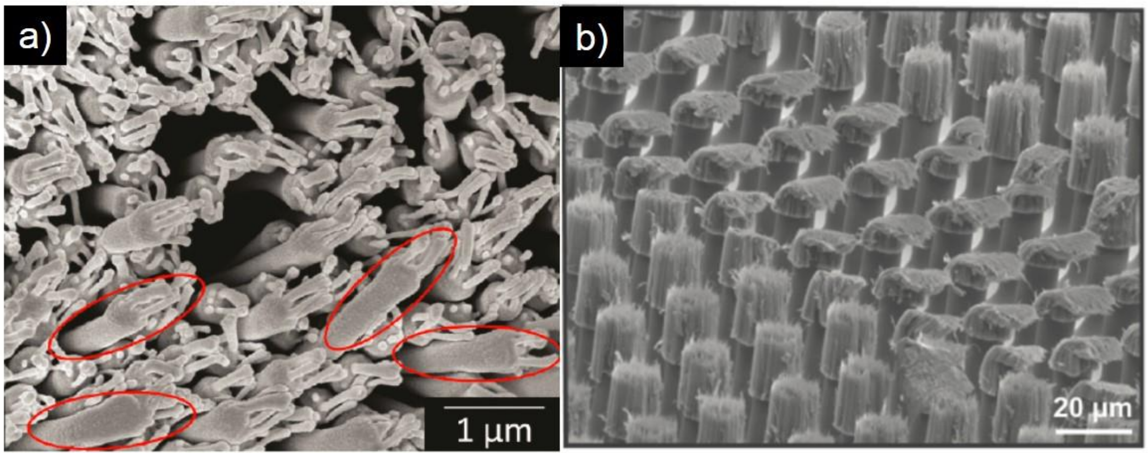

Figure 2.7. SEM images demonstrating the structure damage of hierarchical fibrillar adhesives after shear measurements. a) Polycarbonate (PC) hierarchical fibrils were pulled and bent (noted by red ovals) after shear force measurements [74]. b) CNT hierarchical structure deformed after one time shear force measurement (top layer material: CNT and bottom layer material: SU-8) [52]. Reproduction of the published images complies with copyright protection in Canada.

Another type of hierarchical structure contains a continuous thin film with smaller scale of fibrils on the top; the larger scale fibrils were sandwiched between this thin film and the substrate (Figure 2.8a-b) [75-78]. This type of hierarchical fibrillar structure does not have topography resemblance to the gecko's adhesive, but this design provides a certain compliancy of the fibrillar structure and avoids contact area reduction. Performance of these hierarchical structures has demonstrated improvement on adhesion and friction to some extent, but the linked film limits the moving space of the larger fibrils which results in lower compliancy with shear loading and shear-induced adhesion [79-81]. A variation of the thin film type hierarchical structure is a lamellar like structure (Figure 2.8d-f), with nano-fibrils on the thin flap of polymer [82]. Results of this research focused on the enhanced frictional performance.

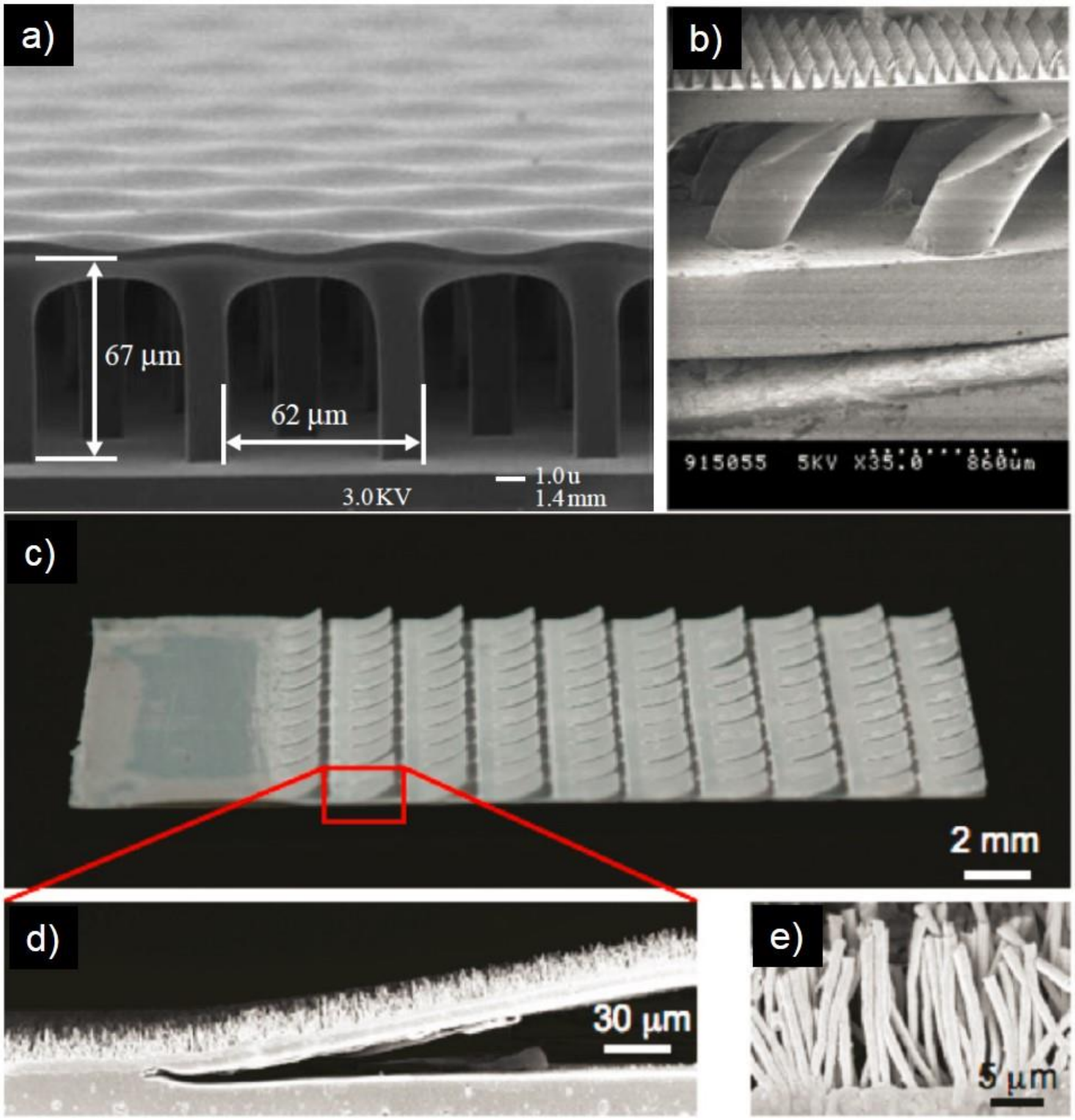

Figure 2.8. **Hierarchical fibrillar structure with thin film terminated at the interaction side. a) SEM image of PDMS hierarchical fibrillar structure with a continuous film on top of fibrils as contact interface with other substrate [75]. b) SEM image of PDMS hierarchical structure with a continuous film on top of the larger fibrils as contact interface with other substrate [77]. c) High density polyethylene (HDPE) hierarchical structure with lamellar shape of flaps, which contains micro-fibrils on top. d) SEM image of side view on one lamellar showing the micro-fibrillar layer. e) SEM image of side view on arrays of micro-fibrils. c)-e) are reproduced from [82]. Reproduction of the published images complies with copyright protection in Canada.**

Advantages and limitations can be summarized on these afore mentioned studies of hierarchical fibrillar adhesives. Contributions to improving artificial fibrillar adhesives with hierarchical fibrillar structures can be made on the following points. First, preparation of these hierarchical structures was generally expensive. Use of special materials, equipment and cleanroom environments haul the development of such adhesives for large-scale applications. Second, most of the previous studies focused on frictional performance rather than adhesion performance. Third, those studies provided results of pull-up force or adhesion performance and had showed limited improvement by utilizing the hierarchical structure. And at last, characterization of these hierarchical structures provided limited information on the relationship between compliancy and adhesion forces. This thesis was proposed based on these observations. The final goal of this thesis study is to prepare a hierarchical fibrillar adhesive which is able to demonstrate the advantage of the topography by correlating compliancy and adhesion force enhancement. To realize this ultimate goal, the preparation of a hierarchical fibrillar adhesive and the development of a characterization method were investigated as necessary steps. The literature presented in this chapter, therefore, offered an insight on the current state of the art technologies and their limitations, which has provided the background of the studies for the following chapters.

2.3. References

[1] Aristotle. The History of Animals, *trans. D'Arcy Wentworth Thompson*. [Online] Sept 2nd 2014, URL: http://classics.mit.edu/Aristotle/history_anim.9.ix.html.

[2] K. Autumn, Y. Liang, T. Hsieh, W. Zesch, W.-P. Chan, T. Kenny, R. Fearing, R.J. Full, *Nature* **2000**, *405*, 681-685.

[3] K. Autumn, A. M. Peattie, *Integr. Comp. Biol.* **2002**, *42*, 1081-1090.

[4] G. Huber, H. Mantz, R. Spolenak, K. Mecke, K. Jacobs, S.N. Gorb, E. Arzt, *Proc. Natl. Acad. Sci. U.S.A.* **2005**, *102*, 16293-16296.

[5] T. Prevenslik, *Tribology in industry* **2009**, *31*, 61-66.

[6] K. Autumn, Properties, Principles, and Parameters of the Gecko Adhesive System. In *Biological Adhesives*; A. M. Smith and J. A. Callow Ed.; Springer: Berlin Heidelberg, **2006**; 225-256.

[7] U. Hiller, *Form. Funct.* **1971**, *4*, 240-253.

[8] U. Hiller, *Z. Morphol.Tiere* **1969**, *62*, 307-362.

[9] K. Autumn, M. Sitti, Y.A. Liang, A.M. Peattie, W.R. Hansen, S. Sponberg, T. Kenny, R. Fearing, J.N. Israelachvili, R.J. Full, *Proc. Natl. Acad. Sci. U.S.A.* **2002**, *99*, 12252-12256.

[10] P.H. Niewiarowski, S. Lopez, L. Ge, E. Hagan, A. Dhinojwala, *PLoS ONE* **2008**, *3*, e2192.

[11] B. Chen and H. Gao*, Int. J. Appl. Mechanics* **2010**, *2*, 1-9.

[12] J. B. Puthoff, M. S. Prowse, M. Wilkinson, K. Autumn, *J. Exp. Biol.* **2010**, *213*, 3699-3704.

[13] M. S. Prowse, M. Wilkinson, J. B. Puthoff, G. Mayer, K. Autumn, *Acta Biomater.* **2011**, *7*, 733-738.

[14] A. B. Kesel, A. Martin, T. Seidl, *J. Exp. Biol.* **2003**, *206*, 2733-2738.

[15] A. B. Kesel, A. Martin, T. Seidl, *Smart Mater. Struct.* **2004**, *13*, 512-518.

[16] S. Niederegger, S. N. Gorb, *J. Comp. Physiol. A* **2006**, *192*, 1223-1232.

[17] S. N. Gorb, M. Sinha, A. Peressadko, K. A. Daltorio, R. D. Quinn, *Bioinspiration Biomimetics* **2007**, *2*, S117-S125.

[18] A. M. Peattie, C. Majidi, A. Corder, R. J. Full, *J. R. Soc. Interface* **2007**, *4*, 1071-1076.

[19] J. F.V. Vincent, U. G.K. Wegst, *Arthropod Struct. Dev.* **2004**, *33*, 187-199.

[20] B. N.J. Persson, *J. Chem. Phys.* **2003**, *118*, 7614-7621.

[21] M. Sitti, R. S. Fearing, *J. Adhes. Sci. Technol.* **2003**, *17*, 1055-1073.

[22] K. Autumn, C. Majidi, R.E. Groff, A. Dittmore, R. Fearing, *J. Exp. Biol.* **2006**, *209*, 3558-3568.

[23] C. A. Dahlquist, Pressure-sensitive adhesives. In *Treatise on Adhesion and Adhesives*. vol. 2; R. L. Patrick Ed.; Dekker, New York; **1969**; 219-260.

[24] T. W. Kim, B. Bhushan, *Ultramicroscopy* **2007**, *107*, 902-912.

[25] P. K. Porwal, C. Y. Hui, *J. R. Soc. Interface* **2008**, *5*, 441-448.

[26] T. W. Kim, B. Bhushan, *J. Adhesion Sci. Technol.* **2007**, *21*, 1-20.

[27] G. Huber, S. N. Gorb, N. Hosada, R. Spolenak, E. Arzt, *Acta Biomater.* **2007**, *3*, 607-610.

[28] A. G. Gillies, A. Henry, H. Lin, A. Ren, K. Shiuan, R. S. Fearing, R. J. Full, *J. Exp. Biol.* **2014**, *217*, 283-289.

[29] Y. Tian, N. Pesika, H. Zeng, K. Rosenberg, B. Zhao, P. McGuiggan, K. Autumn, J. Israelachvili, *Proc. Natl. Acad. Sci. U.S.A.* **2006**, *103*, 19320-19325.

[30] J. O. Wolff, S. N. Gorb, *Sci. Rep.* **2013**, *3*, 1101.

[31] N. Gravish, M. Wilkinson, S. Sponberg, A. Parness, N. Esparza, D. Soto, T. Yamaguchi, M. Broide, M. Cutkosky, C. Creton, K. Autumn, *J. R. Soc. Interface* **2009**, *7*, 259-269.

[32] J. B. Puthoff, M. Holbrook, M. J. Wilkinson, K. Jin, N. S. Pesika, K. Autumn, *Soft Matter* **2013**, *9*, 4855-4863.

[33] B. Zhao, N. Pesika, K. Rosenberg, Y. Tian, H. Zeng, P. McGuiggan, K. Autumn, J. Israelachvili, *Langmuir* **2008**, *24*, 1517-1524.

[34] K. Autumn, S. T. Hsieh, D. M. Dudek, J. Chen, C. Chitaphan, R. J. Full, *J. Exp. Biol.* **2006**, *209*, 260-272.

[35] K. Autumn, A. Dittmore, D. Santos, M. Spenko, M. Cutkosky, *J. Exp. Biol.* **2006**, *209*, 3569-3579.

[36] B. Schubert, J. Lee, C. Majidi, R.S. Fearing, *J. R. Soc. Interface* **2008**, *5*, 845-853.

[37] Y. Tian, J. Wan, N. Pesika, M. Zhou, *Sci. Rep.* **2013**, *3*, 1382.

[38] M. P. Murphy, B. Aksak, M. Sitti, *J. Adhes. Sci. Technol.* **2007**, *21*, 1281-1296.

[39] Y. Li, C. Zh\g, J. H.-W. Zhou, C. Menon, B. D. Gates, *Macromol. React. Eng.* **2013**, *7*, 638-645

[40] Q. H. Cheng, B. Chen, H. J. Gao, Y. W. Zhang, *J. R. Soc. Interface* **2012**, *9*, 283-291.

[41] M. Sitti and R. S. Fearing, *In Proceedings of the IEEE Nanotechnology Conference,* Washington, DC, USA, August, **2002**, pp. 137-140.

[42] D. Campolo, S.D. Jones and R. S. Fearing, *In Proceedings of IEEE Nano,* San Francisco, CA, USA, August 12-14, **2003**.

[43] M. Sitti and R.S. Fearing, *J. Adhes. Sci. Technol.* **2003**, *17*, 1055-1074.

[44] A. K. Geim, S. V. Dubonos, I. V. Grigorieva, K. S. Novoselov, A. A. Zhukov, S. Y. Shapoval, *Nature Materials* **2003**, *2*, 461–463.

[45] T. Kim, H. E. Jeong, K. Y. Suh, H. H. Lee, *Adv. Mater.* **2009**, *21*, 1-6.

[46] M.P. Murphy, B. Aksak, and M. Sitti, *Small* **2009**, *5*, 170-175.

[47] D. Sameoto and C. Menon, J. Micromech. Microeng. 2010, 20, 115037.

[48] B. Chen, P. G. Oppenheimer, T. A.V. Shean, C. T. Wirth, S. Hofmann, J. Robertson, *J. Phys. Chem. C* **2012**, *116*, 20047-20053.

[49] M. P. Murphy, S. Kim, M. Sitti, *ACS Appl. Mater. Interfaces* **2009**, *4*, 849-855.

[50] H. E. Jeong, J.-K. Lee, H. N. Kim, S. H. Moon, and K. Y. Suh, *Proc. Nat. Acad. Sci. U.S.A.* **2009**, *106*, 5639-5644.

[51] A. Y. Y. Ho, L. P. Yeo, Y. C. Lam, I. Rodriguez, *ACS Nano* **2011**, *5*, 1897-1906.

[52] Z. Rong, Y. Zhou, B. Chen, J. Robertson, W. Federle, S. Hofmann, U. Steiner P. Goldberg-Oppenheimer, *Adv. Mater.* **2014**, *26*, 1456-1461.

[53] D. Sameoto, C. Menon, *J. Micromech. Microeng.* **2009**, *19*, 115002.

[54] A. Parness, D. Soto, N. Esparza, N. Gravish, M. Wilkinson, K. Autumn, M. Cutkosky, *J. R. Soc. Interface* **2009**, *6*, 1223-1232.

[55] S. Kim, M. Sitti, *Appl. Phys. Lett.* **2006**, *89*, 261911.

[56] S. Gorb, M. Varenberg, A. Peressadko, J. Tuma, *J. R. Soc. Interface* **2007**, *4*, 271–275.

[57] J. Lee, C. Majidi, B. Schubert, R.S. Fearing, *J. R. Soc. Interface* **2008**, *5*, 835-844.

[58] L. Xue, A. Kovalev, F. Thole, G.T. Rengarajan, *Langmuir* **2012**, *28*, 10781-10788.

[59] L. Qu, L. Dai, M. Stone, Z. Xia, Z.L. Wang, *Science* **2008**, *322*, 238-242.

[60] G. Carbone, E. Pierro and S. N. Gorb, *Soft Matter,* **2011**, *7*, 5545-5552.

[61] L. Heepe, M. Varenberg, Y. Itovich, S.N. Gorb, *J. R. Soc. Interface* **2011**, *8*, 585-589.

[62] D. Sameoto, C. Menon, *J. Micromech. Microeng*. **2009**, *19*, 115026.

[63] A.V. Spuskanyuka, R.M. McMeeking, V.S. Deshpande, E. Arzt, *Acta Biomater.* **2008**, *4*, 1669-1676.

[64] T. Kim, H. E. Jeong, K. Y. Suh, H. H. Lee, *Adv. Mater.* **2009**, *21*, 1-6.

[65] L. Ge, S. Sethi, L. Ci, P.M. Ajayan, A. Dhinojwala, *Proc. Nat. Acad. Sci. U.S.A.* **2007**, *104*, 10792-10795.

[66] H.W. Shim, J.D. Kuppers, H. Huang, *Nanotechnology* **2009**, *20*, 025704.

[67] H. Ko, J. Lee, B.E. Schubert, Y.-L. Chueh, P.W. Leu, R.S. Fearing, A. Javey, *Nano Lett.* **2009**, *9*, 2054-2058.

[68] M. K. Kwak, H.-E. Jeong, K. Y. Suh, *Adv. Mater.* **2011**, *23*, 3949-3953.

[69] C. Greiner, E. Arzt, A. del Campo, *Adv. Mater*. **2009**, *21*, 479-482.

[70] M.P. Murphy, S. Kim, M. Sitti, *ACS Appl. Mater. Interfaces* **2009**, *4*, 849-855.

[71] D. Y. Lee, D. H. Lee, S. G. Lee, K. Cho, *Soft Matter* **2012**, *8*, 4905-4910.

[72] M. Roehrig, M. Thiel, M. Worgull, H. Hoelscher, *Small* **2012**, *8*, 3009-3015.

[73] H. Lee, B. Bhushan. *J. Colloid Interface Sci*. **2012**, *372*, 231-238.

[74] A. Y. Y. Ho, L. P. Yeo, Y. C. Lam, I. Rodriguez, *ACS Nano* **2011**, *5*, 1897-1906.

[75] W.L. Noderer, L. Shen, S. Vajpayee, N.J. Glassmaker, A. Jagota, C.-Y. Hui, *Proc. Royal Soc. A* **2007**, *463*, 2631-2654.

[76] H. Izadi, M. Golmakani, A. Penlidis, *Soft Matter* **2013**, *9*, 1985-1996

[77] A. Asbeck, S. Dastoor, A. Parness, L. Fullerton, N. Esparza, D. Soto, B. Heyneman, M. Cutkosky, in Proceedings of *IEEE Int. Conf. Robotics and Automation*, Kobe Japan, 12-17 May **2009,** pp. 2675-2680.

[78] H. Izadi, B. Zhao, Y. Han, N. McManus, A. Penlidis*, J. Polym. Sci., Part B: Polym. Phys*. **2012**, *50*, 846-851.

[79] H. Yao, H. Gao, *J. Mech. Phys. Solids* **2006**, *54*, 1120-1146.

[80] T.W. Kim, B. Bhushan, *J. Adhes. Sci. Technol.* **2007**, *21*, 1-20.

[81] H. Gao, Wang X, Yao H, Gorb S, Arzt E, *Mech. Mater.* **2005**, *37*, 275-285.

[82] J. Lee, B. Bush, R. Maboudian, R.S. Fearing, *Langmuir* **2009**, *25,* 12449–12453.

Chapter 3.

Enhanced anisotropic and adhesion performance of hierarchical fibrillar adhesive

To demonstrate the advantages of hierarchical fibrillar adhesive, macro- and micro-size fibrils are combined in the same fashion as in the gecko adhesive. Mushroom shape micro-fibrils are attached at the open end of the millimeter size posts. On top of the mushroom cap, micrometer-size fibrils are spread across the surfaces. The hierarchical structure behaves differently from the single level micro-fibrillar adhesive when it is subjected to loads in different directions. This chapter aimed at achieving OBJECTIVE 1. Results obtained demonstrated the advantage of hierarchical structures, which are worth further development to a size scale closer to the gecko adhesive, i.e. nano- and micro-meter size fibrillar arrays. The following contents are published in the paper: Yasong Li, Dan Sameoto and Carlo Menon, "Enhanced compliant adhesive design and fabrication with dual-level hierarchical structure." *Journal of Bionic Engineering*, 2010, *vol. 7*, 228-234.

3.1. Abstract

Artificial dry adhesives inspired by the nano- and micro-scale hairs found on the feet of geckos and spiders have been developed for almost a decade. Elastomeric arrays of micrometre fibrils outperform natural dry adhesives on smooth surfaces under normal loading. However, on the rough surfaces, these single level fibrillar adhesives do not behave as strongly as they do on smooth surfaces. Drastic reduction of surface contact area is the reason of degraded adhesion performance. In nature, contact area is maximized by hierarchically structuring different scales of fibrils capable of conforming to different surface roughness. In this chapter, we adapt nature's solution and propose a novel dual-level hierarchical adhesive design using polydimethylsiloxane (PDMS). A

mold with micro-scale recesses is prepared by laser cutting a poly(methyl methacrylate) (PMMA) plate. PDMS is casted in the PMMA mold and demolded after complete cured of the polymer. A previously prepared PDMS micro-fibrillar adhesive is glued to the demolded PDMS arrays of macro-scale fibrils. The bonded piece of PDMS micro-fibrillar adhesive is then cut into squares so that each small piece of the adhesive functions as a mushroom cap on top of each macro-size fibril. The hierarchical fibrillar adhesive, having millimetre size of fibrils with thin film of arrays of micro-fibrils on top, is able to conform to loads applied in different directions. This hierarchical structure enhances the peel strength on smooth surfaces compared to a single-level dry adhesive, but at the same time weakens the shear strength of the adhesive for a given area in contact. The adhesion performance appears to be very sensitive to the specific size of the fibril tips. Experiments indicate that designing hierarchical structures is not as simple as placing multiple scales of fibrils on top of one another, but can require significant design optimization to enhance the contact mechanics and adhesion strength.

Keywords: Biomimetic, dry adhesive, hierarchical, dual-level adhesive, silicone, polymer

3.2. Introduction

The discovery of intermolecular forces contributing to the gecko’s remarkable climbing ability has inspired the fabrication of artificial dry adhesive for almost a decade [1]. The early efforts in preparing these type of “dry adhesives”, relied on no chemical secretion but simply the dipole attraction in molecular scale, researchers had focused on fabricating arrays of nano- and micro-fibrils and testing them on flat substrates [2-7, 12]. These structures resembled grass, with no particular tip shapes [2-4]. Later, improvements were made by preparing mushroom shape fibrils which boosted the performance of these adhesives when they were tested on smooth surfaces and under normal loading [5-7]. The adhesion performance of these single level adhesives, however, degraded on rough surfaces due to the dramatic decrease of contact with the substrates. To better conform to rough surfaces, hierarchical structures, which have close resemblance to the shape of trees, have evolved in nature. For example, the gecko’s feet, toe, lamella, seta, and spatula provide a compliant mechanism that extends the fibrillar structure to the recesses on the climbing substrate [1]. Recent attempts made to fabricate hierarchical dry adhesives have proved that adapting nature's solution on artificial adhesives is possible [8-10, 12]. Murphy et al. [8] fabricated a triple-level adhesive by dipping bigger size of pillars into an uncured donor layer of polyurethane, followed by placing the uncured side on a silicon mold containing smaller sized structures. This adhesive showed improved adhesion on smooth surfaces, and theoretically on uneven surfaces by testing the contact force using a hemisphere. Lee et al. [9] prepared a macro layer with shape of lamella using a hard polymer, and tested the sample on surfaces with different asperities. The introduction of the lamella structures showed higher shear strengths on stainless steel gratings of 100 µm and 200 µm peak-to-peak. The measured shear adhesion forces of these adhesives were one third of the ones without the lamellar structure on 100 mm gratings. Adhesion forces of the single layer adhesive were almost zero on 200 mm gratings. Asbeck et al. [10] combined macro- and micro-scale directional wedges, which empowered a robot to climb on a wooden door. However, no relationships between adhesion and macro-fibre's shape and size were demonstrated.

In this chapter, we propose a fabrication method for a dual-level adhesive design, and investigate the relationship between adhesion and the macro-fibril's shape and size. The proposed hierarchical structure includes mushroom shaped posts in micro- and macro-scale. Samples are tested for peel and shear strengths, which reveal the dual-level adhesive properties under different circumstances.

3.3. Materials and Methods

3.3.1. Fabrication procedures

All the fabricated samples are made from Sylgard® 184 polydimethylsiloxane (PDMS) from Dow Corning [11], a transparent elastomer having low Young's modulus. First, a poly(methyl methacrylate) (PMMA) mold with macro-scale indentations engraved by a CO_2 laser cutter (Universal Laser Systems VLS3.60) was prepared for casting macro-fibrillar arrays (see Figure 3.1a). Instead of engraving blind holes directly on a PMMA substrate, we found that cutting holes through a piece of PMMA and then bonding it to another flat PMMA substrate with acetone can achieve better resolution of structures. Second, PDMS was poured in the mold, with a layer of cloth soaked with excessive PDMS (Figure 3.1b). The reinforced cloth can prevent the structure destruction when removing the PDMS arrays of macro-size pillars from the PMMA mold. Third, the cured PDMS macro-fibril layer was demolded from the PMMA, ready to be bonded to the micro-fibrillar layer (Figure 3.1c). The fibrillar adhesive containing micro-mushrooms prepared from using a molding method which was introduced in a previous work [7]. The PDMS arrays of macro-size fibrils were dipped into uncured PDMS and placed on the backing layer of PDMS arrays of micro-mushrooms (Figure 3.1d). Bonding of two layers was secured when the PDMS gluing interface is completely cured (Figure 3.1e). Last, the thin layer with micro-mushrooms was cut into design shapes using a laser cutter, forming macro-scale mushroom caps on top of each macro-post (Figure 3.1f). A thin film of plastic is placed on top of the micro-mushrooms during laser cutting in order to protect the microstructures from small flames and debris caused by the laser beam. Figure 3.2 shows the outcomes of the preparation process.

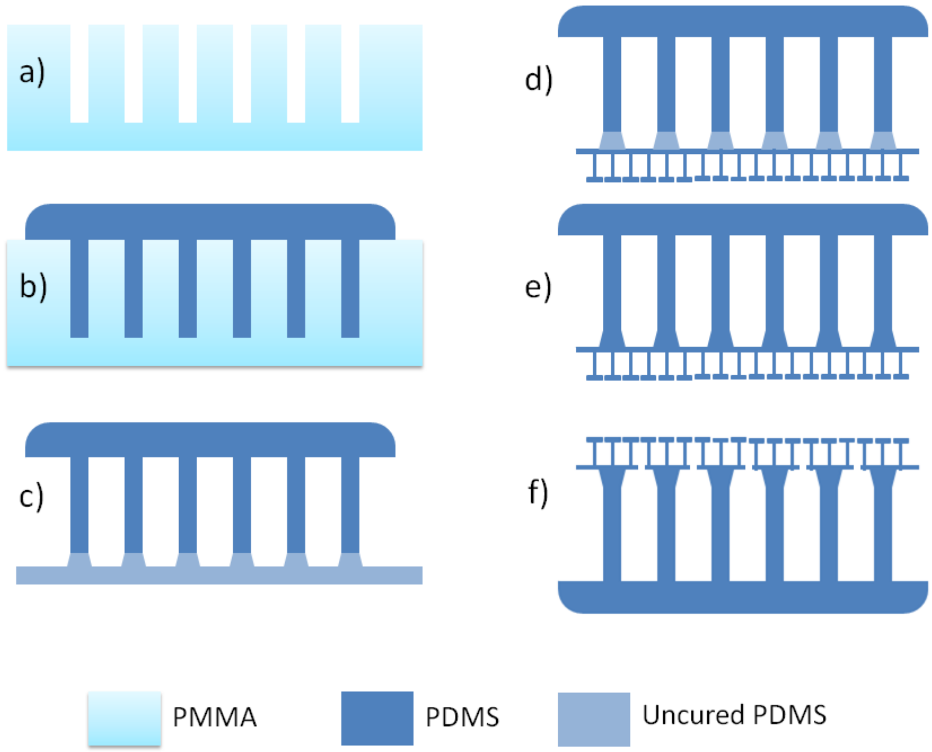

Figure 3.1. Fabrication procedures of dual-level adhesive. a) PMMA mold engraved by a laser cutter; b) PDMS was poured inside the mold; c) macro-scale fibrillar arrays were ready to dip into uncured PDMS as bonding material; d) macro-fibrillar layer put on top of the back of micro-fibrillar layer; e) bonding PDMS cured; f) laser cutting micro-fibrillar layer into small caps.

3.3.2. Parameters selection

In this work, the relationship between adhesion and shape of the macro-scale fibrils was investigated. The size and shape of micro-fibrils as well as the mushroom cap overhang on the microstructures were the same in all the samples we prepared. From this point forward, the mushroom cap, fibril size and shape are all referred to as the macro-scale structures. The smallest circular hole the laser cutter could achieve on the PMMA substrate was 0.03 inch (0.762 mm) in diameter. Therefore we chose 0.03 inch, 0.04 inch (1.016 mm) and 0.06 inch (1.524 mm) as widths of the macro-size fibrils. The PMMA thickness is 0.12 inch (3.048 mm), which corresponds to fibril's height. Thus the aspect ratios of the macro-fibrils with fibril widths of 0.03", 0.04" and 0.06" are 4:1, 3:1 and 2:1. In order to obtain as large of a contact area as possible, the mushroom caps were cut into squares without big gaps between each of them (Figure 3.2c). The mushroom cap overhang is therefore related to the space between two adjacent fibrils. Three space variations (called *space 1*, *space 2* and *space 3* in later context) are chosen, which are 1, 2 and 3 times the fibril's width (e.g., samples with 1 time space and 0.03" fibres width have a 0.03" space between two adjacent fibres and therefore their cap size is 0.06 x 0.06 square inch with overhang of 0.015"). Specifically, mushroom cap overhang in space 1, 2 and 3 for 0.03" fibril width samples are 0.06", 0.09" and 0.12; mushroom cap overhang in space 1, 2 and 3 for 0.04" fibril width samples are 0.08", 0.12" and 0.16"; mushroom cap overhang in space 1, 2 and 3 for 0.06" fibril width samples are 0.12", 0.18" and 0.24.

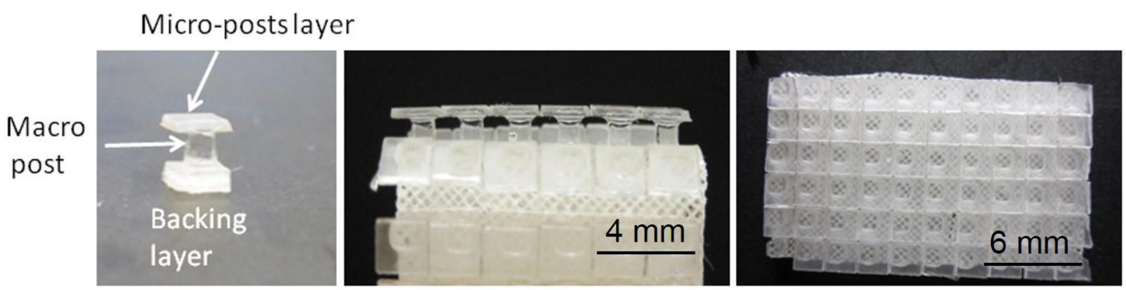

Figure 3.2. Photos demonstrated the hierarchical fibrillar structure. a) a macro-scale fibril with cap; b) side view of arrays of macro-scale fibrils with mushroom caps on a bent sample. Each row consists of 6 micro-fibrils; c) top view of the dual-level adhesive sample.

Three fibril shape variations were also chosen: square, circle and star shapes (see Figure 3.3). Cross section area for these three shapes decrease from square, circle to star, which are resulting in different stiffness in the hierarchical structure. The stiffness is given by the following formula [16]:

$$k = \frac{F}{\delta} = \frac{AE}{L} \qquad \text{(Eq. 1)}$$

where F is the force applied to the object and δ is the displacement due to the force applied to the object; and A refers to the cross sectional area of the object, E is the elastic modulus and L is the length of the object. By using the same material (PDMS) the elastic modulus of the samples are the same. The length or height of the fibrils is also fix in our samples. Thus the stiffness of each fibril is direct proportional to its cross-sectional area. The stiffness of the square fibrillar samples is the greatest, and decrease in circular fibrillar samples. The stiffness of the star shape fibrillar sample has the lowest stiffness.

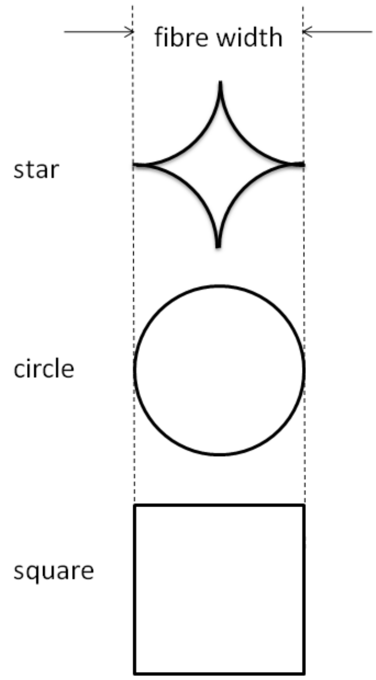

Figure 3.3. Schematics of different fibril shapes with the same fibril width.

The bending stiffness is given as EI, where I is the area moment of inertia about the axis of interest. Here in our three cross-sectional design of the macro-fibrils, all of these geometries are centrosymmetric. Therefore I_x and I_y are the same for these geometries. All fibril width of different shapes are the same (Figure 3.3), and set as 2a. For the square fibrils, the area moment of inertia is

$$I = \frac{1}{12}(2a)(2a)^3 = \frac{4}{3}a^4 = 1.33a^4 \qquad \text{(Eq. 2)}$$

For the circle fibrils, the area moment of inertia is

$$I = \frac{1}{4}\pi a^4 = 0.78a^4 \qquad \text{(Eq. 3)}$$

For the star shape fibrils, the area moment of inertia is calculated from summing up the 4 quarters of inertia in the shape by using perpendicular axis theorem to translate the axis of interest.

$$I = 4\left(\frac{a^4}{3} - \left(\left(\frac{\pi}{16} - \frac{4}{9\pi}\right)a^4 + \frac{\pi a^2}{4}\left(a - \frac{4a}{3\pi}\right)^2\right)\right) = 0.073a^4 \qquad \text{(Eq. 4)}$$

Using the same material for these fibrils in different shape, the bending stiffness is direct proportional to the cross sectional area moment of inertia as given in the above equations (Eq.2-4). The bending stiffness of the square shape of fibrils is the greatest; the circular fibrils have the moderate bending stiffness; and the star shape fibrils have the lowest bending stiffness.

In summary, samples were fabricated with 3 changing parameters: fibril width (or aspect ratio since the height is fixed), space between fibres (or cap size) and fibril shape. Fourteen variations of samples are tested: nine samples of square fibrils with three different fibril widths and three different fibril spaces; two samples of circle shape fibrils and two samples of star shape fibrils with *space 2* and *space 3*; one sample of single layer micro-structure adhesive with a piece of 0.12 inch thick PMMA adhered on the backing layer. All the samples used a micro-fibrillar adhesive fabricated from the same mold, and this layer is 0.25 mm thick.

3.3.3. Experimental setup

Samples were tested for peel strength using a customized setup shown in Figure 3.4a. A linear stage (Zaber Technologies T-LS28-SMV) with a force sensor attached to it

(LSM300 Load Cell from Futek) moved up and down at a constant speed, capable of measuring the pull-up force upon the separation of the two substrates. The load cell was connected to the sample with a flexible rope. The PMMA substrate, which served as the interaction substrate, was tilted with respect to the horizontal ground with an angle θ. The load cell output was acquired by a Data Acquisition Card (National Instruments USB-6259BNC) with a customized software (written in LabVIEW 8.2, National Instruments), which was able to control the movement of the linear stage and record the load cell output.

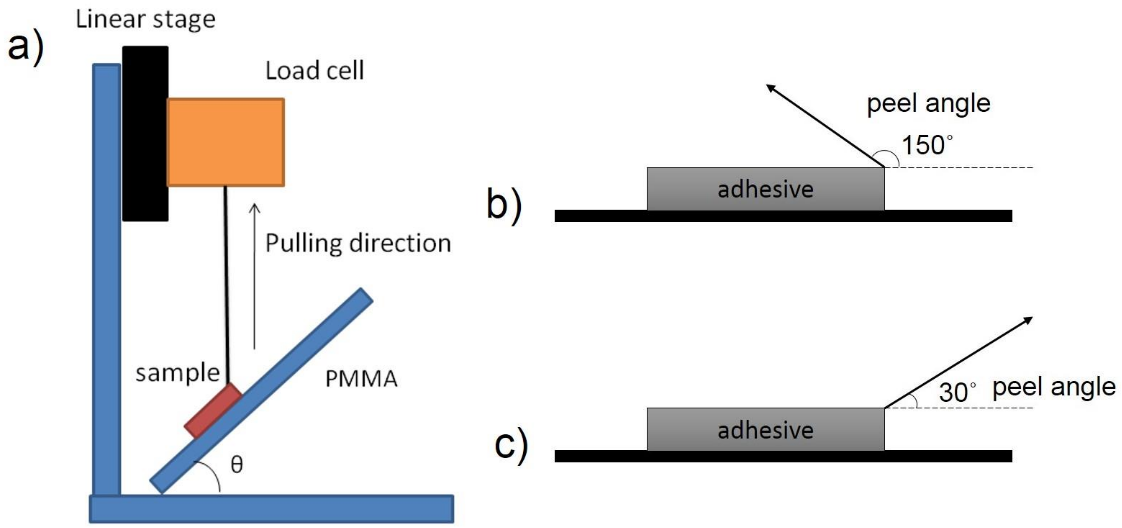

Figure 3.4. a) Schematics of the test system. b) and c) schematics of two testing peel angle at 150˚ and 30˚.

All the tests were performed using a pull speed of 1000 µm/s. Each sample contained 9 macro-fibrils arranged in 3 rows and 3 columns. The flat single layer micro-structured adhesive was cut into a 1x1 cm^2 layer and attached to a PMMA backing layer of the same size. Every sample was preloaded by hand compression and the contact area was confirmed by visual inspection through the transparent PMMA substrate. Measurements using the same set of parameters were repeated for at least 3 times. Pull off forces were recorded and used for comparison of different macro-fibre designs.

3.4. Results and Discussion

3.4.1. Peel tests with peel angle greater than 90 degrees

Peel angles are defined by the angle between the pulling direction and the plane pointing from the connection joint of the sample and the rope to the opposite direction of the sample. Figure 3.4b and 3.4c showed the difference between high peel angle and low peel angle. Figure 3.5 showed a typical force curve of a peel test at high peel angle (specifically a square shape sample with fibril width of 0.04” and space 2). Tests were done by peeling samples vertically from the PMMA flat substrate tilted at 60 degrees. Therefore the peel angle was 150 degrees, as illustrated in Figure 3.4a. Each spike represents the sudden peel off process of a row of macro-fibrils. The peak value of each spike represents the peel off force. The first row of macro-fibrils undergoes the highest peel off force, with decreasing peel off forces for the subsequent rows of macro fibrils. This phenomenon might be an outcome of sudden detachment of the first row of adhesive which slightly influences the contact condition of the second and third rows of caps. A similar situation appeared when the second row of adhesives was peeled off the substrate and influenced the third row of adhesives. It should be noted that during the peeling process, the peel angle was changing slightly with the progression of cracks between the rows of adhesives and contacting substrate. This slight change of the peel angle might also contribute to the differences of the peel off forces on different rows of adhesives.

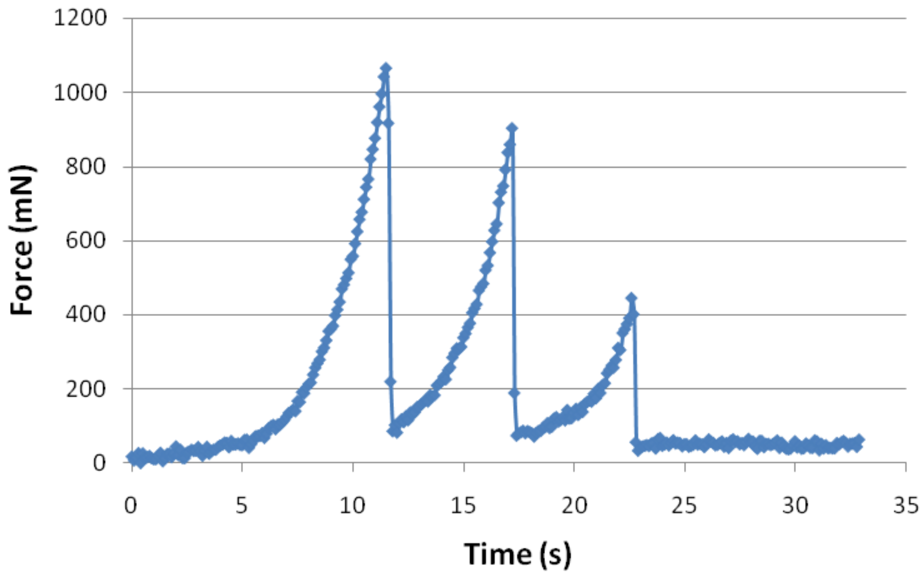

Figure 3.5. **Typical force curve of a peel test using a sample of 0.04" fibril size and *space 2* (adhesive area of ~ 83.6 mm^2) at 150 degrees peel angle.**

Figure 3.6a showed the absolute value of peel off forces for all the samples having square shape fibrils. The large standard deviation was a result of very different peel off forces in the 3 rows of caps as explained previously (Figure 3.5). The adhesion forces increased significantly from samples having *space 1* to samples having *space 2* configurations. This adhesion enhancement was less obvious than the adhesion force increase from samples having *space 2* to *space 3*. In order to better investigate the peel strength regardless of the adhesive width, Figure 3.6b presented the adhesion force divided by the cap edge length as the y axis. Results showed that the 0.03" and 0.04" fibril widths perform best on samples having *space 2* configurations, and samples having fibril width of 0.06" perform best in the *space 1* configuration. Increase of adhesion among the samples having the same space configuration is also observed in Figure 3.6. This increase of adhesion force can be explained from the stiffness of fibrils calculation from the previous section. The stiffness of fibrils is direct proportional to the cross sectional area of the fibrils. This result is demonstrated in *space 1* and *3*, but not in *space 2*. This phenomenon may be explained from the preloading process.

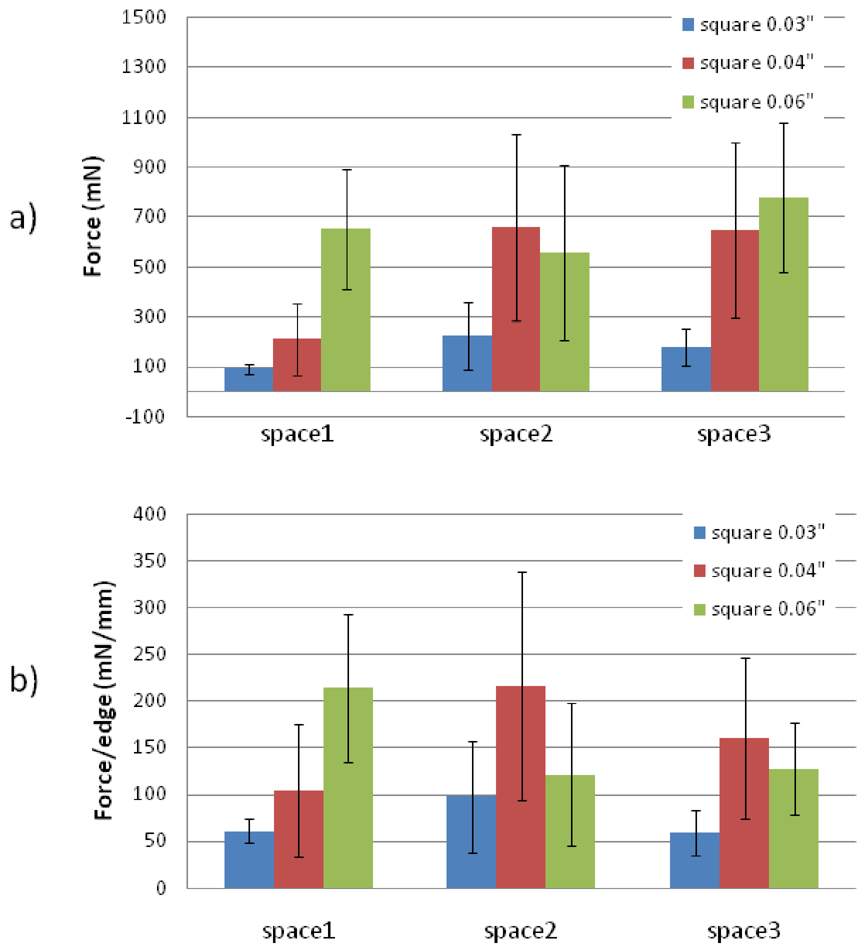

Figure 3.6. **Adhesion force measured using samples having square shape fibrils at 150 degrees peel angle: a) adhesion forces represented by absolute peel off forces; b) adhesion forces represented by peel off force divided by the cap edge lengths.**

Figure 3.7 showed the schematics representing different interacting situations, which could justify the behaviour of the adhesive reported in Figure 3.6. Specifically, Figure 3.7a illustrated the buckling problem caused by slim post and big flat cap under excessive preloading forces. The bending moment of a fibril is calculated from the bending curvature multiplied by the bending stiffness, when the bending stiffness is direct proportional to the fibril width as calculated in Section 3.3.2. The slimmer the fibril was, the easier it was for the fibril to be bent by a preload. The bending moment is transferred to the thin cap layer resulting in uneven forces across the thin cap layer. This uneven force across the thin cap layer increases the probability of contact area reduction within the cap layer. In order to prevent this buckling problem, the fibril size cannot be too slim. On the other hand, the fibril being too thick reduces the flexibility (or increases the stiffness) at pull off. Fibril length of 0.06” having space 2 configurations might have this preloading problem which caused the measured adhesion drop. Figure 3.6b showed that the 0.04” fibril width performs best in the peel tests on average.

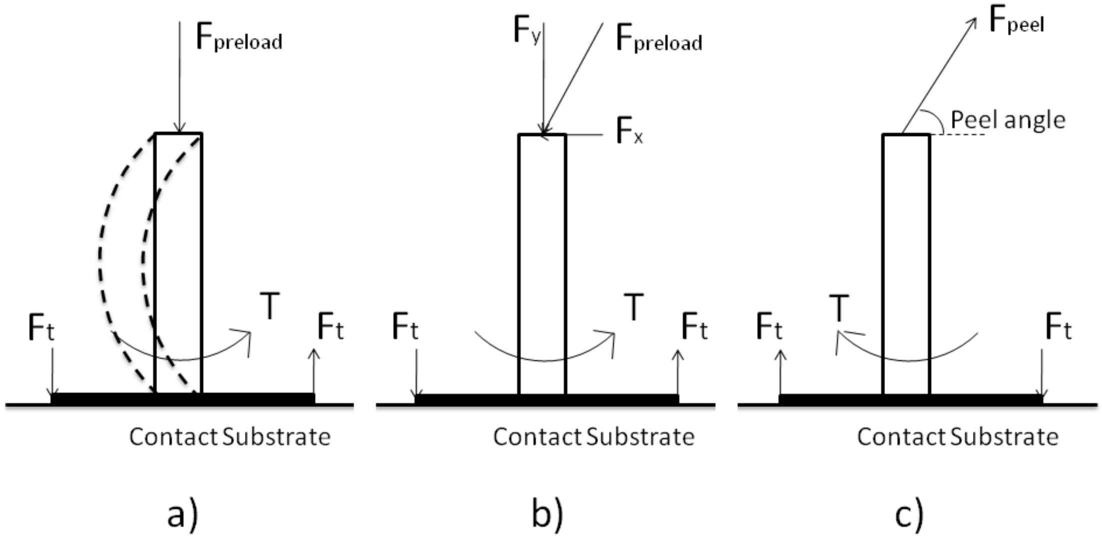

Figure 3.7. Schematics of different loading and peeling conditions. a) Buckling problem due to excessive preload applied on a slim post; b) non-ideal preloading situation due to an off-axial preload; c) influence of peel angle appeared at the edge of cap layer.

The cap size is another element to influence adhesion. Regardless of the fibril width, Figure 3.7b shows the situation of a non-ideal preload. With a larger cap size (e.g. with *space 3* times the post size), the thin caps can easily overlap with adjacent caps, resulting in a decreased overall contact area. With a smaller cap size (e.g. with *space 1* time the post size) small unconventional loads on the cap could easily peel the edge of the thin cap off the substrate. The cap size in *space 2* had generally demonstrated better adhesion performance in the peel tests.

Comparing the peel test results of different fibril shapes, the conclusion gained from the square fibrils was reinforced (Figure 3.8). Generally, *space 2* performed better than *space 3* for the cap size, and square fibrils perform better than slimmer circle and star shape fibrils. The square shape fibrils have the highest bending stiffness among the three shapes; therefore they were rigid enough to adequately preload the full caps. The square shape fibrils were also the least flexible, which is represented by the highest stiffness about the axial loading at pull off process. Hence the square shape fibrils outperformed the circular and star shape fibrils in the peel tests. As a conclusion of the peel tests, the best fibril design appeared to be the sample having fibril width of 0.04” with square shape fibrils and cap size of 2 times fibril width.

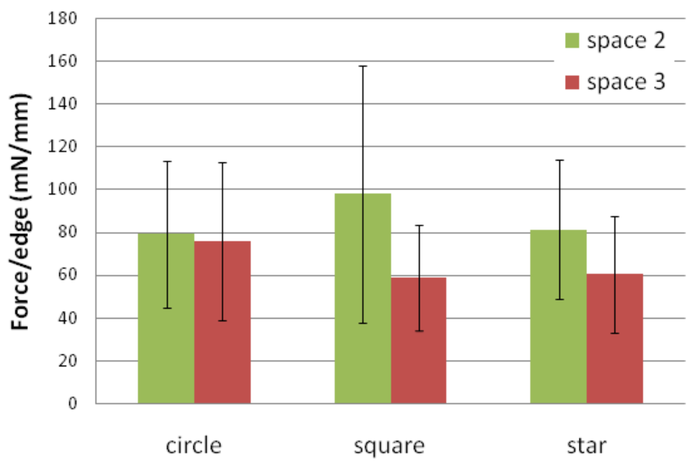

Figure 3.8. Peel test results at 150 degrees peel angle with different post shapes.

We performed additional tests by decreasing the PMMA slope, thus changing the peel angle. Figure 3.9 illustrates the test performed using samples having fibril width of 0.03” in circle shape, and showed that adhesion forces increased with peel angle decrease. The reason for this phenomenon was that a smaller peel angle imposed less torque on the macro-size fibrils, as Figure 3.7c illustrated. With a constant peel off force applied at the same post, the adhesive was more difficult to pull off with a lower peel angle. This trend led to the peel tests at a much lower peel angle which will be described in the next section.

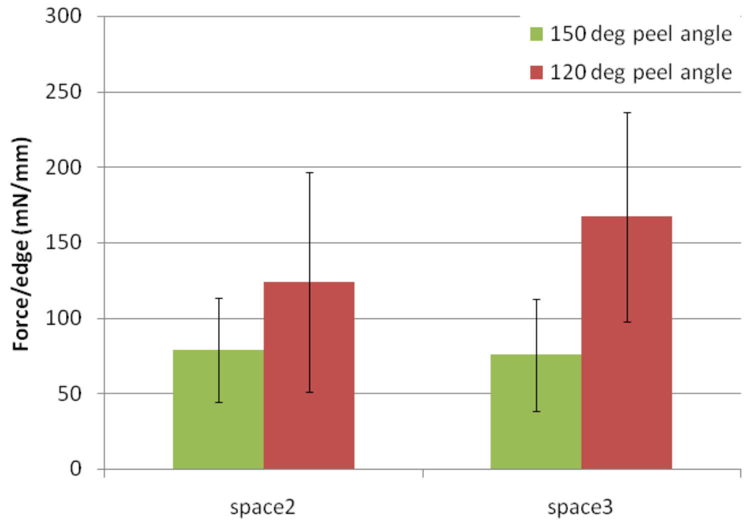

Figure 3.9. Peel test results of two peel angles larger than 90 degrees.

3.4.2. Peel test with peel angle smaller than 90 degrees

Figure 3.10 showed the typical force curve of a peel test having an initial peel angle of 30 degrees on a sample having 0.04” square fibrils with *space 2*, which was the same sample used in the tests of Figure 3.5. Different from the peel test using high peel angle, all the caps on the sample lost adhesion from the substrate at the same time. The pull off forces were therefore generally higher than in the case of tests using high peel angle.

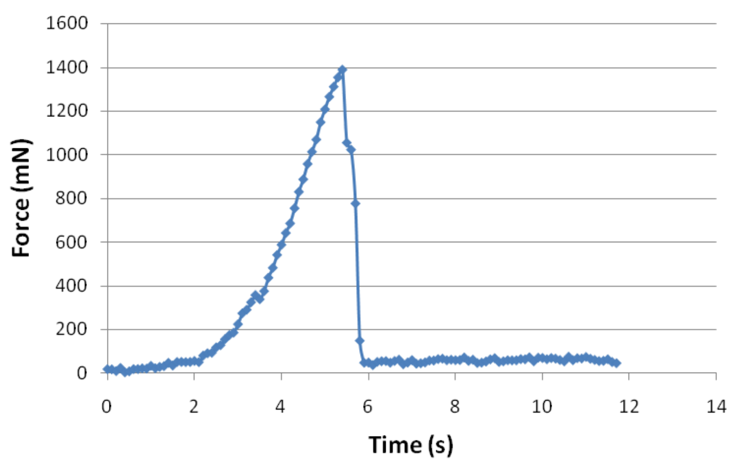

Figure 3.10. Typical force curve of a peel test at peel angle of 30 degrees.

Figure 3.11a showed the absolute value of pull off forces for all the samples of square shape fibrils. The pull off forces increased with the adhesion area increase. The same increasing trend was observed as with the tests using high peel angle. The force was then divided by the length of cap edge to reveal the fibril size and shape as well as the cap size's influence on adhesion performance (Figure 3.11b). The best performing sample had relatively stiff fibrils with close spacing, which is believed to equally load the full areas of the adhesive with a specific pulling direction. As fibril distance and cap size increased, the adhesion strength decreased due to uneven pulling forces distributed among fibrils and also within the caps.

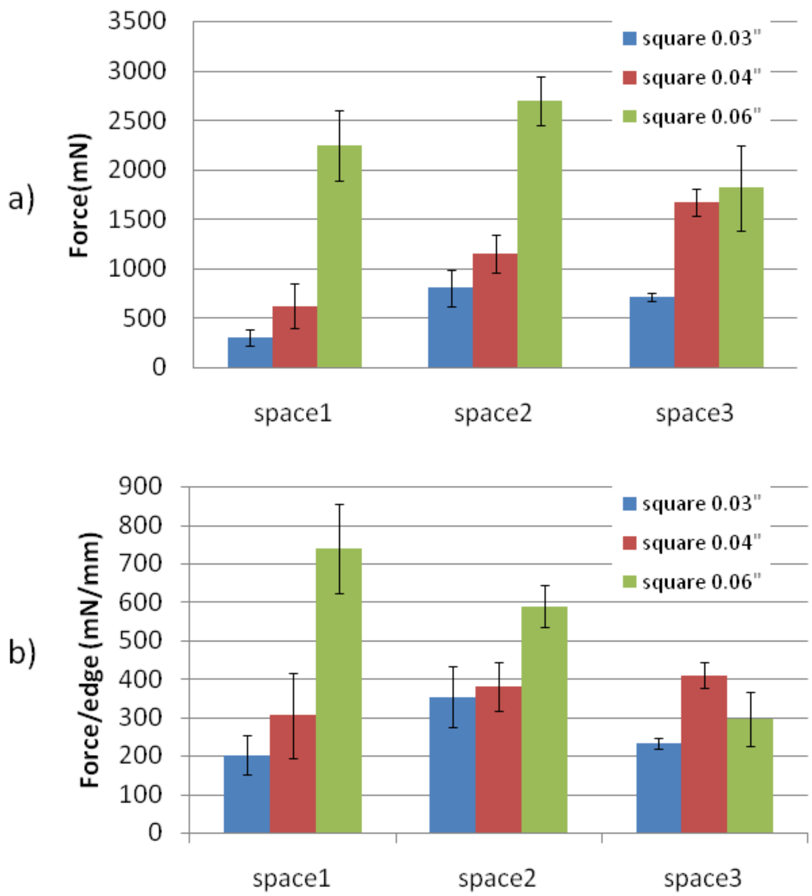

Figure 3.11. **Square samples test at 30 degrees peel angle: a) adhesion forces represented using absolute pull off force; b) adhesion forces represented using pull off force divided by the length of the cap edge.**

Figure 3.12 showed the peel test results comparing samples having different shapes at a smaller peel angle. The result was very similar to that of the peel tests using high peel angles, due to the same buckling problem described above (slim fibrils result in uneven distribution of loads across the cap layer). *Space 2* generally demonstrated stronger adhesion because the close adjacent fibrils can help resist higher pull off force. On the other hand, if the fibrils were too close, overlapping cap layer could be an issue. In conclusion from the peel tests, smaller fibril space and thicker fibril size increased the adhesion strength in a dual-level adhesive design. Fibril sizes that are too slim may be the cause of the buckling problem. The best performing structure among all the samples that were tested for the peel strength was the fibril width of 0.06” having square fibril shape and space of 1 time the fibril width.

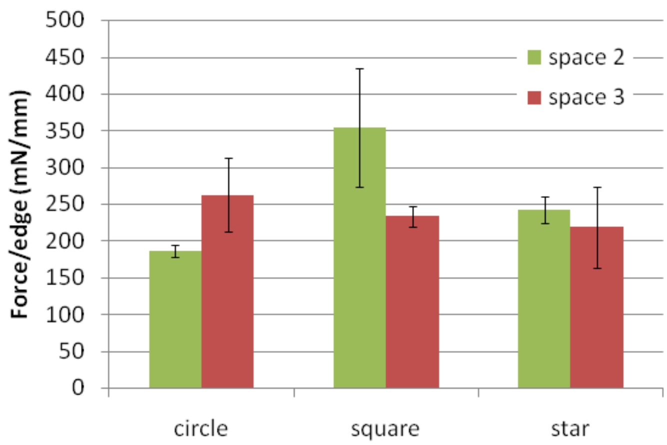

Figure 3.12. Peel tests at 30 degrees peel angle with different post shapes.

3.4.3. Comparison between single and dual level adhesives

The dual level adhesive was compared with the single layer adhesive on their peel strength at 150 and 30 degrees of peel angle. The dual level adhesive used for the comparison was the sample having a fibril width of 0.04” and square fibril shape and space of 2 times the fibril width. Figure 3.13 showed that the dual level adhesive significantly increases the peel strength at high peel angle, although the peel strength at low peel angle was weakened to as much as two thirds of the peel strength for single level adhesive. The reduction in peel strength at the low peel angle was primarily attributed to the separated caps on macro-fibrils, which reduced the length of crack initiation. Improved performance of dual level adhesive at high peeling angle was attributed to the axial loads on the stem of macro-scale fibrils, which absorbed the pull off forces for extension and deformation of the macro-fibrils.

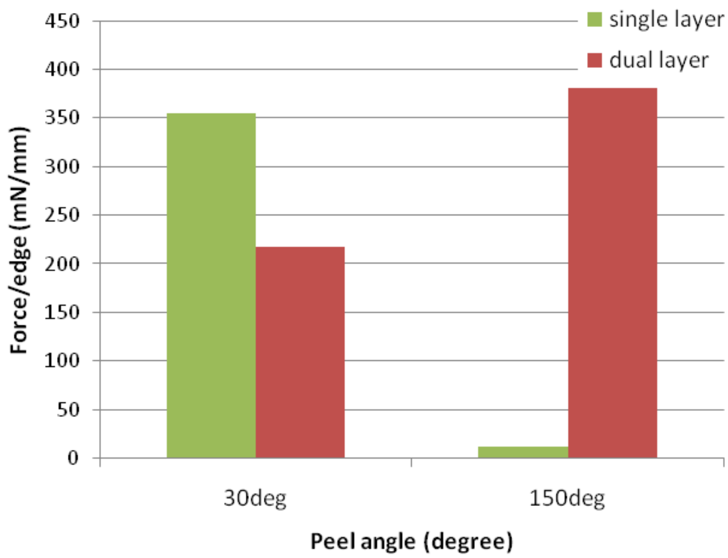

Figure 3.13. Peel strengths at two different peel angles for single and dual level adhesives.

3.5. Conclusions

In this chapter, we proposed a fabrication method for a dual-level adhesive design using PDMS. In order to identify the parameters which maximize adhesion performance, thirteen variations of the design with different cap size, shape, as well as macro-fibrils were tested for peel strength at different peel angles. Experimental results revealed the relationship between adhesion performance and the macro-scale mushroom structure designs, under different loading conditions. The overall result showed that the dual level adhesive improved the peel strength at high peel angle with respect to single level adhesive, but at small peel angle the dual level adhesive was more vulnerable to torques applied on the macro-size fibrils induced by tangential components of the loads. The improvement of peel strengths in the dual level adhesive could potentially make the adhesive comply with rough surfaces and resist loading from different directions without easily detaching in particular orientations. Our work indicates that proper design of each hierarchical level of fibrillar adhesive need careful consideration to maximize adhesion performance under a variety of loading conditions.

3.6. Acknowledgments

We would like to acknowledge the assistance of Simran Sirai and Zeeshan Khokhar with the development of the force testing system, and Ben Chang for his assistance in laser cutting. Financial support was provided by the Natural Sciences and Engineering Research Council of Canada (NSERC) and the European Space Agency (ESA).

3.7. References

[1] K. Autumn, M. Sitti, Y. A. Liang, A. M. Peattle, W. R. Hansen, S. Sponberg, T. W. Kenny, R. Fearing, J. N. Israelachvili, R. J. Full, *Proc. Natl. Acad. Sci. U.S.A* **2002**, *99*, 12252-12256.

[2] A. K. Geim, S. V. Dubonos, I. V. Grigorieva, K. S. Novoselov, A. A. Zhukov, S. Y. Shapoval, *Nat. Mater.* **2003**, *2*, 461-463.

[3] N. J. Glassmaker, A. Jagota, C.-Y. Hui, J. Kim*, J. R. Soc. Interface* **2004**, *1*, 23-33.

[4] D. Sameoto, Y. Li, C. Menon, *Advances in Science and Technology* **2008**, *54*, 439-444.

[5] S. Kim, M. Sitti*, Appl. Phys. Lett.* **2006**, *89*, 261911.

[6] M.P. Murphy, B. Aksak, M. Sitti, *Small* **2009**, *5*, 170-175.

[7] D. Sameoto, C. Menon, *J. Micromech. Microeng.* **2009***, 19*,115002.

[8] M.P. Murphy, S. Kim, M. Sitti, *ACS Appl. Mater. Interfaces* **2009**, *1*, 849-855.

[9] J. Lee, B. Bush, R. Maboudian, R.S. Fearing, *Langmuir* **2009**, *25*, 12449-12453.

[10] A. Asbeck, S. Dastoor, A. Parness, L. Fullerton, N. Esparza, D. Soto, B. Heyneman, M. Cutkosky, in proceedings of IEEE Int. Conf. Robotics and Automation, Kobe, Japan, 12-17 May **2009,** pp. 2675-2680.

[11] Dow Corning Corporation, Sylgard® 184 Silicone Elastromer Kit, [Online] Sept 2nd 2014, URL: http://www.dowcorning.com/applications/search/products/details.aspx?prod=01064291.

[12] D. Sameoto, C. Menon, *Smart Mater. Struct.* **2010**, *19*, 103001.

[13] R. K. Shukla, A. Srivastava, Mechanics, New Age International, Daryaganj, Delhi, IND. Available from: ProQuest ebrary. [16 December 2014].

Chapter 4.

Replica molding for low cost and high yield fabrication of nano-fibrillar adhesive using desired material

Having proven the advantage of the hierarchical fibrillar structure, a smaller scale of hierarchical fibrillar adhesive should be the next step to investigate. Fabrication of nano-fibrillar arrays, in literature, usually was a cost consuming procedure and limited to certain construction material. With these limitations, procedures implanting nano-fibrils on top of micro-fibrils are complicated and expensive. In this chapter, a low cost and high yield fabrication procedure for nano-fibrillar arrays is introduced, with the advantage of freedom to choose various construction materials. The procedure made use of a replica molding method and allow highly reproducible polymeric nano-fibrillar arrays. Since the construction material is polymer, binding of nano-size and micro-size fibrils can be easily realized by applying another layer of same polymer as binding interface. This chapter aimed at achieving OBJECTIVE 2. The following contents are published in paper: Yasong Li, Him Wai Ng, Byron D. Gates and Carlo Menon, "Material versatility using replica molding for large-scale fabrication of high aspect-ratio, high density arrays of nano-pillars" in *Nanotechnology*, 2014, *vol. 25*, 285303.

4.1. Abstract

Arrays of high aspect-ratio nano-pillars have attracted a broad interest for various applications, such as for use in solar cells, surface acoustic sensors, tissue engineering, bio-inspired adhesives and anti-reflective surfaces. Each application may require a different structural material, which can vary in the required chemical composition and mechanical properties. In this chapter, a low cost fabrication procedure is proposed for

large scale, high aspect-ratio and high density arrays of nano-pillars. The proposed method enables the replication of a master with high fidelity, using the subsequent replica molds multiple times, and preparing arrays of nano-pillars in a variety of different materials. As an example applied to bio-inspired dry adhesion, polymeric arrays of nano-pillars are prepared in this work. Thermoset and thermoplastic nano-pillar arrays are examined using an atomic force microscope to assess their adhesion strength and its uniformity. Results indicate the proposed method is robust and can be used to reliably prepare nano-structures with a high aspect-ratio.

4.2. Introduction

The advancement of innovative fabrication technologies, such as electron beam lithography (EBL) [1-3], nano-imprint lithography (NIL) [4-6], and deep reactive ion etching (DRIE) [7], have enabled the development of a large number of novel nano-structured devices. Arrays of high aspect-ratio (AR) pillars continue to receive widespread interest among many nano-structured devices. Applications include solar cells [8-9], surface acoustic sensors [10-11], structural frames for tissue engineering [12], anti-reflective instruments [13], super-hydrophobic surfaces [14], and bio-inspired dry adhesives [15-17]. While the topographic profile of these nano-structured devices is very similar, their materials are rather diverse. For example, solar cells use semiconducting materials [8-9], and acoustic wave resonance sensors are constructed from metals and piezoelectric materials [10-11], and anti-reflective devices usually utilize transparent plastics [13]. On the other hand, bio-inspired dry adhesives [15], cell growing beds [18-19], microfluidic devices [20], and super-hydrophobic self-cleaning surfaces [21] are often prepared using a variety of polymers. The development of a novel manufacturing method that could enable the reproduction of the same pattern using a variety of different materials would be desirable. This work aims to widen the choice of materials we are able to replicate using the same soft mold, which would lower the overall cost of fabricating large scale arrays of high AR nano-pillars.

The fabrication of arrays of high AR nano-pillars is generally expensive as it involves the use of sophisticated masks and expensive equipment and instrument setup, which very often have a low throughput. For example, minimum feature size is limited by the wavelength of light used in traditional photolithography processes and, therefore, the use of more sophisticated equipment is required to achieve smaller dimensions [22]. Alternatively, EBL and focused ion beam (FIB) lithography that can create nano-scale features require a relatively long time for direct writing into photoresist or other materials of interest [1-3, 23]. Nano-imprint lithography can greatly reduce the cost of making replicas, but fabricating the silicon masters still requires the use of EBL or FIB processes with a high overall cost to prepare the templates [4-6]. Colloidal masks [24-25] prepared from the self-assembly of polymer beads can facilitate control over both feature size and coverage of large areas, but the precise control over the uniformity in the single layer polymer beads can be a challenge during fabrication. A method that may reduce the time and cost of fabricating arrays of nano-pillars could rely on the use of nano-templates, such as polycarbonate (PC) membranes. However, the pores in PC membranes lack the necessary periodicity to be suitable for creating uniformly distributed nano-pillars [26].

An alternative solution is to use anodic aluminum oxide (AAO) membranes as nano-templates. Membranes of AAO formed by a two-step anodization have been pursued for replication of nano-pillars as they have highly ordered arrays of hexagonal cells, each with a cylindrical pore that can span the entire substrate [27-30]. Pore periodicity, density and diameter—usually down to a hundred nanometers or less—can be finely controlled by the choice of acid and anodization voltage. The fabrication of this type of nano-structure is well established and large sheets of AAO membranes are available by either preparation in the laboratory or from commercial suppliers. The highly uniform membranes of regular nano-sized holes have attracted a large interest as suitable for use as templates to fabricate arrays of pillars [31-43].

Various methods can be used to fill material the array of voids within an AAO nano-template. These methods include atomic layer deposition (ALD), which can grow metal or oxide pillars in the AAO template [31-33]. Another method is electroplating that can deposit various metals in the pores followed by release of the metal nano-wires from the template [34-35]. Chemical vapor deposition (CVD) can grow carbon nanotubes inside the template and can form a uniform nano-forest [36-37]. Hot embossing can be used to fill in the AAO template with thermo-plastic materials [38-44]. Among these methods, hot embossing appears to be an advantageous method to fabricate polymeric pillar arrays. By finely controlling the temperature and pressure of the hot embossing process, Teflon® [39], poly (methyl methacrylate) (PMMA) [40], UV curable polymers [41], polypropylene [42], polyimide [43] and polycarbonate (PC) [44] pillared arrays can be prepared with a range of desired diameters and aspect-ratios for various applications.

In this work, we report a replica molding method based on hot embossing that enables the preparation of arrays of nano-posts from different materials. The use of different materials is a key aspect of this work in order to satisfy the needs of multiple applications [8-21] and also enables the ability to experimentally assess the advantages that specific materials can provide. The method proposed herein shows the feasibility of manufacturing high AR (approximately 25) arrays of nano-pillars (diameter from 200 nm and below) covering large surfaces. One of its specific features is that the proposed method yields high AR nano-pillars that do not collapse, a primary drawback of most manufacturing processes proposed in the literature [38-44]. Another specific feature is that the process does not require the use of clean-room facilities, which drastically reduces the cost related to the required infrastructure. The proposed process enables the control of both diameter and length of the pillars by opportunely selecting the appropriate nano-template and processing conditions.

4.3. Sample preparation and evaluation methods

There are mainly three steps for the replication process proposed in this work. First, the thermoplastic pillars are fabricated through a hot embossing process. Second, the polydimethylsiloxane (PDMS) negative replica is cast from the polymeric pillars. Last, other materials, such as thermoset plastics, are cast against the negative PDMS replica containing arrays of holes to prepare the positive replica. By the end of the process, these thermoset plastics have features with the same shape and dimensions as the initial thermoplastic pillars. The overall process is illustrated in Figure 4.1.

4.3.1. Fabrication of arrays of nano-pillars in PMMA using AAO

Arrays of thermoplastic pillars were obtained from the AAO template during the first fabrication step, as shown in Figure 4.1a. Specifically, a commercially available AAO membrane (Whatman© Anopore™ inorganic membrane, Anodisc™ 25) was used in this work. PMMA (OPTIX® acrylic) was selected as the thermoplastic test substrate because of its low glass transition temperature (105 °C), low refractive index (1.49) and high elastic modulus (3.37 GPa) [45], which reduces the possibility of the pillars collapsing upon release from the mold. A 1 mm thick PMMA sheet was initially cut into 25 x 25 mm^2 pieces using a CO_2 laser cutter (VLS3.60, Universal Laser Systems) to cover the circular AAO membrane, which had a 21 mm diameter. A hot embossing setup was prepared in the laboratory. The setup included a hot plate (HS40A, Torrey Pines Scientific), two glass slides (Corning® Glass Slides, 75 x 50 mm^2) used as backing layers to sandwich the AAO template and the PMMA substrate, and a 1 liter volume glass beaker, which was used to provide the necessary embossing pressures.

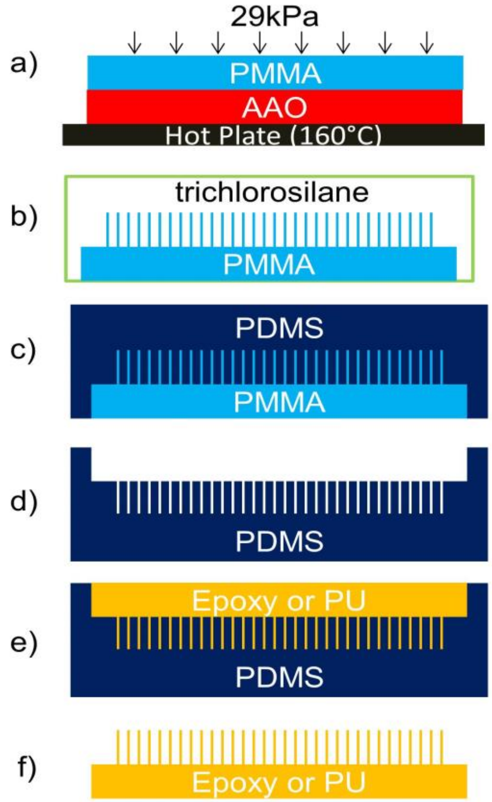

Figure 4.1. Overall fabrication process to demonstrate material versatility using replica molding of nano-fibrillar arrays: a) thermoplastic PMMA was initially embossed with an anodic aluminum oxide (AAO) template at 160 °C under 29 kPa pressure; b) a silanization procedure created a release layer for the subsequent molding steps; c) PDMS precursors were cast against the PMMA fibrillar structure and cured; d) PDMS negative mold was released from the PMMA master; e) epoxy was cast and thermally cured against the PDMS mold containing an array of holes; f) epoxy replica was released from the PDMS mold, having same shape and dimensions of the arrays of PMMA pillars.

The following three parameters were fine-tuned to achieve the desired aspect-ratio of the nano-pillars: i) pressure; ii) temperature; and iii) embossing time. The beaker was filled with up to one liter of water to provide ~10 N embossing force. This load was applied over a 346 mm^2 area, yielding a 29 kPa embossing pressure. The load was applied while the PMMA substrate was heated to just above its melting temperature (148-157 °C [45]). Specifically, it was experimentally determined that 160 °C for the embossing temperature under the 29 kPa load formed a low AR nano-structure in about

15 min. It should be noted that this embossing time does not include the ramp up of the hot plate, which had a maximum ramp rate of 450 °C/hr.

Following the hot embossing process, the samples were cooled without any added pressure until reaching room temperature. Mold release was achieved by etching the AAO template in a NaOH (3 M) solution for ~15 minutes. The samples were subsequently washed with deionized water and dried under a stream of N_2 gas.

This first fabrication step yielded positive PMMA molds having arrays of nano-posts. Different aspect-ratios of the nano-posts were obtained by varying the embossing time, while keeping pressure and temperature at 29 kPa and 160 °C, respectively.

4.3.2. Fabrication of arrays of nano-holes in PDMS

A negative mold was obtained by casting PDMS (Sylgard 184, Dow Corning) against the arrays of PMMA nano-pillars. To ensure mold integrity after demolding, a release layer was applied to guarantee proper mold release (Figure 4.1b). A solution phase silanization process was used to deposit this release layer onto the surfaces of the nano-pillars. The PMMA nano-structured sample was placed in an air based plasma (PDC-001, Harrick plasma) at a pressure of ~0.3 Torr for 1 min at 10.7 W to activate the surfaces. The sample was subsequently placed into a flask containing 50 mL hexanes (ACS reagent grade, 98.5%) and 200 μL of silane (1H, 1H, 2H, 2H – perfluorodecyldimethylchlorosilane, Alfa Aesar, >90%) heated to 80 °C in an oil bath for 3 h. The sample was rinsed by immersion in a fresh solution of hexanes and dried under a N2 gas stream after being retrieved from the solution. Part A and B precursors to the PDMS were mixed in a 10:1 (w/w) ratio, respectively, and poured in a petri dish containing the silanized PMMA sample (Figure 4.1c). The petri dish was subsequently placed in a vacuum chamber in order to degas the sample for 30 min. After degassing, the sample was left to cure at room temperature for 24 h. After curing, the PDMS was peeled away from the petri dish to obtain the negative mold (Figure 4.1d). This PDMS mold was used for subsequently casting arrays of nano-pillars from different materials.

4.3.3. Replication of nano-pillar arrays

In order to demonstrate the proposed process for enabling the fabrication of arrays of nano-pillars in different materials, replicas were prepared using two different polymers: i) polyurethane (V-825, BJB enterprise); and ii) epoxy (TC-1622, BJB enterprise). The polyurethane had a shorter curing time (6-8 min working time before reaching its gel point) than the epoxy (with a 2 h working time). The Young's modulus of the polyurethane and epoxy were 2.3 GPa and 2.2 GPa, respectively. Both polymers were mixed from two initial components and subsequently poured over the negative replica or PDMS mold. The samples were degassed in a vacuum chamber and cured at room temperature (Figure 4.1e). Replicas of the cured polymer were subsequently peeled away from the PDMS mold to obtain arrays of nano-pillars (Figure 4.1f).

4.3.4. Evaluation of quality of the mold and replica

The geometry of the molds and replicas were examined using a scanning electron microscope (SEM) (Strata DB-235 and Nova NanoSEM 430, FEI). Static water contact angle (WCA) measurements (OCA 15, Dataphysics) were conducted to assess the quality of the various surfaces. In these measurements, the volume of the water droplet was set to 0.5 μL. An average contact angle measurement was obtained from 10 independent measurements for each sample from different locations. To demonstrate their potential for use in applications, polymeric arrays of nano-pillars were tested for their adhesion force using an atomic force microscope (AFM, MFP-3D-SA, Asylum Research). A silicon nitride cantilever (NP-O10, Bruker) without a sharp tip was employed in the adhesion measurements, which have been determined to be suitable for evaluating the adhesion properties of the arrays of nano-pillars [46]. To dissipate the surface static charges during these measurements due to the dielectric properties of the polymers, the edges of the samples were painted with silver paste and connected to a conductive wire that was fixed to the metallic surfaces of the AFM acoustic isolation chamber.

4.4. Results and Discussion

4.4.1. Properties of arrays of PMMA nano-pillars

In order to obtain nano-pillars of PMMA with different aspect-ratios, a range of embossing times were selected for the process. Figure 4.2 shows typical SEM images of the top view of the arrays of nano-pillars obtained using 1 and 2 h of embossing time. The PMMA samples that underwent 1 h of embossing did not exhibit significant collapse of the nano-pillars (Figure 4.2a), but pillars from samples embossed for 2 h collapsed as they were too tall to withstand lateral adhesion forces exerted by nearby pillars (Figure 4.2b).

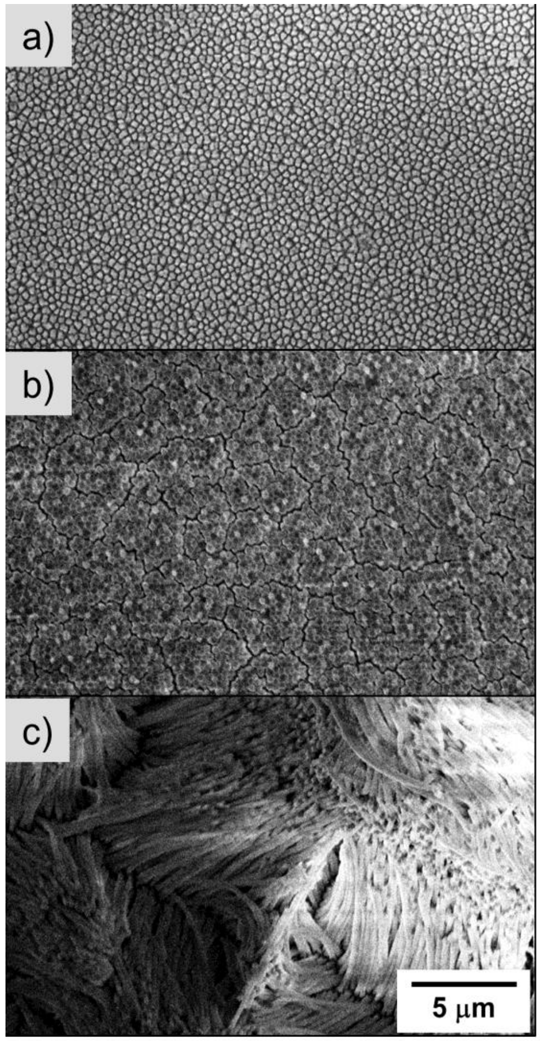

Figure 4.2. Scanning electron microscopy (SEM) images of the PMMA nano-pillar samples after various embossing times; a) sample prepared by 1 h of embossing; b) sample prepared by 2 h of embossing; c) sample prepared by 1 h of embossing and subsequently treated with Zonyl, which collapsed the pillars and exposed their lengths. All images were obtained at under the same magnification.

The AAO membrane used in the experiments had a thickness of 60 μm, a pore size of 200 nm and pore density of 10^9 pores/cm^2 [47]. The space between the individual PMMA nano-posts, prepared by the embossing process was very small (~50 nm averagely) due to the geometry of the selected AAO membrane. The pores in this template also did not have a very regular pattern or individual shape. The resulting PMMA pillars, therefore, each had a relatively irregular cross-section as shown in Figure 4.2. It should, however, be noted that the pore size, pore density and the overall membrane size could be further controlled by customizing the anodizing process [27-30]. Nano-posts having different diameters, spacing between pillars, and improved symmetry could potentially be obtained by fabricating a customized AAO membrane.

To estimate the aspect-ratio of the nano-pillars, a cross sectional view of the fabricated PMMA samples is desirable. However, these acrylate samples were difficult to cut through without damaging the nanoscale-features using traditional equipment, such as milling machines, focused ion beams or laser cutters. A fluorinated solvent was used to intentionally collapse the slender pillars and an SEM image obtained to estimate their height (Figure 4.2c). From the top view of the bent pillars, the average length was estimated to be 5 μm for samples that underwent 1 h embossing time. The aspect-ratio of this sample was estimated to be 25, which greatly exceeds the requirements of most applications mentioned previously.

In the experiments to obtain nano-pillars in different aspect ratios, we chose to vary embossing time while fixing the embossing pressure and temperature. Other approaches to prepare the arrays of nano-pillars could vary the pressure with a fixed embossing time and temperature, or vary temperature with a fixed embossing time and pressure. Any of these methods could be used to calibrate a fabrication process to accurately prepare nano-pillars of specific aspect ratios, once a best method is established to overcome the intrinsic difficulties of systematically and accurately determining the aspect ratio of the nano-pillars.

Figure 4.3a shows an optical image of the sample containing PMMA nano-pillars, which were obtained from a one hour embossing time. This nano-structured PMMA sample preserved most of the transparency of the original PMMA material because the array of nano-pillars remained upright without collapsing upon release from the AAO mold. The outline of a circular shape in Figure 4.3a indicates the boundary of the deformed PMMA surfaces that were in contact with the 21 mm diameter polypropylene ring that protected the rim of the brittle AAO commercial membrane. On the other hand, the PMMA samples that underwent a two hour embossing process appeared to have a foggy gray coloration (Figure 3b). This color change was due to the formation of collapsed posts that reduced transparency of the sample.

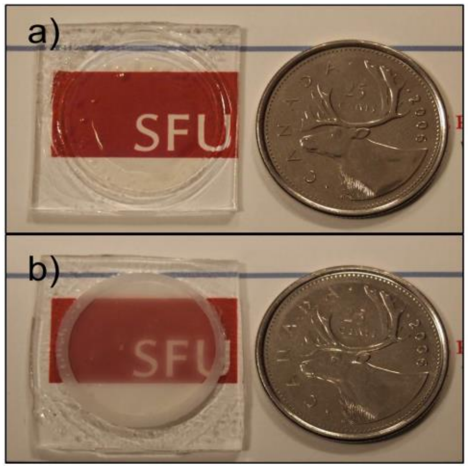

Figure 4.3. **Samples of PMMA nano-pillars placed on top of the SFU logo with a C$ 0.25 coin placed next to the sample to indicate the scale: a) sample prepared by 1 h of embossing; b) sample prepared by 2 h of embossing.**

Figure 4.3 also shows that the entire embossed area was roughly the size of a C$ 0.25 coin. This large nano-patterned area was prepared using a single embossing stamp, indicating that the proposed process, which required very affordable fabrication equipment, could potentially provide a high yield manufacturing process.

4.4.2. Release layer and mold release

A soft polymer was selected to obtain a negative mold from the PMMA positive mold in order to retain the integrity of the PMMA template after demolding. PDMS was chosen for its low viscosity and low surface energy, which facilitated the mold filling and mold releasing processes. However, directly casting PDMS and peeling it away from the very high aspect-ratio PMMA nano-structures could have damaged the PDMS sample due to the low tear strength of PDMS. A release layer of perflouroalkylsilane molecules was applied to the PMMA samples prior to casting PDMS. Specifically, a solution phase silane deposition process was used to ensure the molecules could reach deep into the trenches of the high AR nano-pillars. Unlike traditional release layers, such as polyvinyl alcohol (PVA) or silicon oil, that are usually applied using spin coating, the perfluoroalkylsilane molecules can coat the surfaces of the nano-pillars using either a gas or solution based medium. These molecules form a thin layer that protects and alters the surface energy of the original mold during the demolding process. Solution based coating processes enable faster and more uniform transport of the silane molecule through the help of a solution media. PMMA is sensitive to a large variety of solvents, leaving few choices for the deposition media. Among this remaining list, hexanes were selected for dispersion of the perfluoroalkylsilane molecules during the deposition process. WCA measurements were performed on the samples nano-pillars after coating with the silane molecules to determine the quality of these coatings. Results and discussion of these WCA measurements are provided in further detailed in the supporting material.

Figure 4.4a shows SEM images of arrays containing PMMA nano-pillars after demolding of PDMS when the PMMA mold was not treated with the perfluoroalkylsilane release layer. Although PDMS is a material that is widely used in replica molding, we could only release a thin layer of PDMS from the PMMA pillars. The resulting PDMS negative replica had either no nano-holes or holes with a very low aspect-ratio, which were not suitable for subsequent replica molding processes. Figure 4.4b shows the PMMA sample after demolding of the PDMS when the PMMA was treated with a silane release layer before casting the PDMS. The aspect-ratio of the features in the resulting PDMS negative mold significantly increased following this treatment and facilitated the further use of the PDMS negative mold in subsequent molding steps of the process. However, this PDMS release layer was not perfect, as parts of the PDMS remained trapped deep within the trenches surrounding the PMMA nano-pillars. This phenomenon could be caused either by the very low tear strength of PDMS or by an incomplete coating with silane molecules, which may not cover all surfaces of the nano-pillars. Improvement of the silane treatment process would need to be addressed to enable further improvements in the quality of this replica molding method. An alternative method of silane deposition could be through the use of an atomic layer deposition process, but the appropriate equipment is necessary to perform these studies. Despite the presence of some defects, the PDMS samples were suitable for use as negative molds and enabled the preparation of arrays of high AR nano-pillars, as discussed in the following sections.

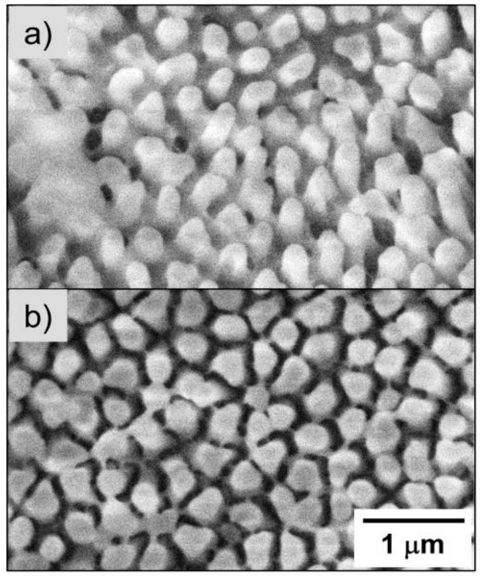

Figure 4.4. **SEM images of dense arrays of PMMA pillars after demolding of PDMS; a) arrays of PMMA pillars that did not utilize a release layer applid prior to casting PDMS; b) arrays of PMMA pillars with a release layer applied prior casting the PDMS. The two SEM images were taken at the same magnification.**

4.4.3. Positive replica using epoxy and polyurethane

Thermoset materials can be cast directly against the AAO template to form nano-pillars. This approach has been reported to have multiple drawbacks including a very limited control over length of the pillars and a subsequent collapse of these fibers [48]. In addition, obtaining the final nano-pillar arrays directly from the AAO membranes would require using one AAO template per casting, which makes the process very expensive for the fabrication of large quantities of nano-pillar containing arrays.

The use of replica molding was, therefore, selected to minimize the use of AAO membranes. Thermoset materials were cast against the PDMS negative molds to obtain the final arrays of nano-posts. Epoxy and polyurethane were both evaluated to prove the proposed method could be used to prepare nano-posts in substantially different materials.

Figure 4.5 shows SEM images of the fabricated epoxy (Figure 4.5b) and polyurethane (Figure 4.5c) nanostructures against the original arrays of PMMA nano-pillars (Figure 4.5a). It can be seen that the density of pillars decreased for both replicas. Aspect-ratio of both the epoxy and polyurethane based nano-pillars was about 5. The decrease of pillar density and aspect-ratio was primarily attributed to the well-known low wettability of PDMS [49]. The use of vacuum to improve the ability of epoxy or polyurethane to fill the PDMS nano-holes was unsuccessful, possibly due to nano-bubbles of trapped air residing in a large number of the nano-holes. The longer curing time of epoxy (24 h) with respect to polyurethane (~7 min to reach a very viscous phase) negligibly improved the density of the nano-pillars.

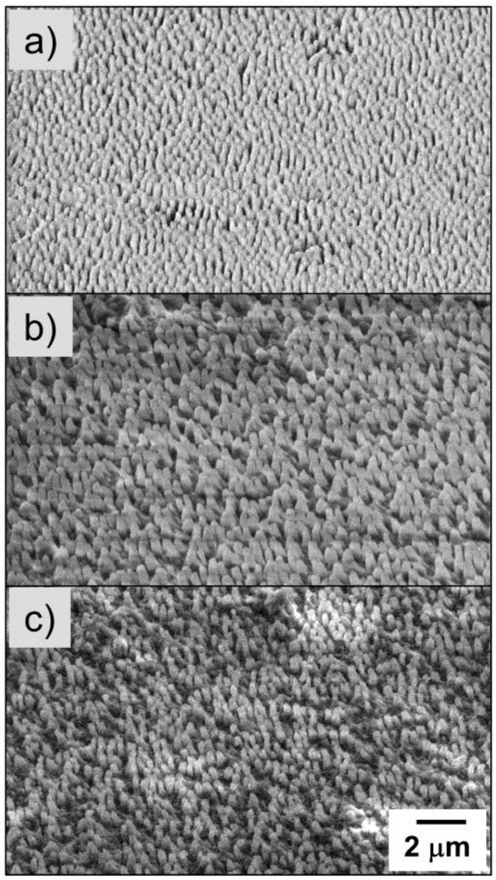

Figure 4.5. SEM images of the original dense arrays of PMMA nano-pillars (a), epoxy replica of these arrays (b) and a polyurethane replica of the arrays of nano-pillars (c). All of the images were taken at the same magnification and a 45° tilt.

Figure 4.5 also shows that the cross-sectional circumference of the thermoset pillars increased in comparison to the initial PMMA nano-pillars. This phenomenon was attributed to expansion of the nano-pillars during the elastomers' cross-linking phase, which was only partially constrained by the surrounding soft PDMS mold.

Despite these limitations, arrays of nano-pillars with an AR of 5 were reliably and repeatedly prepared from the same PDMS molds. It should be noted that an aspect-ratio of 5 is suitable for a large variety of applications [9-11, 13-17]. This final step of the process shows that the use of expensive AAO membranes can be limited to the initial fabrication of the PMMA positive molds, but can enable the preparation of a number of replicas from different materials.

4.4.4. Case study: a bio-inspired dry adhesive

As an example of a potential application, epoxy based arrays of nano-pillars were studied to assess their use as gecko-inspired dry adhesives. These nano-pillars of epoxy were compared to PMMA nano-pillars from the initial positive mold to demonstrate that an appropriate selection of material can increase the adhesion performance of these arrays.

A nanoscopically flat silicon nitride AFM cantilever was controlled to vertically approach the arrays of nano-pillars and stop after reaching a predetermined force. The AFM cantilever was subsequently vertically withdrawn until the fibers detached from the cantilever. This specific motion of the AFM cantilever has been proven to be particularly suitable for evaluating nano-structured gecko-inspired adhesives [46]. The adhesion force between the nano-pillar and the cantilever surface was calculated through deflection of the cantilever. The contact area between the cantilever and the nano-fibrils was estimated to be ~16 μm^2. In order to gather detailed information on the uniformity of the adhesion force for these surfaces, a program was written to automatically move the cantilever and repeat the aforementioned movements to acquire a large set of measurements over an array, as well as from different locations within the sample. Each unique position was separated by at least 1 μm. The adhesion forces were plotted in grey scale with a lateral offset of the data corresponding to the physical location where the measurements were performed on the sample in order to create a force map (Figure 4.6). The uniformity or variations in the adhesion forces across the sample can be easily visualized by examining the grey scale force maps obtained from different areas. Random patterns and trends in the measured adhesion forces within one force map indicate the anticipated variation for these measurements. The random variation in adhesion forces measured across a sample is the result of randomized test conditions, including a random numbers of pillars interacting with the AFM cantilever during each measurement and small variations in the aspect ratio of those pillars. On the other hand, a localized decrease in adhesion forces within the map indicates the possible presence of defects (e.g., missing fibers). Identification of these defects can help improve the fabrication process. By observing the trends in the appearance of the arrays of nano-pillars and the corresponding force map, the effect of variations in shape, size and density of these nano-pillars can be correlated to the resultant adhesion forces. This method also permits an automated collection of large sets of data, which enable a detailed statistical analysis of adhesion forces for samples in order to characterize their performance as a dry adhesive and the quality of the developed manufacturing process [46].

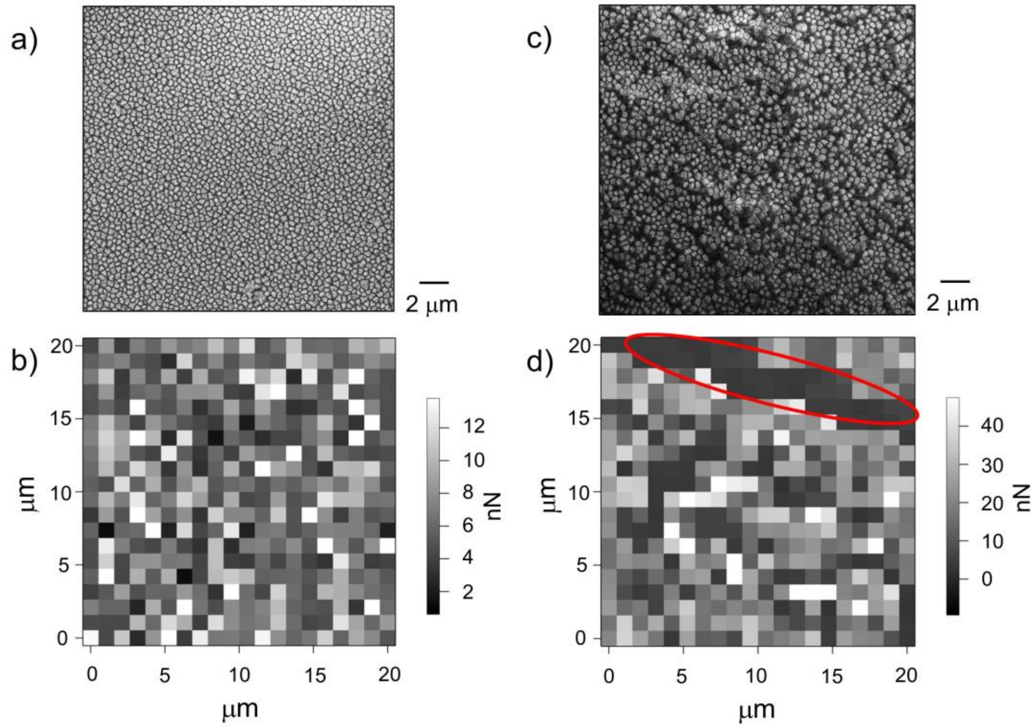

Figure 4.6. **(a) Representative SEM image of a sample containing an array of PMMA pillars whose adhesion forces were measured using an atomic force microscopy (AFM) based technique, and (b) the corresponding force map obtained from these measurements. Both the SEM and force map have the same lateral dimensions. (c) SEM image obtained from a representative region of an array of epoxy pillars whose adhesion forces were measured by an AFM based technique, and (d) a corresponding force map with the same lateral dimensions. All images correspond to an area of 20 x 20 μm^2. The red oval in (d) indicates a defect in the sample, possibly due to the partial collapse of neighboring nano-pillars or missing nano-pillars.**

Figure 4.6b shows the force map obtained from an array of PMMA nano-pillars, which was prepared by 1 h of hot embossing. An SEM image of the PMMA sample having the same magnification (20 x 20 μm^2) used to obtain the force map is provided in Figure 4.6a to facilitate the visualization of the area analyzed by the force map within the PMMA sample. It should be noted that the AFM and SEM images do not correspond to an identical region; these images were obtained from two unique regions of the sample, but with the same lateral dimensions. Subsequently testing the adhesion force of a region after imaging with an SEM was avoided as the focused electron beam modifies the surfaces and the geometrical features of the polymer.

The results plotted in Figure 4.6b indicate that the values of the measured force were random across the tested area without an apparent spatial trend. These results suggest there are small variations across the sample, but this trend in adhesion forces conforms to the variation anticipated for an array of nano-pillars as described above. The adhesion force measurements for the epoxy sample had a larger variation in measured values and in the force maps. For example, the region highlighted with the red oval in Figure 4.6d shows an area in which adhesion was low, presumably due to the presence of defects in the sample. These defects could be missing or collapsed pillars that reduced the contact area between the epoxy nano-pillars and the AFM cantilever resulting in a decrease in the measured adhesion forces. The PMMA nano-pillars had a better preservation of the original template geometry than the epoxy nano-pillars. The PMMA based pillars could be preferred for a range of optical and biological applications, while the epoxy nano-pillars could be more suitable for use as a dry adhesive.

Figure 4.7 shows histograms that summarized the force measurements acquired from the arrays of PMMA and epoxy nano-pillars. In addition, a third histogram was added for a PMMA sample that contains shorter pillars (0.5 h of hot embossing). All of the histograms were obtained by collecting force measurements from a large number of locations (400 points) in order to perform proper statistical analysis. The two histograms for the hot embossed PMMA contain a single peak while analysis of the epoxy replica contains multiple peaks spanning a much larger range of forces. The reason for this discrepancy is that the arrays of PMMA nano-pillars had a more uniform topography than that observed in the epoxy based samples (e.g., compare Figures 4.6a and 4.6c). The latter sample had a higher number of defects, such as missing pillars.

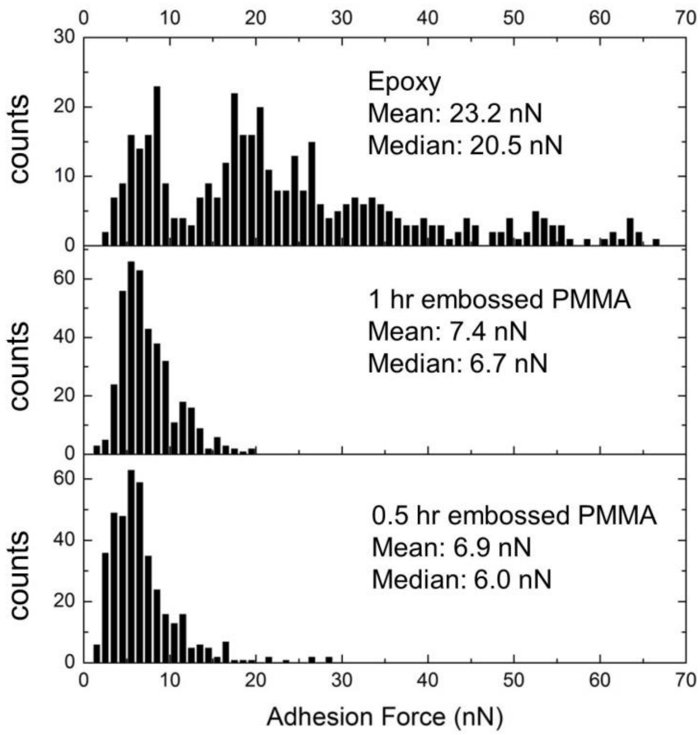

Figure 4.7. Histograms of the adhesion force measured for samples containing arrays of nano-pillars prepared from epoxy, as well as PMMA nano-pillars prepared using either 0.5 h or 1 h of hot embossing as indicated on these plots. These measurements were obtained using an atomic force microscope, a flat cantilever, and a set of customized software routines for manipulating the cantilever.

For the arrays of PMMA pillars, samples having shorter pillars (prepared using 0.5 h of embossing) induced a lower adhesion force than the taller pillars (from a 1 h embossing process). This difference is shown in both the mean and median of the histograms in Figure 4.7. The taller pillars may be able to provide a higher flexibility and ability to bend when the AFM cantilever was pressed against these structures. Bending of the pillars might have created an increased contact area between the sides of the pillars and the flat AFM cantilever. These interactions between the nano-structures and the AFM cantilever would correspond to a higher measured adhesive force. While statistically significant, the effect of the AR was not very noticeable; the variation in mean and median for the two PMMA samples was 7.2% and 11.7%, respectively. A much larger variation in the adhesion force was observed within the epoxy based samples. In fact, despite the decrease in pillar density and aspect-ratio, the measured adhesion for the epoxy samples was more than 3 times higher than that for the PMMA samples. This change was attributed to the higher surface energy of epoxy (44.5 mJ/m^2) with respect to PMMA (37.5 mJ/m^2) [50]. This increase of adhesion supports our conclusion that this method of replicating nano-pillars can be successfully utilized to select the most suitable material for a specific application, in this case the preparation of a biomimetic dry adhesive. It can be envisioned that future research on the preparation of complex structures will take advantage of this replica molding method.

The combined analysis of the adhesion maps and histograms (Figures 4.6 and 4.7) indicated the presence of defects in the epoxy-based samples and a consequent large variation in measured adhesion. It should, however, be noted that the presence of such localized defects is believed to not largely affect the macroscopic performance of the sample because the area occupied by these defects is very small in comparison to the overall surface area of the sample. In addition, a suitable preloading force applied to the sample can potentially create an improved contact with the shorter nano-pillars and, thus, improve the overall adhesion strength of the sample. Despite any possible influence of these defects, an investigation was performed to identify their potential sources. These sources included: 1) PDMS not properly demolding from the PMMA nano-pillars, resulting in a reduced AR and density of the nano-holes in the PDMS mold; 2) the epoxy might not have completely filled the PDMS nano-holes due to its low surface energy; and 3) the epoxy could not properly demold from the PDMS mold (epoxy nano-pillars could remain trapped in the PDMS nano-holes). Figures 4.2, 4.5, 4.6 and 4.7 each provide evidence that the replication process yielded an array of high quality nano-pillars with high adhesion properties, but future work will tackle the above-mentioned potential causes for defects in the replicated structures to improve the uniformity of the final arrays of nano-pillars.

4.5. Conclusions

This chapter introduces a replica molding technique that enables the preparation of dense arrays of nano-pillars in a variety of materials. This high yield method requires low cost fabrication facilities. A thermoplastic material (PMMA) was pressed against an AAO template to form arrays of high aspect-ratio nano-pillars. The transparency of the nano-structured polymer indicated these nano-pillars retained their upright or columnar structure and did not collapse. The arrays of PMMA nano-pillars were subsequently used as a positive mold to form a PDMS negative mold. A silane based release layer was applied on the PMMA surfaces to enable improved release of this PDMS mold. The quality of the release layer was examined using water contact angle measurements and SEM imaging. Two thermoset plastics, PU and epoxy, were subsequently cast against the PDMS negative molds to obtain positive replicas. The pillar density and shape within these replicas were examined by SEM analysis. As a case study, the adhesion properties of the replicas were investigated for samples containing arrays of nano-pillars that were similar in size and shape to a gecko's setae. The adhesion force for arrays of epoxy (replica) and PMMA (master) nano-pillars were measured using AFM based techniques. The average adhesion force of the epoxy sample was more than three times higher than that of the PMMA sample. This improvement was associated to the higher surface energy of the epoxy. This case study demonstrated that the selection of the structural material could play an important role in the performance of the fabricated nanostructures. The proposed method has an advantage over existing fabrication processes as it enables the selection of a variety of materials from which to fabricate arrays of nanostructures.

4.6. Acknowledgements

This work was supported by the Natural Sciences and Engineering Research Council (NSERC) of Canada and the Canada Research Chairs Program (B.D. Gates). This research also made use of 4D LABS shared facilities supported by the Canada Foundation for Innovation (CFI), British Columbia Knowledge Development Fund (BCKDF), Western Economic Diversification Canada, and Simon Fraser University.

4.7. References

[1] Vieu C, Carcenac F, Pépin A, Chen Y, Mejias M, Lebib A, Manin-Ferlazzo L, Couraud L, Launois H 2000 Electronbeamlithography: resolution limits and applications. *Appl. Surf. Sci.* **164** 111-117.

[2] Grigorescu AE and Hagen CW 2009 Resists for sub-20-nm electron beam lithography with a focus on HSQ: state of the art. *Nanotechnology* **20** 292001.

[3] Kolodziej CM, Kim SH, Broyer RM, Saxer SS, Decker CG, Maynard HD 2012 Combination of Integrin-Binding Peptide and Growth Factor Promotes Cell Adhesion on Electron-Beam-Fabricated Patterns. *J. Am. Chem. Soc.* **134** 247-255.

[4] Guo LJ 2007 Nanoimprint lithography: methods and material requirements. *Adv. Mater.* **19** 495-513.

[5] Lee S-W, Lee K-S, Ahn J, Lee J-J, Kim M-G, ShinY-B 2011 Highly Sensitive Biosensing Using Arrays of Plasmonic Au Nanodisks Realized by Nanoimprint Lithography. *ACS Nano* **5** 897-904.

[6] Balla T, Spearing SM, Monk A 2008 An assessment of the process capabilities of nanoimprint lithography*. J. Phys. D: Appl. Phys.* **41** 174001.

[7] Chekurov N, Grigoras K, Peltonen A, Franssila S, Tittonen I 2009 The fabrication of silicon nanostructures by local gallium implantation and cryogenic deep reactive ion etching. *Nanotechnology* **20** 065307.

[8] Maiolo III JR, Kayes BM, Filler MA, Putnam MC, Kelzenberg MD, Atwater HA, Lewis NS 2007 High Aspect Ratio Silicon Wire Array Photoelectrochemical Cells *J. Am. Chem. Soc.* **129** 12346-12347.

[9] Nakayama K, Tanabe K, Atwater HA 2008 Plasmonic nanoparticle enhanced light absorption in GaAs solar cells. *Appl. Phys. Lett.* **93** 121904.

[10] Ramakrishnan N, Nemade HB 2011 Mass Loading in Coupled Resonators Consisting of SU-8 Micropillars Fabricated Over SAW Devices. *IEEE Sens. Jl.* **11** 430-431.

[11] Xua J, Dapinoa MJ, Gallego-Perezb D, Hansfordb D 2009 Microphone based on Polyvinylidene Fluoride (PVDF) micro-pillars and patterned electrodes. *Sensor Actuat. A-Phys.* **153** 24-32.

[12] Chandra D, Taylor JA, Yang S 2008 Replica molding of high-aspect-ratio (sub-)micron hydrogel pillar arrays and their stability in air and solvents. *Soft Matter* **4** 979-984.

[13] Shin HG, Kwon JT, Seo YH, Kim BH 2008 Fabrication of Polymer Master for Antireflective Surface Using Hot Embossing and AAO Process. *Int. J. Mod Phys. B* **22** 5887-5894.

[14] Krishnamoorthy S, Gerbig Y, Hibert C, Pugin R, Hinderling C, Brugger J, Heinzelmann H 2008 Tunable, high aspect ratio pillars on diverse substrates using copolymer micelle lithography: an interesting platform for applications. *Nanotechnology*, **19** 285301.

[15] Choi MK, Yoon H, Lee K, Shin K 2011 Simple Fabrication of Asymmetric High-Aspect-Ratio Polymer Nanopillars by Reusable AAO Templates. *Langmuir* **27** 2132–2137.

[16] Jeong HE, Lee J-K, Kim HN, Moon SH, Suh KY 2009 A nontransferring dry adhesive with hierarchical polymer nanohairs. *Proc. Natl. Acad. Sci. U.S.A.* **106** 5639-5644.

[17] Kim T, Jeong HE, Suh KY, Lee HH 2009 Stooped Nanohairs: Geometry-Controllable, Unidirectional, Reversible, and Robust Gecko-like Dry Adhesive. *Adv. Mater.* **21** 2276-2281.

[18] Lee J-L, Shen Y-K, Lin Y, Chen D-R 2010 The Nano-topology Influence of Osteoblast-like Cell on the Bio-nanostructure Thin Film by Nanoimprint. In Int. Conf. on Nanotechnology and Biosensors, Hong Kong, PR China, December 28-30, 2010.

[19] Chen G, McCarley RL, Soper SA, Situma C, Bolivar JG 2007 Functional Template-Derived Poly(methyl methacrylate) Nanopillars for Solid-Phase Biological Reactions. *Chem. Mater.* **19** 3855-3857.

[20] Chen G, McCandless GT, McCarley RL, Soper SA 2007 Integration of large-area polymer nanopillar arrays into microfluidic devices using in situ polymerization cast molding. *Lab Chip* **7** 1424-1427.

[21] Yoon Y, Lee D-W, Lee J-B 2012 Surface modified nano-patterned SU-8 pillar array optically transparent super-hydrophobic thin film. *J. Micromech. Microeng.* **22** 035012.

[22] Harriott LR 2001 Limits of Lithography. *P. IEEE* **89** 366-374.

[23] Reyntjens S, Puers R 2001 A review of focused ion beam applications in microsystem technology. *J. Micromech. Microeng.* **11** 287.

[24] Skupinski M, Sanz R, Jensen J 2007 Surface patterning by heavy ion lithography using self-assembled colloidal masks. *Nucl. Instrum. Meth. B* **257** 777-781.

[25] Kustandi TS, Samper VD, Yi DK, Ng WS, Neuzil P, Sun W 2007 Self-Assembled Nanoparticles Based Fabrication of Gecko Foot-Hair-Inspired Polymer Nanofibers. *Adv. Funct. Mater.* **17** 2211-2218.

[26] Palacio MLB, Bhushan B, Schricker SR 2013 Gecko-inspired fibril nanostructures for reversible adhesion in biomedical applications. *Mater. Lett.* **92** 409-412.

[27] Fureaux RC, Rigby WR, Davidson AP 1989 The formation of controlled-porosity membranes from anodically oxidized aluminium. *Nature* **337** 147-149.

[28] Belwalkar A, Grasing E, Van Geertruyden W, Huang Z, Misiolek WZ 2008 Effect of processing parameters on pore structure and thickness of anodic aluminum oxide (AAO) tubular membranes. *J. Membrane Sci.* **319** 192-198.

[29] Zhao S, Chan K, Yelon A, Veres T 2007 Novel structure of AAO film Fabricated by constant current anodization. *Adv. Mater.* **19** 3004-3007.

[30] Poinern GEJ, Ali N, Fawcett D 2011 Progress in Nano-engineered anodic aluminum oxide membrane development. *Materials* **4** 487-526.

[31] Martinson ABF, Elam JW, Hupp JT, Pellin MJ 2007 ZnO Nanotube based Dye-sensitized Solar Cells. *Nano Lett.* **7** 2183-2187.

[32] Banerjee P, Perez I, Henn-Lecordier L, Lee SB, Rubloff GW 2009 Nanotubular metal-insulator-metal capacitor arrays for energy storage. *Nat. Nanotechnol.* **4** 292-296.

[33] Lee P-S, Lee O-J, Hwang S-K, Jung S-H, Jee SE, Lee K-H 2005 Vertically Aligned Nanopillar Arrays with Hard Skins Using Anodic Aluminum Oxide for Nano Imprint Lithography *Chem. Mater.* **17** 6181-6185.

[34] Saedi A, Ghorbani M 2005 Electrodeposition of Ni-Fe-Co alloy nanowire in modified AAO template. *Mater. Chem. Phys.* **91** 417-423.

[35] Yoo W-C, Lee J-K 2004 Field-dependent Growth patterns of metals electroplated in nanoporous alumina membranes. *Adv. Mater.* **16** 1097-1101.

[36] Sui YC, Acosta DR, Gonzalez-Leon JA, Bermudez A, Feuchtwanger J, Cui BZ, Flores JO, Saniger JM 2001 Structure, Thermal Stability and deformation of multibranched carbon nanotubes synthesized by CVD in the AAO template. *J. Phys. Chem. B* **105** 1523-1527.

[37] Guo J, Xu Y, Wang C 2011 Sulfur-Impregnated Disordered Carbon Nanotubes Cathode for Lithium–Sulfur Batteries*. Nano Lett.* **11** 4288-4294.

[38] Rohrig M, Schneider M, Etienne G, Oulhadj F, Pfannes F, Kolew A, Worgull M, Holscher H 2013 Hot pulling and embossing of hierarchical nano- and micro-structures. *J. Micromech. Microeng* **23** 105014.

[39] Izadi H, Zhao B, Han Y, McManus N, Penlidis A 2012 Teflon hierarchical nanopillars with dry and wet adhesive properties. *J. Polym. Sci. Pol. Phys.* **50** 846-851.

[40] Pan CT, Wu TT, Chen MF, Chang YC, Lee CJ, Huang JC 2008 Hot embossing of micro-lens array on bulk metallic glass. *Sensor Actuat. A-Phys.* **141** 422-431.

[41] Kim DS, Lee HS, Lee J, Kim S, Lee K-H, Moon W, Kwon TH 2007 Replication of high-aspect-ratio nanopillar array for biomimetic gecko foot-hair prototype by UV nano embossing with anodic aluminum oxide mold. *Microsyst. Technol.* **13** 601-606.

[42] Lee H, Bhushan B 2012 Fabrication and characterization of hierarchical nanostructured smart adhesion surfaces. *J. Colloid Interf. Sci.* **372** 231-238.

[43] Liu K, Du J, Wu J, Jiang L 2012 Superhydrophobic gecko feet with high adhesive forces towards water and their bio-inspired materials. *Nanoscale* **4** 768-772.

[44] Chang W-Y, Lin K-H, Wu J-T, Yang S-Y, Lee K-L, Wei P-K 2011 Novel fabrication of an Au nanocone array on polycarbonate for high performance surface-enhanced Raman scattering. *J. Micromech. Microeng.* **21** 035023.

[45] Plaskolite INC. (USA), OPTIX properties, [cited 2014 Jan 15], Available from: http://www.plaskolite.com/Fabrication/Acrylic/Optix.

[46] Zhang C, Zhou J, Sameoto D, Zhang X, Li Y, Ng HW, Menon C, Gates BD 2014 Determining adhesion of nonuniform arrays of fibrils. *J. Adhes. Sci. Technol.* **28** 320-336.

[47] SPI supplies/Structure Probe, Inc. (USA), ANOPORE™ Inorganic Aluminum Oxide Membrane Filters, [cited 2014 Jan 15], Available from: http://www.gelifesciences.com/webapp/wcs/stores/servlet/catalog/en/GELifeSciences-ca/products/AlternativeProductStructure_16220/28420418.

[48] Menon C, Murphy M, Sitti M 2004 Gecko Inspired Surface Climbing Robots. In IEEE Int. Conf. on Robotics and Biomimetics, Shenyang City, PR China, Aug. 22-26, 2004.

[49] Efimenko K, Wallace WE, Genzer J 2002 Surface Modification of Sylgard-184 Poly(dimethyl siloxane) Networks by Ultraviolet and Ultraviolet/Ozone Treatment. *J. Colloid. Interf. Sci.* **254** 306-315.

[50] Diversified Enterprises (USA), Critical surface tension and contact angle with water for various polymers, [cited 2014 Jan 15], http://www.accudynetest.com/polytable_03.html?sortby=contact_angle.

4.8. Supporting Information

4.8.1. Pillar collapse due to an increase in aspect ratio

By increasing the embossing time, it is anticipated that the aspect ratio of the nano-pillars would increase. The size and shape of the nano-pillars can also depend on the embossing time. A longer embossing time can create higher compression forces on the soft molding materials, as suggested by an increase in the diameter of the pillars with increased embossing times. The collapse of these pillars with increase of their aspect ratio interferes with the light path through these otherwise transparent samples, causing a macroscopic change in their color and transparency as described in the main text.

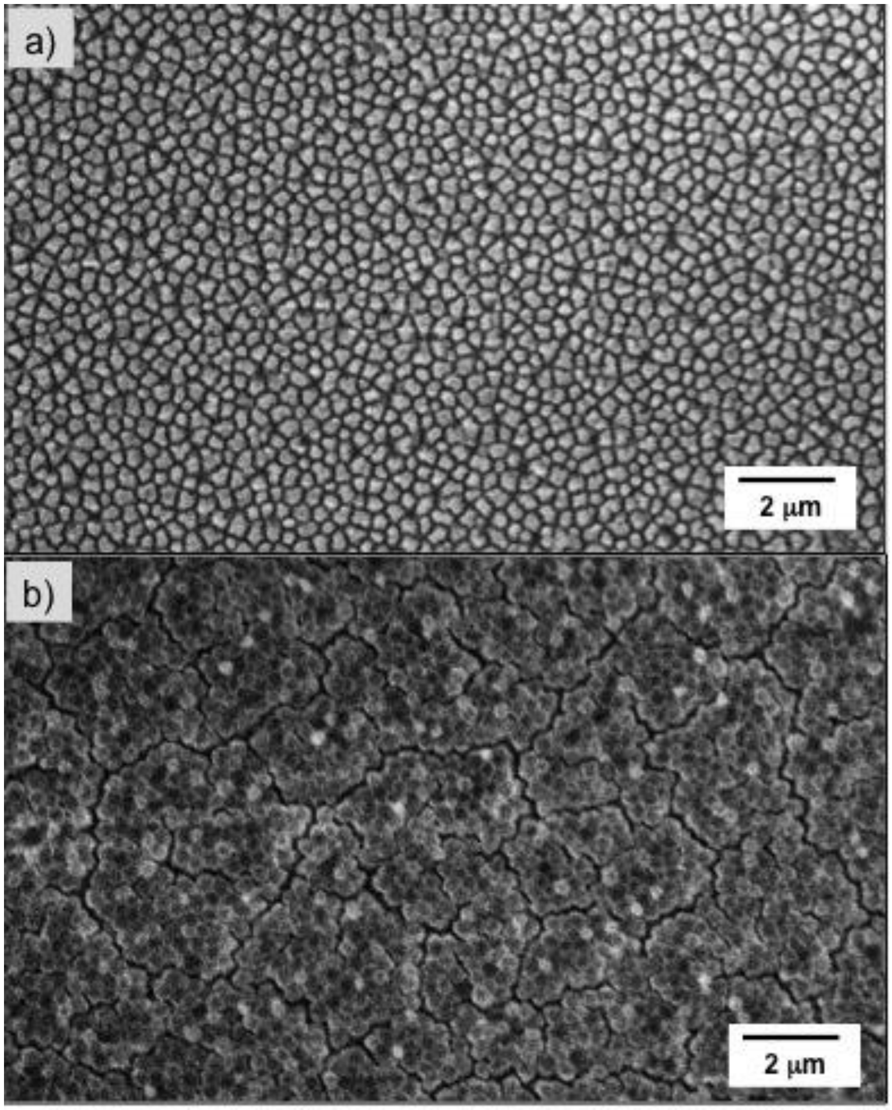

Figure 4.8. **Scanning electron microscopy (SEM) images of the PMMA nano-pillar samples after various embossing times: a) sample prepared by 1 h of embossing; b) sample prepared by 2 h of embossing.**

4.8.2. Quality assessment of the release layers using static water contact angle (WCA) measurements

Figure 4.9 shows the WCA of the PMMA surface before (Figure 4.9a) and after (Figure 4.9b) hot embossing, as well as after silane treatment (Figure 4.9c). As observed in Figure 4.9b, the nano-structured PMMA surfaces had a slight decrease in water contact angle from that of the pristine flat PMMA surfaces, which indicated the capillary effect of the nano-pillars drew the water droplet in between the high AR features. A significant increase in contact angle was observed after treating the array of PMMA nano-pillars with a perfluoroalkylsilane. Results in Figure 4.9 indicate that the water droplet sat on the surfaces of the silane coated nano-structures in a Cassie-Baxter mode, indicating the silane molecules coated at least the top layer of these nano-scale features.

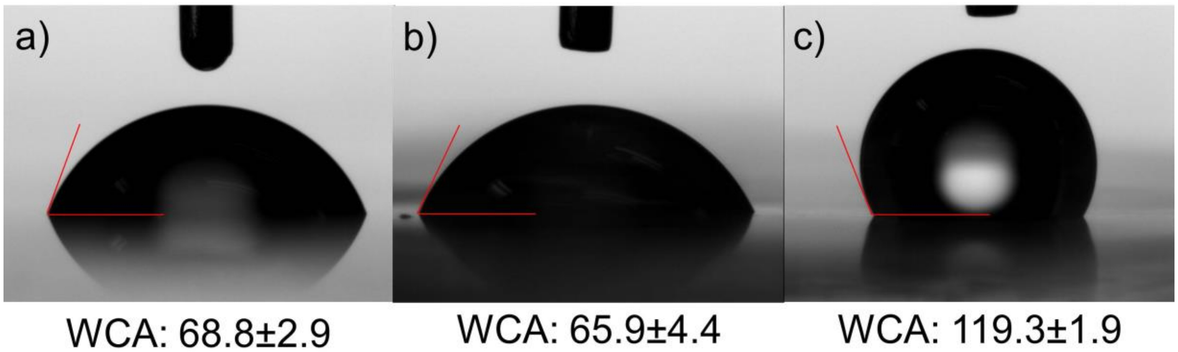

Figure 4.9. Static water contact angle measurements of PMMA before (a) and after (b) hot embossing, and for the nano-pillar PMMA after treatment with a silane based release layer (c).

4.8.3. Comparison of the shapes of the nano-structures during each step of the replication process

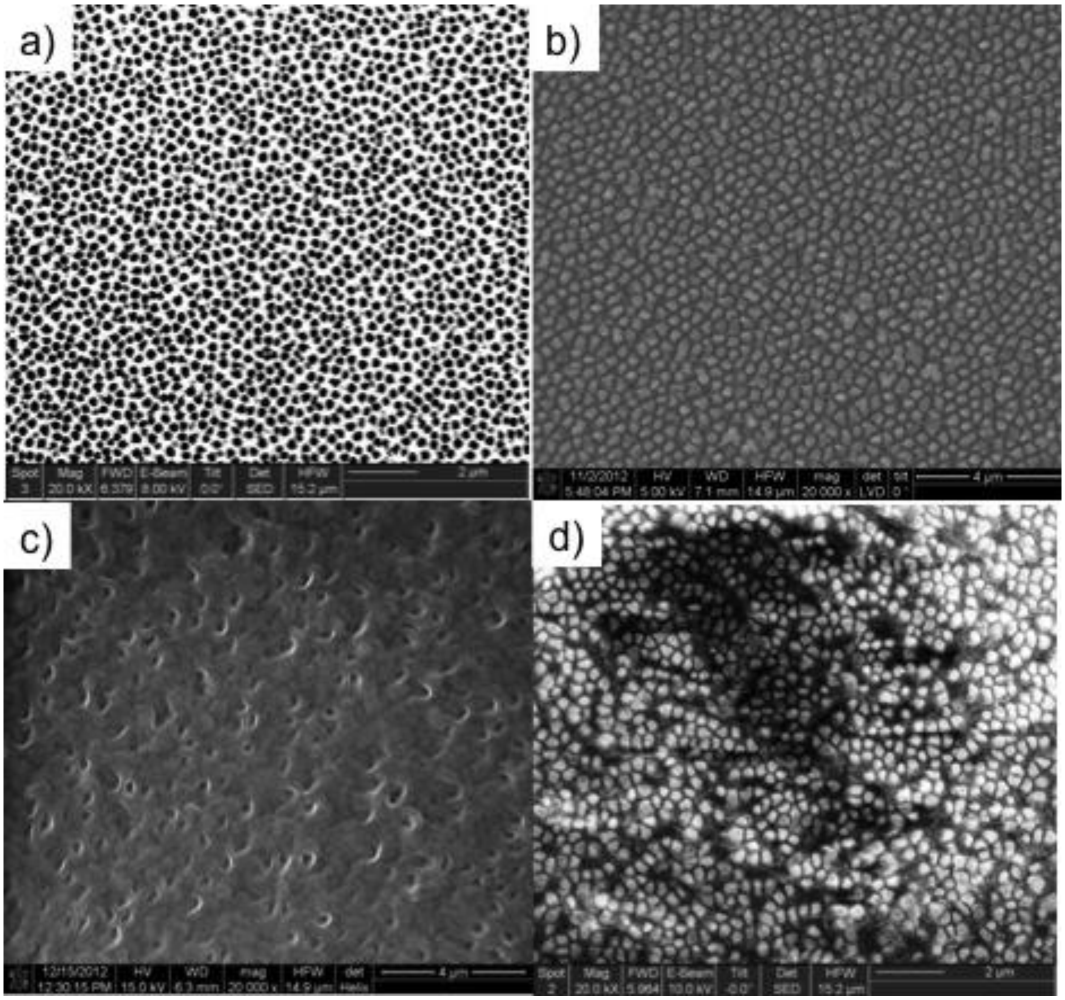

Figure 4.10. SEM images of: a) an AAO template used as the initial master; b) PMMA nano-pillars arrays demolded from the AAO template; c) arrays of nano-holes in PDMS after demolding from the arrays of PMMA nano-pillars; and d) epoxy based arrays of nano-pillars after demolding from the PDMS nano-holes. The PMMA, PDMS and epoxy nano-structures all retain the shape of the initial features.

Chapter 5.

Measuring shear-induced adhesion of gecko-inspired fibrillar arrays using scanning probe techniques

Current research of adhesion measurement methods applied on micro-scopic fibrillar arrays rarely focus on characterizing uniformity and fibril-substrate interaction. As described in Chapter 2, counter substrates used to measure adhesion or friction forces were usually a lot larger than the fibril itself. On the other hand, nano-fibrillar arrays behaved differently from the microscopic and macroscopic fibrillar arrays in those adhesion tests. To properly assess adhesion properties of nano-fibrillar arrays, a measurement method making use of a scanning probe microscope was developed in this chapter. Although the fibrillar arrays were observed uniformly distributed on the substrate, the adhesion forces were different from area to area due to complicated interaction conditions. Inspired from the gecko climbing with their natural fibrillar adhesive, a shear movement was added in between the attaching and detaching process. Applying such shear-induced adhesion measurement method, improvement of adhesion force was observed from contact area optimization. Interaction between the substrate and fibrillar arrays was also discussed. This chapter aims at realization of OBJECTIVE 3. The following contents are published in: Yasong Li, Cheng Zhang, James H.-W. Zhou, Carlo Menon and Byron D. Gates, "Measuring shear-induced adhesion of gecko-inspired fibrillar arrays using scanning probe techniques" in *Macromolecular Reaction Engineering*, 2013, *vol. 7*, 638-645.

5.1. Abstract

The natural ability of geckos and spiders to climb almost all surfaces using the compliant, nano-structured components on their feet provides motivation for making bio-inspired adhesives. The brush-like fibrillar structures have only minimal adhesion upon

initial contact. Maximum adhesion is realized after a dragging motion of the gecko's or spider's foot that aligns the fibrillar structures to be almost parallel to the contacting surfaces. The goal of the studies described in this chapter is to create an analytical technique to improve our ability to characterize dry adhesives modeled after these biological systems. The technique described herein uses a scanning probe microscope to manipulate a flat test surface in contact with biomimetic fibrillar arrays while monitoring the adhesion forces. Adhesion forces were measured after both normal contact and shear induced contact between the nano-structured fibrils and the test surface. Results confirm that the adhesion forces are higher for bio-inspired adhesives after a shear induced contact. Variations in these forces can be measured across the sample with micron-scale lateral resolution. This method of analysis can be extended to evaluating bio-inspired dry adhesives with realistic mechanisms of attachment utilized in robotic and similar applications of these materials.

Keywords: adhesion forces, dry adhesive, nano-structured fibrils, scanning probe microscopy, shear loading

5.2. Introduction

Following the scientific identification that van der Waals forces contribute remarkably to a gecko's ability to climb [1-3], numerous attempts have been pursued to make artificial adhesives that mimic the fibrillar structures found on a gecko's foot [4-8]. The gecko adhesive does not rely upon fluid secretion and, therefore, is widely referred to in the literature as a "dry adhesive" [1-3,9]. Pressure sensitive adhesive (PSA) tapes, including office and duct tape, form a tacky connection between the tape and the contacting surfaces. Geckos, on the other hand, rely on fibrillar nano-structures to form millions of interactions through weak van der Waals forces with the surfaces [10]. The synergistic effect of millions of weak interactions translates into a collectively strong adhesion force that supports every step of the climbing animal. Fibrils on the skin of the gecko are made from beta-keratin, which is non-tacky and stiff. These materials properties provide wear resistance for the fibrillar structures. The combination of composition and shape of these nano-structures permit the gecko feet to adapt to surfaces of different roughness. To conform to rough surfaces, the gecko adhesive contains a hierarchical structure of branching fibrils of different diameters ranging from nanometers to millimeters. These slender and brush-like structures have a high compliancy to various surface topographies and ensure a maximized number of contact points with the surfaces.

The formation of contact points between the hierarchical fibrillar structures and the contacting surfaces is a dynamic process. A close examination of the climbing motion of the animals reveals that the adhesion mechanism includes a dragging movement of the animal's foot to assist in achieving a high conformation between the fibrils and various surfaces [11-12]. Experiments have been performed that demonstrate this observation for both gecko [13-15] and spider [16-17] seta. In one study, Autumn et al. attached a gecko seta to a cantilever in order to manipulate the seta with control in all three dimensions. This control was essential for their ability to bring the seta into contact with surfaces, to subsequently provide a shear movement across these surfaces, followed by removal of the seta by a pulling in a direction perpendicular to the surfaces. This series of manipulations to the seta is referred as the "load-drag-pull" (LDP) method [18]. Experimental results indicate that the adhesion force between the seta and various surfaces increases with the additional shear movement after bringing the seta into contact with the test surfaces. Theories and models have been developed to explain the mechanism of increased adhesion resulting from the LDP method. Results of these studies highlight the improvement of fibril alignment during the shear movement applied to the seta. Tian et al. [19] have demonstrated that frictional forces contribute significantly to the adhesion force of gecko setae, but the angle of peeling the seta from surfaces is relatively low. Other models on pre-tension [20] of the adhesive were modeled as a thin film, and analyzed by Kendall's [21] thin film peeling model, which provide further insight into the shear induced adhesion forces utilized by geckos to climb walls and suspend from ceilings. Mathematical modeling of experimental adhesion force measurements for gecko setae by Yamaguchi et al. show a close fit with the LDP experimental results and advances the concept that lateral movement increases adhesion force [22]. Studies by Majidi and Fearing [23] and Cheng et al. [24] also suggest that alignment of the fibrillar arrays is an important aspect of increased adhesion. A mathematical model and supporting experimental results of Filippov et al. [25] suggest that spiders also align their fibrils through a dragging motion of their feet.

This study indicated the adhesion force between the fibrils and contacting surfaces is enhanced through an increase in the area of contact. A combination of the hierarchical nano-structures in setae of geckos or spiders and a shear induced alignment of these nano-structures work in conjunction to enhance their adhesion to various surfaces.

Artificial dry adhesives have been prepared to mimic the properties observed in setae of geckos and spiders. A key component of the development of these dry adhesive materials is the verification of their adhesive properties and validation that their adhesion forces are similar to their natural counterparts. In one study, Schubert et al. [26] demonstrated the use of a large spherical probe (contact region ~1x1 mm^2) in conjunction with LDP based adhesion force measurements to evaluate an array of polypropylene nano-fibrils. In an array of nano-scale fibrils with a common directionality (i.e. a specific tilted orientation), Lee et al. [27] evaluated the adhesion force by the LDP method and a "push-pull" (PP) method. In the later technique, various surfaces are contacted with and separated from fibrils while maintaining a direction of motion parallel to the orientation of the fibrils. The comparative analysis by Lee et al. demonstrated that the adhesion characteristics of the tilted fibrils were similar to those of the gecko adhesive. In contrast, Varenberg and Gorb [28] tested their adhesive composed of an array of micro-scale mushroom shapes with fibril-like stalks by applying a shear force, but the adhesion force decreased due to the smaller area of contact between the test surfaces. A wedge shaped adhesive was similarly evaluated by Parness et al. [29] using the LDP method. In this study, the applied shear forces created a compliant interface between the wedges and the contacting surfaces to increase the area of contact, which also increased the measured adhesion force. In summary, if a shear force is applied between the fibrillar array and the contacting surfaces which results in an increase of contact area, then the adhesion force also increases. The applications on this discovery include construction of climbing robots [30-31] that use gravitational forces to induce a shear loading between their feet and the surfaces of a wall. This demonstration also provides further evidence that a shear assisted contact between the dry adhesive and the contacting surfaces helps to ensure a reliable and strong adhesion interaction.

The study described below investigates the implementation of the LDP and PP measurement techniques using an atomic force microscope to assess the adhesion forces of an array of artificial fibrils. The benefits of using an atomic force microscope (AFM) for these analyses include micro-scale control over position of the measurements within the samples, fine control over the contacting forces, and precise control of both speed and direction of motion during the force measurements. Previous implementation of AFM techniques to measure adhesion forces of fibrillar arrays includes the use of a colloidal probe [32-33] and a flat probe [34-35]. These measurements implemented PP methods. We extend these demonstrations here to LDP techniques and compare the results with those of the PP method. A benefit of the use of an AFM for administering these adhesion measurements is a fine control over the interactions between the test surfaces and the fibrillar array and the ability to take force measurements from small (e.g., micro-scale) regions of the sample. The latter ability is especially important when evaluating the adhesion forces of a non-uniformly distributed array of nano-structured fibrils. The results of the study reported herein indicate that the adhesion forces for non-uniform arrays of fibrils increase when using a shear loading (LDP rather than PP methods) with the AFM controlled cantilever. Further results indicated a divergence in the adhesion forces across these samples. These measurements could be useful in determining correlations between structure and function in such non-uniform dry adhesives samples, or for identifying non-uniformities in adhesive forces within well-ordered fibrillar arrays.

5.3. Experimental Section

5.3.1. Preparation of fibrillar arrays as dry adhesives

The artificial fibrillar arrays were fabricated using a Reactive Ion Etching (RIE) method we discussed in detail within a previous paper [35-36]. Epoxy based (SU-8 2010, MicroChem) arrays of nano-scale fibrils were prepared upon a regular arrangement of squares measuring 1 mm x 1 mm and with a spacing of 0.5 mm between each pad. The etching time of the RIE process determined the average length of the fibrils within each sample. For the purposes of this study, we present results on samples etched for 10 min, producing fibrils with a nominal length of ~250 nm. Samples were inspected by scanning electron microscopy (Strata DB-235, FEI) to verify the length of the fibrils, monitor for the presence of defects in samples, and to identify changes to the fibrillar arrays after performing the various adhesion tests outlined below in further detail. All samples were also inspected for defects using an optical microscope (Axio Imager M1m, Zeiss) throughout these studies.

5.3.2. Measurement of adhesion forces in fibrillar arrays

An atomic force microscope (MFP-3D-SA, Asylum Research) was adapted for adhesion force measurements on the fibrillar arrays described above. A specific script was written (with assistance from Jason Bemis, Asylum Research, Santa Barbara, CA) to control the position, movements, and dwell time of a cantilever, including after being brought into contact with the sample. In addition, the implementation of a "sewing" type of an action enables the cantilever to sequentially measure adhesion forces across the sample by moving from one position on the sample to an adjoining position upon completion of each measurement cycle. Tipless silicon nitride cantilevers (NP-O10, Veeco Instruments) were used for the measurements performed in this study. Each AFM probe contains four cantilevers each with a different spring constant. The spring constant of the selected "C" triangular cantilever is ~320 nN/μm, which is calibrated prior to each test by performing a single force curve and determining the resonance frequency (~60 kHz) of this cantilever. The adhesion force normal to the test surface is calculated using the calibrated spring constant and the measured cantilever deformation. The pointed end of the triangular shaped cantilever was directed towards the sample surfaces with an angle between the tipless cantilever and the samples maintained at ~11° when the cantilever was approaching the test samples. The loading force was set to ~10 nN and during the LDP method the contacting cantilever moved a distance of 1 μm during the subsequent shear step at a speed of 20 μm/s. A preload force of 10 nN was chosen for these measurements because it is within the range of adhesion forces (i.e. 0 to 60 nN) that can be measured through the use of this cantilever as determined empirically. From our experience, higher preload values could compress or otherwise significantly deform the fibrillar surfaces as will be discussed below in relation to Figure 5.3. The vertical retraction speed of the cantilever was set at 1 μm/s. Adhesion force measurements were acquired in a sequence of analyses conducted in a square array of 20 measurements in either direction (x or y). Each of these 400 independent measurements had a corresponding force-distance (FD) curve that was acquired from the beginning to end of the sequences outlined in Figure 5.1 and discussed in further detail below. Further information on the measurement of adhesion forces by the PP method are described in [35].

5.3.3. Statistical analysis of experimental results

As indicated above, 400 measurements were acquired for each experiment. Results of each experiment were plotted in a histogram for ease of analyzing for trends. Both the median and a 12.5% trimmed mean were calculated for each set of results as a combined indicator of the average adhesion force and the distribution of adhesion forces for each sample. The median was chosen to indicate the center of the distribution, and the 12.5% trimmed mean to portray the average value of each data set while excluding 100 data points (out of a data set of 400) from either side of the entire population. The portion that is trimmed was determined after a close examination of the normal probability plot for each data set (see Supporting Information for further details).

5.4. Results and Discussion

A number of approaches are being pursued for making bio-inspired dry adhesives. An essential component of characterizing these materials is to determine the correlation between structure and function on a scale proportional to the dimensions of the components within the adhesives. Often the key features within these materials are micro- to nano-scale fibrils with spacing on an equivalently small scale. We have previously demonstrated the usefulness of measuring the adhesion forces within non-uniform arrays of fibrils through the use of an AFM [35]. In these previous tests, a flat cantilever was brought into contact with an array of vertically oriented fibrils to a predetermined loading force and directly retracted. The direction of movement of the cantilever was maintained parallel to the orientation of these fibrils. The adhesion forces between the fibrillar array and the contacting surfaces (i.e. flat surfaces of the cantilever) were determined from the calibrated deflection of the cantilever. This method has been referred to as a “test without dragging”, “tap test”, or the “push-pull” technique. We refer to this method here as the push-pull or the PP technique. In this manuscript, we extend the PP method with further modifications to mimic the load-drag-pull or LDP method. The LDP method is adapted from previous demonstrations [18] to demonstrate this method in conjunction with use of commonly available AFM hardware. Because the dragging or shear motion of the cantilever is the essential difference between the PP and LDP methods, we sometimes refer to the latter as the shear induced contact method or the dragging test.

An overview is provided in Figure 5.1 of the implementation of the LDP method using a scanning probe microscope to manipulate a flat cantilever as a probe in order to measure adhesion forces for arrays fibrils. The tipless cantilever is first located above an array of fibrils (Figure 5.1a). The cantilever is controlled through a series of sequential steps (Figure 5.1a-5.1d): i) vertical approach of the cantilever to the test surfaces, bringing the fibrils in contact with the cantilever (load step); ii) lateral movement of the cantilever across a predetermined distance (drag step); iii) cantilever vertically withdraws from the surface and control system records the adhesion force generated from the contacts (pull step); and iv) movement of the cantilever to an adjacent spot to start a new measurement. During each measurement the cantilever approaches the fibrillar array until reaching a predetermined force, referred to as the loading force, of ~10 nN (Figure 5.1b). After the cantilever has been brought into contact with the array of nano-structured fibrils, its position is controlled to slide laterally over these surfaces (Figure 5.1c). The direction and distance of this movement can be precisely controlled through a series of piezoelectric stacks that control the position of the stage relative to the position of the cantilever. In these studies, we moved the cantilever in a direction opposite of the pointed end of the triangular shaped cantilever. This direction of motion was chosen to avoid unintentional damage to the surfaces of the dry adhesive (potential damage to the samples following the LDP method is assessed later in this manuscript). Because the average length of artificial fibrils was ~250 nm, the lateral movement of the cantilever during the dragging step was set to 1 μm. This length of movement was chosen in order to travel at least the height of the contacting fibrils in order to align and efficiently contact these fibrils. The cantilever was moved during this shear step (Figure 5.1c) at a rate of 20 μm/s and subsequently retracted in a vertical direction (Figure 5.1d) at a speed of 1 μm/s, which were indiscriminately selected as starting points to assess the efficacy of implementing the LDP method using an AFM.

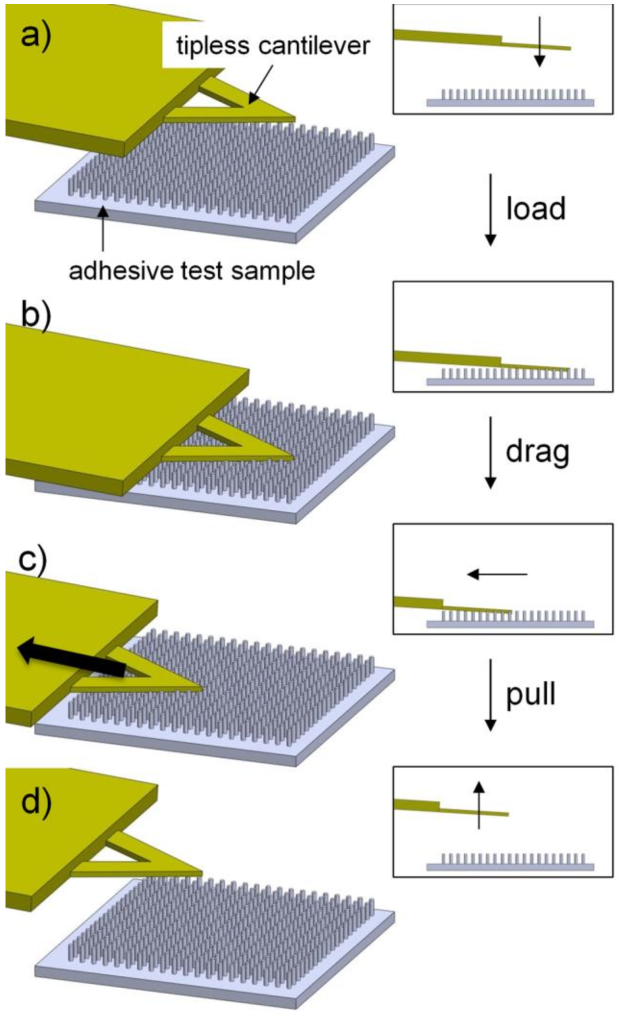

Figure 5.1. **Schematic of the sequential steps implemented during a shear induced alignment of bio-inspired fibrils during adhesion force measurement implemented with a scanning probe microscope. (a) A tip-less cantilever is positioned over the fibrillar array. The cantilever subsequently (b) approaches the fibrillar array in a vertical direction (i.e., load step), and (c) the cantilever is laterally moved across the sample providing a shear force to the initially vertically oriented fibrils (i.e., drag step). (d) The last step of this method is to vertically unload, or pull the cantilever away from the sample. During this entire process deflection of the cantilever is recorded and translated into an adhesion force between the cantilever and fibrillar array.**

The adhesion forces of the polymeric fibrils under test were measured from the calibrated deflection of the tipless cantilever during retraction from the contacting surfaces. The force to pull the cantilever away from the fibrillar arrays is one aspect of the data contained within the acquired force-distance (or FD) curves (Figure 5.2). The corresponding force-time response curve is described in detail in the supporting information (Figure 5.7). The adhesion force for this measurement was ~19.8 nN. There are also many other details within these traces that contain useful information about the fibrillar arrays as they interact with the flat surfaces of the cantilever. This figure depicts the force curve during approach of the cantilever to the fibrillar arrays and during the load step of the LDP method (red trace in Figure 5.2, read from right to left). The inset depicts the oscillations in the force curve observed during both the dragging movement of the cantilever and the subsequent withdrawal of the cantilever from contact with the fibrils (blue traces in Figure 5.2, read from left to right). The dragging motion of the cantilever initially induces oscillations that likely correspond to changes in the tilt of the cantilever during alignment of the fibrillar structures. These deflections to the cantilever could be attributed to release of some of the fibrils (considering that the lateral distance traveled is greater than the average height of the fibrils), contact with a non-uniform array of fibrils (essentially these are roughened surfaces), and reorientation of the fibrillar structures during this shear induced alignment process. These interactions reach a steady state during the dragging motion of the cantilever (Figure 5.7), suggesting alignment of the fibrils in the direction of the moving cantilever. During movement of the cantilever away from the fibrils, the “retraction” trace is a smooth line. The subsequent trace depicts the force necessary to remove the cantilever from these surfaces of aligned fibrils. It may be possible to extend this work in the future with narrower cantilevers to the analysis of adhesion forces between either individual or smaller clusters of fibrils and the cantilever in order to more easily discern these individual processes, but these analyses are beyond the scope of this current study.

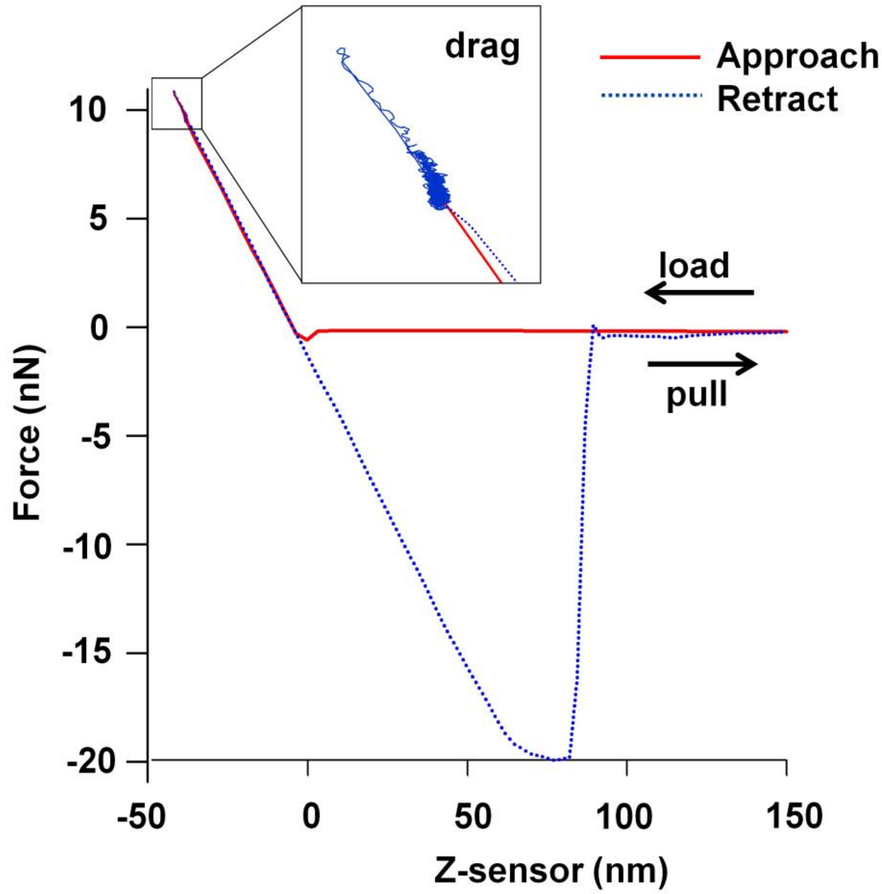

Figure 5.2. **A typical force-distance (FD) curve used to measure the adhesion forces resulting from shear induced contact between a flat cantilever and arrays of nano-structured fibrils. This plot contains traces recorded while the cantilever was approaching (red) and retracting from (blue) these fibrils, indicating the forces of interaction between these surfaces. The inset provides a magnified view of the FD curve during the final load, drag, and initial withdrawal steps of the LDP method.**

The measurement of adhesion forces for arrays of polymer based fibrils could induce damage during the initial load, shear movement, and retraction of the cantilever. The initial load force could deform the polymer surfaces. The lateral movement during shear induced alignment of the fibrils could deform, cut or otherwise damage the fibrils, and the retraction of the cantilever from these arrays could stretch or snap the polymer fibrils that have a significant area of contact with the cantilevers. Although the samples had extensive contact with the tipless cantilever, especially during the LDP method, no obvious damage was observed in our studies. Analysis of the samples by optical microscopy and scanning electron microscopy did not reveal any noticeable changes to the fibrillar arrays. The SEM results in Figure 5.3 depict regions of the sample as observed before the adhesion force measurements (Figure 5.3a), after measurements using the LDP method (Figure 5.3b), and subsequent to using the PP method (Figure 5.3c). Remarkably, there were no observed collapse of the fibrillar nano-structures after either of these force measurements, and the density of fibrils remains the same as that observed in the as-prepared samples.

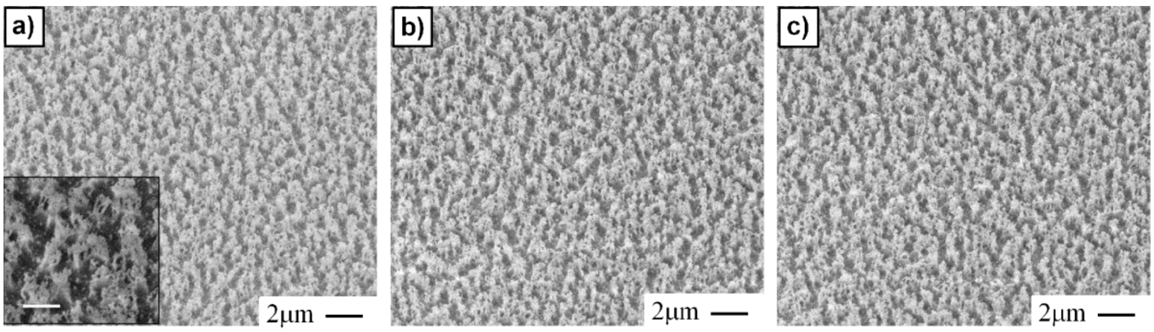

Figure 5.3. Scanning electron microscope images of polymeric fibril samples (a) before measuring their shear induced adhesion (inset: close-up of the fibrils, scale bar: 1μm), (b) following the drag step of this measurement, and (c) after measuring their adhesion using a normal force loading of the cantilever. All images are taken in 45 degrees tilt. The nominal length of the fibrils is ~250 nm.

The hypothesis that the fibrils have aligned during the shear step of the LDP method is further confirmed by comparing the results of these measurements with those obtained from the PP method on the same samples. An increase of adhesion force is predicted by theoretical studies and has been observed in previous reports [18-24]. Histograms of the adhesion forces measured by the LDP and PP methods for the polymeric fibrils are depicted in Figure 5.4. The distribution of results in these histograms provides a simple comparison between the LDP and PP methods. The histogram associated with the PP or tap test (Figure 5.4a) contained adhesion forces ranging from 0 to 26 nN with a standard deviation of 3.0 nN. In comparison, the results of the LDP or drag test (Figure 5.4b) had a wider distribution of adhesion forces ranging from 0 to 55 nN with a standard deviation of 9.4 nN. Furthermore, the median adhesion force from the PP method was 3.8 nN in comparison to a value of 8.7 nN for the measurements from the LDP method. We also calculated the 12.5% trimmed mean for each study in order to account for potential outliers in these datasets (i.e. due to any random events that may otherwise bias the results). The LDP method yielded a trimmed mean of 9.9 nN in comparison to 3.9 nN for the PP method. Each analysis demonstrates a higher average adhesion force resulting from the drag test. The adhesion forces of the shear aligned fibrils are more than twice those of the same fibrils under test by direct contact and pull-off of the cantilever. The divergence of these results can be attributed to alignment of the fibrils during the LDP method, and the subsequent increased interactions between the fibrils and the flat surfaces of the cantilever. The shear movement of the cantilever during the “drag step” leads to possible compression, stretching, elongation, and alignment of the fibrils along the direction of cantilever motion. During this process any overlapping and otherwise curling fibrils untangle and are exposed to the flat surfaces of the cantilever. The contacting surfaces with the cantilever can come from many different parts of a single fibril. These points of contact will depend on the shape and stiffness of the fibril and its relative position with respect to the cantilever. These differences in tip-sample interactions vary between each location on the sample and, therefore, between each adhesion force measurement. These variations contribute to the diverse range of adhesion forces observed for the measurements subsequent to shear alignment.

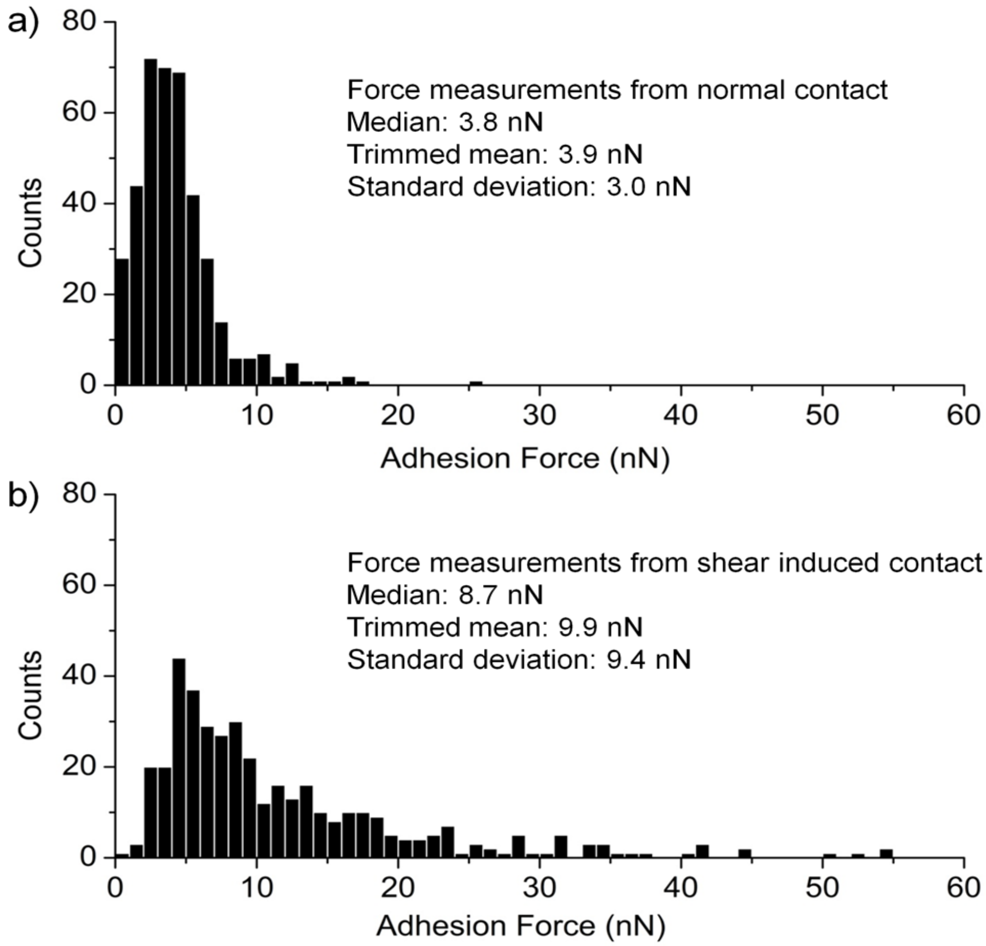

Figure 5.4. Histograms of adhesion tests acquired from (a) normal contact between the cantilever and the fibrillar array (i.e. non-shear loading of the cantilever in a direction parallel to the orientation of the fibrils), and (b) measurements from shear induced contact between fibrillar arrays and the cantilever by implementing a dragging motion. The total number of measurements for each test was 400. Trimmed mean is calculated by trimming the 12.5% of outliers at the smaller and larger end of the measurements. Standard deviation is calculated from the square root of the variance of the entire population.

The histograms for the adhesion force measurements indicate a large variation in the results as a function of position across the sample. The variations in adhesion force observed from the LDP method are clearly observed in a force map (Figure 5.5). This map depicts the adhesion force measured from 400 independent measurements made in a square array across the sample, and the gray scale coloration indicates the strength of these interactions (the lighter the color, or more white, the stronger the adhesion force) in accordance with the scale bar. There is a seemingly random distribution to the measured adhesion forces. In comparison to the spatial arrangement observed for the fibrillar structures (Figure 5.3), it might be surprising that the adhesion forces vary non-uniformly across the sample. These results are, however, consistent with our previous observations [35] for the spatially correlated variation in adhesion forces measured for a similar array of fibrillar structures using the PP method. The local variations in contact between the tipless cantilever and the fibrils may be larger in accordance with the larger variation in adhesion forces observed for these samples (Figure 5.4). It is clear that the dragging motion of the cantilever induces changes within the arrangement of the fibrils and increases the contact points between the contacting surfaces and the fibrils.

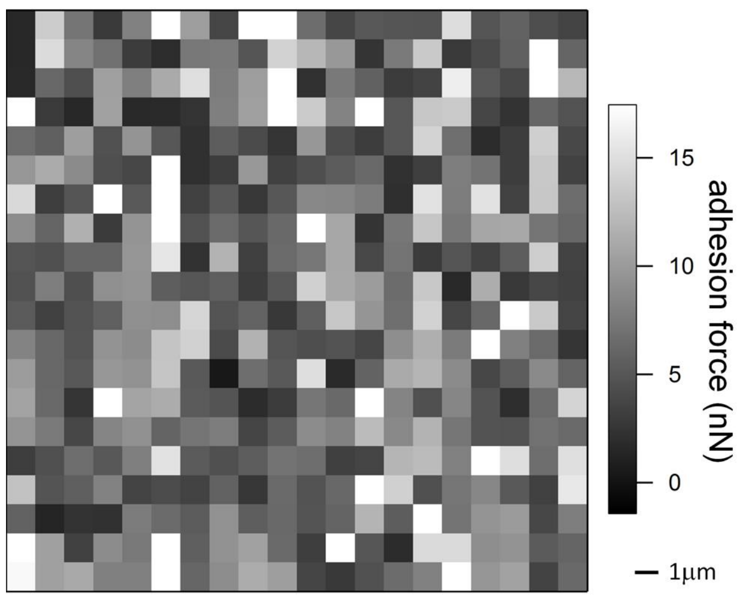

Figure 5.5. A representative map of the lateral variation in adhesion forces resulting from a series of sequential LDP based measurements performed across an array of ~250-nm tall fibrils. The force map was collected from a total 400 independent measurements, each corresponding to a different lateral position on the sample (varying in x and y by 1 μm movements).

5.5. Conclusion

A lateral or shear movement is essential for climbing animals to efficiently engage the fibrillar structures on their feet to contacting surfaces. The same is true for climbing robots and in other applications of an artificial dry adhesive. We have developed a method to assist in establishing the correlation between structure and function of nano-structured dry adhesives as a result of this shear induced movement. An atomic force microscope was used to manipulate a flat cantilever that could be controllably brought into contact with fibrillar arrays. The distances and directions over which the cantilever moved, as well as the speeds with which it moved could be controlled in order to induce a shear motion of the cantilever across an array of fibrils. A technique was demonstrated that can move the cantilever in a sewing-like manner across the surfaces of a dry adhesive to acquire sufficiently large data sets in order to both assess trends in adhesion forces and spatial variations in these measurements. The shear induced alignment of the fibrils increases the adhesion force measured for polymer-based fibrils, which is consistent with prior studies using macro-scale measurements of adhesion forces after shear alignment. This shear induced alignment of the fibrils increases the number of contact points between the cantilever and the fibrils. This lateral movement between the cantilever and sample also increase the variability in observed interactions and, thus, variations in measured adhesion forces. Results of these studies coincided with predictions from theoretical models and prior research in this field. This new implementation of the shear induced alignment of fibrillar arrays and the subsequent measurement of their adhesion forces expands our ability to understand structure-function correlations in nano-structured dry adhesives. Development of improved methods of making and using these bio-inspired adhesives could benefit from this adaptation of scanning probe microscopy techniques for measuring adhesion forces from normal and shear induced contact.

5.6. Acknowledgements

This work was supported in part by the Natural Sciences and Engineering Research Council (NSERC) of Canada, and the Canada Research Chairs Program (B.D. Gates). This work made use of 4D LABS shared facilities supported by the Canada Foundation for Innovation (CFI), British Columbia Knowledge Development Fund (BCKDF), Western Economic Diversification Canada, and Simon Fraser University. We appreciate the assistance of Jason Bemis at Asylum Research for assistance in co-developing the software necessary for measuring adhesion forces resulting from shear induced alignment of fibrils using scanning probe microscopy techniques. We also thank Michael C.P. Wang for his assistance with atomic force microscopy.

5.7. References

[1] K. Autumn, M. Sitti, Y. A. Liang, A. M. Peattie, W. R. Hansen, S. Sponberg, T. Kenny, R. Fearing, J. N. Israelachvili, R. J. Full, *Proc. Natl. Acad. Sci. U.S.A.* **2002**, *99*, 12252.

[2] E. Arzt, S. Gorb, R. Spolenak, *Proc. Natl. Acad. Sci. U.S.A.* **2003**, *100*, 10603.

[3] K. Autumn and N. Gravish, *Phil. Trans. R. Soc. A* **2008**, *366*, 1575.

[4] A. K. Geim, S. V. Dubonos, I. V. Grigorieva, K. S. Novoselov, A. A. Zhukov, and S. Y. Shapoval, *Nat. Mater.* **2003**, *2*, 461.

[5] G. Huber, S. N. Gorb, R. Spolenak, and E. Arzt, *Biol. Lett.* **2005**, *1*, 2.

[6] M. P. Murphy, S. Kim, and M. Sitti, *ACS Appl. Mater. Interfaces* **2009**, *1*, 849.

[7] D. Sameoto and C. Menon, *J. Micromech. Microeng.* **2009**, *19*, 115002.

[8] D. Y. Lee, D. H. Lee, S. G. Lee and K. Cho, *Soft Matter* **2012**, *8*, 4905.

[9] K. Autumn, *MRS Bulletin* **2007**, *32*, 473.

[10] H. H. Schleich, W. Kästle, *Amphibia-Reptilia* **1986**, *7*, 141.

[11] K. Autumn, Y. Liang, T. Hsieh, W. Zesch, W.-P. Chan, T. Kenny, R. Fearing, and R. J. Full, *Nature* **2000**, *405*, 681.

[12] K. Autumn, M. Sitti, Y. A. Liang, A. M. Peattie, W. R. Hansen, S. Sponberg, T. Kenny, R. Fearing, J. N. Israelachvili, and R. J. Full, *Proc. Natl. Acad. Sci. U.S.A.* **2002**, *99*, 12252.

[13] G. Huber, S. N. Gorb, R. Spolenak, and E. Arzt, *Biol. Lett.* **2005**, *1*, 2.

[14] N. Gravish, M. Wilkinson, and K. Autumn. *J. R. Soc. Interface* **2008**, *5*, 339.

[15] B. Zhao, N. Pesika, K. Rosenberg, Y. Tian, H. Zeng, P. McGuiggan, K. Autumn, and J. Israelachvili, *Langmuir* **2008**, *24*, 1517.

[16] S. Niederegger and S. N. Gorb, *J. Comp. Physiol. A* **2006**, *192*, 1223.

[17] J. O. Wolff and S. N. Gorb, *Sci. Rep.* **2013**, *3*, 1101.

[18] K. Autumn, A. Dittmore, D. Santos, M. Spenko, and M. Cutkosky, *J. Exp. Biol.* **2006**, *209*, 3569.

[19] Y. Tian, N. Pesika, H. Zeng, K. Rosenberg, B. Zhao, P. McGuiggan, K. Autumn, and J. Israelachvili, *Proc. Natl. Acad. Sci. U.S.A.* **2006**, *103*, 19320.

[20] B. Chen, P. D. Wu, and H. Gao, *J. R. Soc. Interface* **2008**, *6*, 529.

[21] K. Kendall, *J. Phys. D: Appl. Phys.* **1975**, *8*, 1449.

[22] T. Yamaguchi, N. Gravish, K. Autumn and C. Creton, *J. Phys. Chem. B* **2009**, *113*, 3622.

[23] C. Majidi and R. S. Fearing, *Mater. Res. Soc. Symp. Proc.* **2008**, *1086*, U01-11.

[24] Q. H. Cheng, B. Chen, H. J. Gao, and Y. W. Zhang, *J. R. Soc. Interface* **2012**, *9*, 283.

[25] Alexander Filippov, Valentin L. Popov, and Stanislav N. Gorb, *J. Theor. Biol.* **2011**, *276*, 126.

[26] B. Schubert, J. Lee, C. Majidi, and R. S. Fearing, *J. R. Soc. Interface* **2008**, *5*, 845.

[27] J. Lee, R. S. Fearing, K. Komvopoulos, *Appl. Phys. Lett.* **2008**, *93*, 191910.

[28] M. Varenberg and S. Gorb, *J. R. Soc. Interface* **2007**, *4*, 721.

[29] A. Parness, D. Soto, N. Esparza, N. Gravish, M. Wilkinson, K. Autumn and M. Cutkosky, *J. R. Soc. Interface* **2009**, *6*, 1223.

[30] S. N. Gorb, M. Sinha, A. Peressadko, K. A. Daltorio and R. D. Quinn, *Bioinspir. Biomim.* **2007**, *2*, S117.

[31] D. Santos, B. Heyneman, S. Kim, N. Esparza, and M. Cutkosky, presented at IEEE Int. Conf. on Robotics and Automation, Pasadena, CA, USA, May 19-23, 2008.

[32] D. S. Kim, H. S. Lee, J. Lee, S. Kim, K-H. Lee, W. Moon, and T. H. Kwon, *Microsyst. Technol.* **2007**, *13*, 601.

[33] M. L. B. Palacio, B. Bhushan, and S. R. Schricker, *Mater. Lett.* **2013**, *92*, 409.

[34] B. Bhushan, X. Ling, A. Jungen, and C. Hierold, *Phys. Rev. B* **2008**, *77*, 165428.

[35] C. Zhang, J. Zhou, D. Sameoto, X. Zhang, Y. Li, H. W. Ng, C. Menon, and B. D. Gates, *J. Adhes. Sci. Technol.* **2012**, *28,* 320-336.

[36] D. Sameoto, Y. Li, C. Menon, *Advances in Science and Technology, Trans. Tech. Publications* **2008**, *54*, 439.

5.8. Supporting Information

5.8.1. Statistical analysis of experimental results

As described in the chapter, 400 measurements were taken in each experiment. Histograms of each experiment are plotted showing an obvious departure from a Gaussian distribution. Traditional statistical measurements may be suitable to describe this data. Therefore, three statistical indicators-- the median, the 12.5% trimmed mean, and the standard deviation -- were chosen to describe the majority of the population and the span of the data. The median was derived from the middle value of the entire data set and the standard deviation was calculated from the square root of the data variance. Both of these terms are traditional indicators of variance in a dataset, and each represents the central tendency and range over which the data spans. Trimmed mean is a measure from robust statistical analysis to estimate the central tendency of the dataset [1-3]. We chose the trimmed mean analysis because we have a large quantity of data points and the original data is heavily left skewed. The skewness of the data is not expected since the sample is prepared by a uniform process and the measurements are taken without any discrimination. We suspected that there are outliers in the original data from experimental error or sample contamination. The percentage of trimmed data is determined by assessing a normal probability plot. Figure 5.6 depicts the data before and after trimming the head and tail, which contain suspected outliers. The original data (Figure 5.6a) indicates that the populations are left skewed due to the long tail at a high probability. Some data points at either end of the population (low or high probability) deviated from the main group as defined by the dash. After trimming the 12.5% of suspected outliers from either end of the data, the resulting normal probability plot is obtained (Figure 5.6b). This trimmed population is symmetric and is closer to a normal distribution, but still contains long tails. The calculated mean of the trimmed data reflex a more accurate measure of the central tendency.

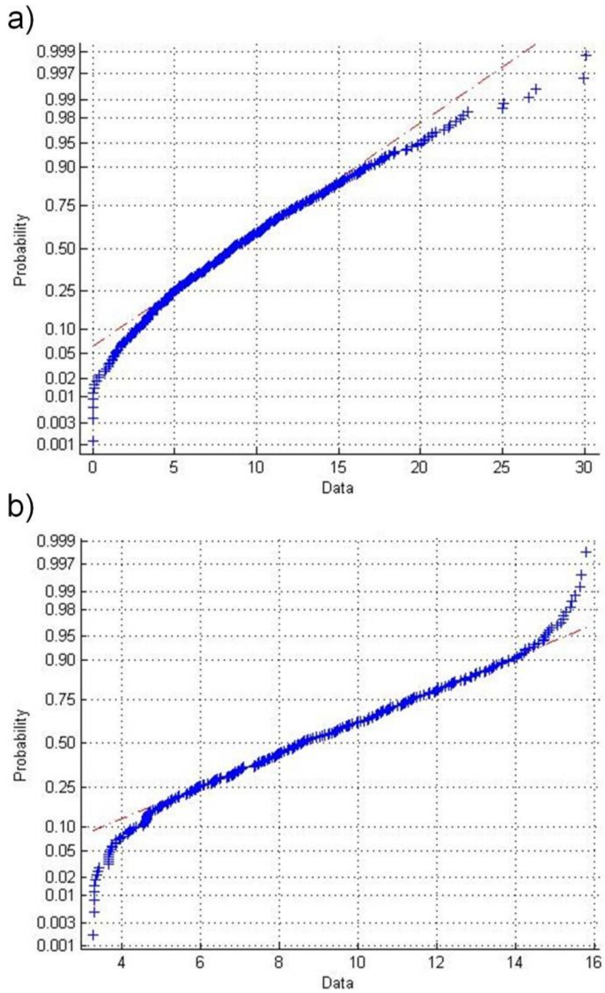

Figure 5.6. **Normal probability plots of the data (a) before and (b) after trimming 12.5% from the head and tail of the data. The red dash line indicates the data that fits to a normal distribution, and the blue markers represent each data point. After trimming of the data, the distribution is more symmetric and is closer to a normal distribution.**

5.8.2. Force-Time (FT) response of a single measurement using AFM

A typical time response of the forces acting on the cantilever in a force measurement is shown in Figure 5.7. During approach of the cantilever to the fibrillar surface a “snap-in” force is observed at ~0.7 sec. The “snap-in” force is due to a sudden attraction of the electrostatic or van der Waals forces between the two surfaces. The subsequent compressive force rapidly increases to a pre-set force of ~10 nN. The cantilever then starts to move horizontally, with a slight increase of cantilever deformation. The compressive force normal to the test surface then is maintained for ~1 sec. Slight oscillation was observed during this period of time as the cantilever moves horizontal to the test surface. The cantilever is subsequently lifted from the sample with a peak adhesion force of ~19.8 nN. The deformation of the cantilever returns to its original state with a force of ~0 nN. This force-time (FT) curve can be compared with the force-distance (FD) curve as reported in the manuscript to correlate each of these interactions and cantilever deformation.

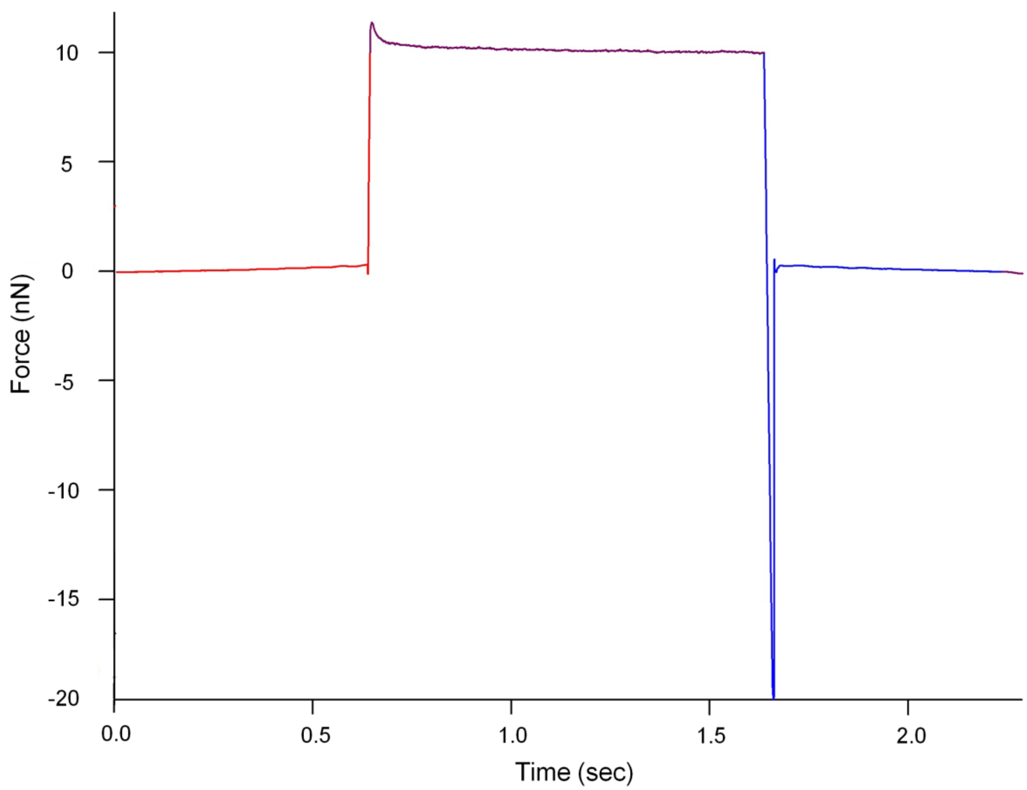

Figure 5.7. Force-Time (FT) curve of a typical drag test. The cantilever first approaches the sample with a small "snap-in" representing the engagement of cantilever to the sample surface. The cantilever then reaches the pre-set loading force of ~10 nN followed by a shear induced contact of the cantilever over the test surfaces. The alignment of the fibrils is associated with the oscillations in the measured force during the drag experiments. An adhesion force (~ 19.8 nN) of the test surface is recorded as the cantilever is retracted vertically from the surfaces following the shear induced contact.

5.8.3. References for supporting information

[1] D. M. Erceg-Hurn, V. M. Mirosevich, *Am. Psychol.* **2008**, *63*, 591.

[2] R. R. Wilcox, H. J. Keselman, *Psychol. Methods.* **2003**, *8*, 254.

[3] R. R. Wilcox, Robust, Fundamentals of Modern Statistical Methods, Springer, New York, NY, USA 2010.

Chapter 6.

Optimization of parameters used in shear-induced adhesion measurements using scanning probe techniques

The ability to manipulating test substrate is provided by the technique in the previous chapter intrigued the study of optimal parameters to obtain desire fibril-substrate interactions. By closely examining the parameters involved in the shear-induced adhesion measurements, substrate drag distance, drag velocity and retract velocity were investigated for their influence on the adhesion forces. Experimental results revealed the fibril-substrate interaction which provided useful insight of adhesive applications. This chapter aims at solving the question raised in OBJECTIVE 4. The following contents are submitted as paper: Yasong Li, James H.-W. Zhou, Cheng Zhang, Carlo Menon and Byron D. Gates, “Harnessing tunable scanning probe techniques to measure shear enhanced adhesion of gecko-inspired fibrillar arrays” to ACS Applied Materials & Interfaces.

6.1. Abstract

The hierarchical arrays of mesoscale to nanoscale fibrillar structures on a gecko’s foot enable the animal to climb surfaces of varying roughness. Adhesion force between the fibrillar structures and various surfaces is maximized after the gecko drags its foot in one direction, which has also been demonstrated to improve the adhesion forces of artificial fibrillar arrays. Essential conditions that influence the magnitude of these interactions include the lateral distance travelled and velocity between the contacting surfaces, as well as the velocity at which the two surfaces are subsequently separated. These parameters have, however, not been systematically investigated to

assess the adhesion properties of artificial adhesives. We introduce a systematic study that investigates these conditions using a scanning probe microscope to measure the adhesion forces of artificial adhesives through a process that mimics the mechanism by which a gecko climbs. The measured adhesion response was different for arrays of shorter and longer fibrils. The results from 9000 independent measurements also provide further insight into the dynamics of the interactions between fibrillar arrays and contacting surfaces. These studies establish scanning probe microscopy techniques as a versatile approach for measuring a variety of adhesion properties of artificial fibrillar adhesives.

Keywords: adhesion forces, dry adhesive, nanostructured fibrils, scanning probe microscopy, shear loading

6.2. Introduction

Geckos can maneuver themselves freely on various surfaces, irrespective of gravity, thanks to millions of nano-size fibrils on their climbing feet [1]. Numerous intermolecular forces collectively form a strong adhesion through contact between these slender fibrils and the surfaces upon which the gecko is climbing. The hierarchical fibrillar structures on the gecko's feet have a critical dimension in the range from micrometers to nanometers that provide both a compliancy and stickiness with the climbing surfaces [2]. The bonds formed between the nanofibrils and the contacting surfaces reach their strongest values after the gecko applies a lateral dragging movement of the foot towards their body [3]. This dragging movement has been proven to assist in the fibril alignment with the surfaces, increasing the contacting area of the interfaces and, hence, improving the adhesion forces measured in subsequent pull up experiments [4-5]. Test procedures that include this dragging movement have been named the "Load-Drag-Pull" (LDP) method [6]. This method can be described in the following three steps: i) the fibrillar patch first vertically approaches the contacting surfaces; ii) a lateral shear force is applied in one direction to the patch upon contact with the surfaces; and iii) a vertical withdrawing force is applied to the patch until the two interfaces have been completely separated. This test procedure has been performed for the analysis of gecko adhesives [7-8] and artificial polymeric adhesives [9-11]. Results of these studies generally demonstrated an increase of adhesion measured using the LDP method in contrast to methods without the dragging movement. These results further support the idea that fibrils are aligning during the dragging process. Alignment of the fibrils optimizes the contact area during these LDP based adhesion force measurements.

Geckos have developed certain patterns to efficiently climb. Autumn et al. [12] investigated the dynamics of a living gecko while climbing vertically at different speeds. Geckos generally use a stable stride pattern no matter how fast they climb, indicating that there should be an optimal set of attaching and detaching parameters that the gecko uses for efficient climbing. Artificial fibrillar adhesives are designed to mimic the geometry of the gecko fibrillar adhesives, yet can have a significant variation in their shape, size and density depending on the different preparation methods [13-16]. There will also be an optimal set of parameters to efficiently utilize each specific type of artificial adhesive. The LDP characterization method described above could be adapted as a technique to identify an optimal set of operating parameters for artificial engineered adhesives. The outcome of this study would be beneficial to applications involving artificial adhesives, such as climbing robots [17], surgical tapes [18] and handling tools of microelectronic chips [19].

The LDP technique for measuring adhesion forces involves a dynamic interaction of the contacting interface. These dynamics can be characterized by the lateral distance and velocity of movement between the contacting surfaces and the velocity at which the two surfaces are subsequently separated. In addition to measuring adhesion forces, frictional forces are one of the most investigated properties using the LDP method [9-11, 20-22]. Studies by Gravish et al. [23] demonstrated a different friction and adhesion response of gecko setae and synthetic fibrillar adhesive while varying the lateral drag velocities during LDP based measurements. Puthoff et al. [24] also provided evidence of the effects of drag distance and drag velocity on the adhesion and friction of fibrillar adhesives measured using LDP methods. Similar results were reported for this study on synthetic dry adhesives. The drag distance and velocity were, generally, directly proportional to the measured adhesion and friction forces when studying gecko setae. The result from the analysis of artificial fibrillar adhesives indicated that the adhesion and friction response each reach a point of saturation at a certain combination of drag distance and velocity. Both of the studies used relatively large areas of each sample. For example, an analysis would use an entire gecko seta and an artificial adhesive of a similar size (e.g. ~5 mm^2 in [24]).

A technique developed in our laboratory demonstrated the utility of a scanning probe microscope (SPM) to characterize the uniformity and adhesion properties of fibrillar arrays [5,25]. This technique enabled the automatic collection of data on adhesion response and the ability to observe the interactions between two contacting substances for a smaller number of fibrils (i.e. small contact area). Experimental results indicated that adhesion forces were randomly distributed across fibrillar arrays, even for those that are spatially distributed in a uniform manner. This phenomenon indicated that each measurement could produce a unique result even though the test conditions were almost identical. This SPM based technique provides flexibility to conduct measurements either with or without the inclusion of a lateral motion. Various parameters that control the movement of the two contacting surfaces are tunable for each measurement, within the limitations of the SPM system.

In this study, we investigated the influence of lateral drag distance, drag velocity and the velocity at which two substrates are separated during LDP measurements used to characterize an artificial fibrillar adhesive. Adhesion forces between arrays of polymeric fibrils and a flat atomic force microscope cantilever were measured utilizing the SPM techniques described above. These techniques offer the flexibility of independently controlling each of the measurement parameters. The lateral drag distance, drag velocity and cantilever retract velocity were each individually studied for their effect on the measured adhesion forces. Statistical analysis was performed on the large data sets collected under same test conditions at different locations of each sample. These results revealed an optimal set of parameters necessary to obtain desirable performance of the artificial fibrillar adhesive. These optimal parameters are potentially useful for various applications requiring a quick attachment and release mechanism.

6.3. Results and Discussion

In the study described in Chapter 5, we introduced a comparison of two methods to characterize adhesion forces between surfaces through the use of a SPM system [5]. One of these methods, referred to as a Push-Pull (PP) method, manipulates an SPM controlled cantilever to vertically approach an array of fibrillar nanostructured surfaces until these opposing contacting surfaces are in intimate contact. The cantilever is subsequently withdrawn in a vertical motion until the two substrates are completely separated. The second method, referred to as the Load-Drag-Pull (LDP) method, introduces an additional movement of the cantilever between the other two movements used in the PP method. During this new step, the cantilever moves horizontally (i.e. applies a shear force) across the fibrillar arrays after the two substrates were brought into a complete contact during the preloading of the compression force. A vertical retraction or pull up of the cantilever follows this drag movement of the cantilever. The schematics in Figure 6.1 depict the differences between the two methods. The maximum deflection of the cantilever is converted into force based on a pre-test calibration of the cantilever spring constant. The force measured upon cantilever retraction is the adhesion force recorded as a single data point in the datasets used for statistical analysis. The use of an SPM system to incorporate the shear dragging movement proved to be an effective method for enhancing the adhesion force between a flat cantilever and the fibrillar arrays, which is also the method used by the biological adhesion system (e.g., gecko). As indicated from the existing research [12], geckos use a relatively stable process of gripping and releasing of surfaces regardless of their climbing speed for a given gait. The animal generally increases stride length, which is the distance between two steps, instead of changing the stride frequency, leg phase (sequences of movements within one step) and attachment/detachment time (intervals of the interaction between the feet and the contact surfaces until forming complete contact) [12]. These experimental results suggest that there should be an optimal set of parameters that the animals use to create a firm grip with the climbing surfaces. The complete set of optimal parameters has not yet been confirmed with living animals. The rate-dependent adhesion force during the attachment process has been proven using separated gecko setae and artificial micro-scale dry adhesives, but the results provide no specific optimal set of parameters [12,23-24]. Considering the actual size of the fibrillar structure in the biological system, the SPM measurement system that we adapted for measuring nanoscale fibrillar arrays would be a suitable platform to provide further insight into a set of optimal parameters. Based on the dynamics taking place during contact between two surfaces, the force describing this interaction is related to the derivative of velocity and the second derivative of distance. Controlling the velocity and displacement of a substrate under test can, therefore, modify its interactions with an array of fibrils. Thus, three parameters that are of specific interest for further investigation include the drag distance (the relative displacement of two substrates in a lateral direction during the process of “drag”), the drag velocity (the relative velocity of two substrates in a lateral direction during the process of “drag”) and the retract velocity (the relative velocity of two substrates in a vertical direction during the process of “pull”).

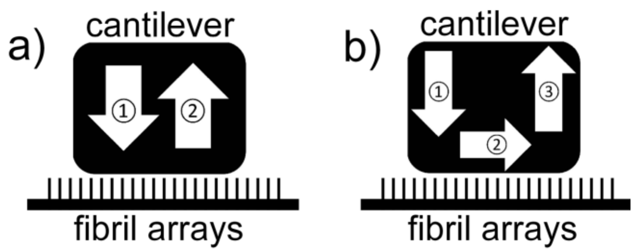

Figure 6.1. Schematic depiction of two methods used to measure adhesion forces of nanoscale fibrillar arrays: (a) the Push-Pull (PP) method, and (b) the Load-Drag-Pull (LDP) method. The PP method is implemented by manipulating a scanning probe microscope (SPM) controlled tipless cantilever to vertically approach the fibrillar arrays (step 1) until the interaction force between the two surfaces reaches a pre-set value. The cantilever is subsequently withdrawn from the fibrillar arrays in a vertical motion (step 2) until achieving separation between the fibrils and the cantilever. The LDP method includes an additional step (see step 2 in b) between two identical steps to those of the PP method. In this additional step the cantilever is dragged in a lateral motion over the surfaces of the fibrillar arrays to enhance fibril-cantilever interactions.

6.3.1. Investigation of the drag distance in LDP experiments

The optimal drag distance should provide insight into the point at which a system achieves maximum alignment of the fibrils. Excessive drag applied to the fibrils during the initial contact with a flat surface will reduce the benefit observed by the additional dragging movement. On the other hand, a relatively long drag distance will increase the likelihood of fibril damage. The process of the fibril alignment can be observed from the

Force-Time (FT) curve, such that the one shown in Figure 6.2 that was obtained using an artificial fibrillar adhesive (see experimental section for further details). The interaction force measured over the time elapsed during the contact between the cantilever and fibrillar surfaces are observed in this FT curve for one measurement cycle. In Figure 6.2, the cantilever started at a position of non-contact (showing no interaction force in the beginning of the curve), and the cantilever was brought into contact with the fibrillar arrays until the compression/preloading force reaches a preset value (compression forces are indicated by a positive value). The cantilever was subsequently dragged over a specific distance, which was varied as a test parameter (insets in Figure 6.2), at a dragging speed of 20 μm/s. The cycle ended with a 2 s dwell time, followed by a vertical retraction of the cantilever to separate the surfaces as indicated by the negative force in the curve. The lowest value in the force curve was recorded as the adhesion force for a single measurement. The measured force oscillated as the cantilever was dragged across the fibrillar surfaces, as indicated in the insets of Figure 6.2. This oscillation corresponds to the variable contact of the cantilever with the roughened surfaces using an interaction force of ~5 nN. The time period over which the oscillation occurred was proportional to the dragging distance. During this lateral shear, the positive “spikes” in the force curve were attributed to the cantilever encountering an array of newly contacted fibrils. The initial interactive force is restored when the cantilever continues moving over an array of aligned fibrils. When a sufficient number of these fibrils release from the cantilever, a retraction force is measured as indicated by the negative “spikes” in the force curve. A similar effect was observed in the FT curves for both the longer (~1 μm) and shorter (~0.1 μm) fibrils. Figure 6.2 only demonstrates the FT curves for the shorter fibrils.

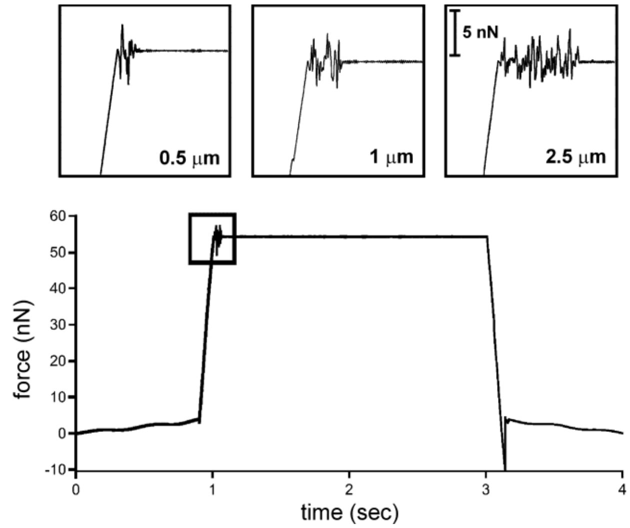

Figure 6.2. **A representative Force-Time (FT) curve (bottom) measured using the LDP method for a cantilever in contact with an array of fibrils (in this example the fibrils had an average height of ~ 0.1 μm). Drag velocity was set to 20 μm/s. The magnified views of FT curves (from the region denoted by the black box) depict the force response corresponding to different drag distances (e.g., 0.5, 1.0 and 2.5 μm, respectively). The length of time over which the measured forces oscillate corresponds to the distance (and thus the period of time) the cantilever is moved across the fibrillar arrays. The range of the oscillations in force during this drag step of the LDP method is ~5 nN.**

The effect of drag distance on the measured adhesion force was statistically analyzed for the samples consisting of longer (~1 μm) and shorter (~0.1 μm) fibrils. The drag and retract velocities were maintained at 20 μm/s and 1 μm/s, respectively, while 400 measurements were obtained for each of the different drag distances (0.5, 1 and 2.5 μm). The ratio of drag distance to fibril length (referred to as the distance-to-length ratio, or DL ratio) for the sample of shorter fibrils was 5, 10 and 25, while the DL ratio for the sample of longer fibrils was 0.5, 1, and 2.5. The results of measurements performed using the PP method are also included for comparison. Figure 6.3 and 6.4 are histograms for measurements obtained from samples with fibril lengths of ~0.1 μm and ~1 μm, respectively. For the shorter fibrils (~0.1 μm), the longer drag distances resulted in a smaller adhesion force. However, for the longer fibrils (heights of ~1 μm), the longer drag distances corresponded to higher average adhesion forces. Considering the DL ratio and the median or trimmed mean of the adhesion measurements, the tests at a DL ratio of 5 for the sample of shorter fibrils gave a similar result to that from the PP method. In contrast, the results of tests at a DL ratio of 2.5 for the sample of longer fibrils gave the highest measured adhesion forces. The data suggest that a proper alignment of the fibrillar arrays could be achieved using a DL ratio between 0 and 5.

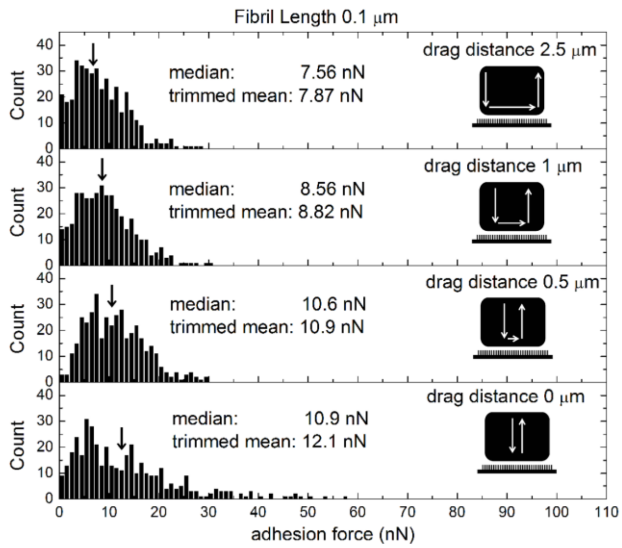

Figure 6.3. Histograms of adhesion forces measured by the LDP and PP methods for an array of relatively short fibrils (average heights of ~ 0.1 μm) for different drag distances. Drag velocity was set at 20 μm/s. Arrows above the histograms indicate the location of the medians for each set of data.

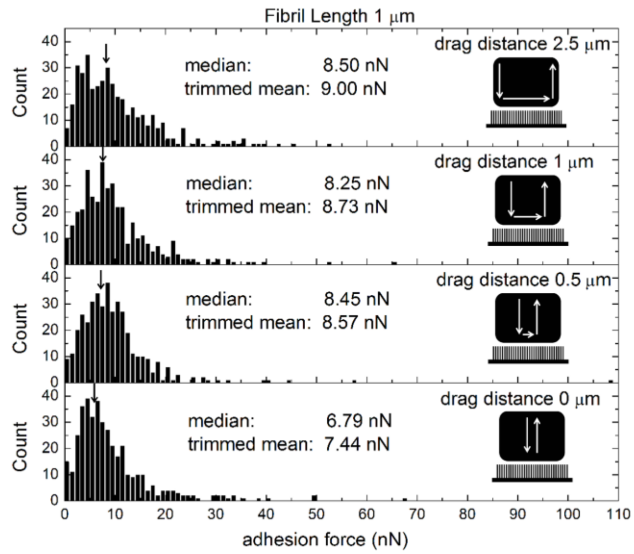

Figure 6.4. **Histograms of adhesion forces measured by the LDP and PP methods for arrays of relatively long fibrils (average heights of ~1 μm) under different drag distances. Drag velocity was set at 20 μm/s. Arrows above the histograms indicate the location of the medians in each set of data.**

In the measurements using the longer fibrils (heights of ~1 μm), the cantilever start dragging after compressing the fibril arrays to the preset force. Most of the fibrils underneath the cantilever might be compressed into a folded structure at this point in the measurement. The shear movement of the cantilever moves from this initial contact point, stretching the attached fibrils to an extended position. Fibrils will likely point in the same direction that the cantilever is moving. Fully extended fibrils would expose more of their surface area to potential contact with the cantilever, creating more contact area. Thus higher adhesion forces would be measured during the subsequent cantilever pull-up. However, if the dragging distance is much greater than the average length of the fibrils, the result could be a stick-slip effect as reported in [28]. The sudden release of the fibrils from the flat cantilever causes an unstable interaction and, subsequently, a loss of the optimized contact points formed during the previous shear movement. In the case of the shorter fibrils (heights of ~0.1 μm), the adhesion forces measured by the PP method are the result of contact between the cantilever and both the fibrils and the substrate recesses between the fibrils. After initiating the drag movement, the cantilever contacted other fibrils and reduced its contact with the recessed regions. A decrease in the measured adhesion force for these samples in correlation to extensive dragging reflects the reduction of contact area between the sample and the tipless cantilever (Figure 6.3).

A significant variation was observed in the distribution of the data for the shorter fibrils (Figure 6.3). The longer the drag distance, the tighter the observed distribution in measured adhesion force. Although a lower average adhesion force was measured for a drag distance of 2.5 μm, its tighter distribution indicates the contact between the fibrils and the cantilever was more uniform between different measurements. A similar phenomenon was observed in the data from the longer fibrils. The distributions in the data for all drag distances had a similar appearance for the longer fibrils (Figure 6.4). The data also indicates that any shear movement during the fibril-cantilever interactions will increase the adhesion force in comparison to that measured by the PP method. The effect of fibril alignment during the “drag” step is more obvious in the longer fibrils. The p-values of the Kruskal-Wallis ANOVA, a non-parametric test suitable for non-Gaussian distributions [27], on data collected for each sample was significantly small (<0.01) suggesting that the drag distance is significantly influencing the measured adhesion force. The influence of drag distance on the measured adhesion force revealed that the interactions between the flat cantilever and the fibrillar arrays are not as simple as predicted by classical friction laws and contact mechanics. Further studies that varied the drag velocity were performed to further investigate the range of effects resulting from the lateral shear movements of the cantilever.

6.3.2. Investigation of the drag velocity in LDP experiments

Velocity of the cantilever during the drag movement of the LDP measurements could be important for its influence on providing sufficient time to form a significant number of interactions between the contacting surfaces. Figure 6.5 depicts a typical FT curve of a LDP measurement on the ~0.1-μm tall fibrils. The magnified traces within the insets located above the FT curve depict the force response during the dragging process for different drag speeds. The magnitude of the variation in force observed during this dragging increased significantly within increase in the speed of the lateral shear. The magnitudes of the oscillation in force measured at a drag speed of 2, 20 and 200 μm/s were ~1, ~3 and ~15 nN, respectively. The duration of the drag can also be observed in these plots. A 2 s dwell time was introduced after the drag movement in order to provide a sufficient amount of time for the system under study to relax and maximize the interactions between the contacting surfaces. The energy needed to overcome the maximum static friction of the sample is theoretically the same for the higher drag speed as that for the lower drag speed. Therefore, when the drag speed is increased (i.e. drag time decreases) the force response should increase proportionally based on the conservation of energy.

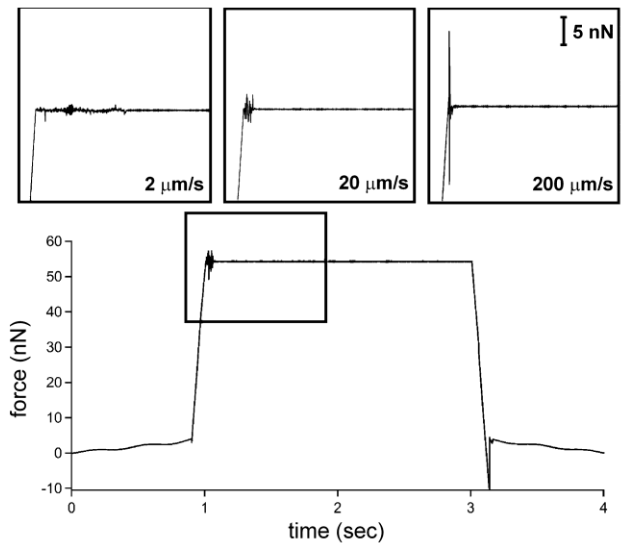

Figure 6.5. A typical Force-Time (FT) curve (bottom) measured using the LDP method for an array of 0.1 μm tall fibrils. Drag distance was set at 1 μm. The insets are magnified FT curves that depict the variation observed in these curves for different drag velocities (e.g., 2, 20, and 200 μm/s) using the LDP method. The oscillations in the measured force increased in proportion to the drag velocity (as noted in the insets) when the cantilever was in motion (i.e. the dragging step) while in contact with the fibrillar arrays. The magnitude of oscillations in the measured force varied from ~1 nN to ~15 nN.

A slower drag movement could, however, generate a higher measured adhesion force because of a longer interaction time between the two types of surfaces establishing more points of contact. This hypothetical situation is supported by results of the statistical analysis of the LDP measurements from samples having both longer (~1 μm) and shorter (~0.1 μm) fibrils. Histograms for the results of the LDP measurement on the shorter fibrils are plotted in Figure 6.6. Although the differences in average adhesion force between the three different drag speeds are within 1 nN of each other, the slower drag speed had a slightly higher average adhesion force than the results of the faster drag speed. The variance in the data, from slower to faster drag, was 36.8, 31.5 and 28.4 nN. Levene's test was used to indicate if equal variance existed between the groups of data [27] (see experimental section for further details). The p-value of Levene's test was 0.079, which indicated a small possibility for equal variance among these data sets. The lower variance in the data for the higher drag speed implies that the uniformity of the adhesion force is greater at fast lateral shear movements. The shapes of the distribution in results for all the three sets of data were similar to each other. The decrease in average adhesion force in the faster drag experiments might also be the result of surface damage due to the high forces applied over a relatively short duration to overcome frictional forces. The rapid movement of the cantilever might also introduce more random points of contact with the sample, such as slip between the fibrils and the flat cantilever. This tendency was more obvious in the experiments performed on the samples with longer fibrils (Figure 6.7).

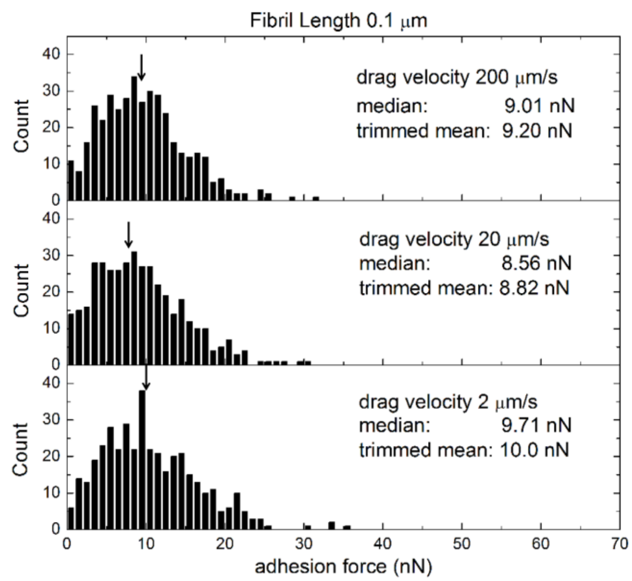

Figure 6.6. Histograms of the adhesion forces acquired by the LDP method for arrays of relatively short fibrils (average heights of ~0.1 μm) using different drag velocities (e.g., 2, 20 and 200 μm/s). Drag distance was set at 1 μm. Arrows indicate the location of the medians of each set of data.

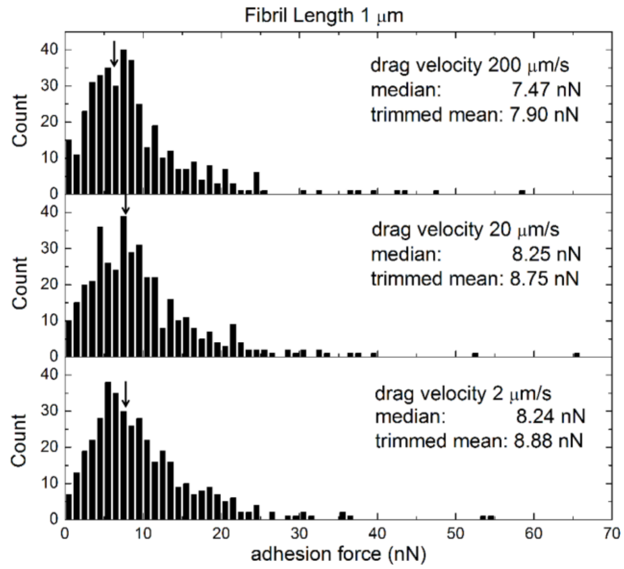

Figure 6.7. **Histograms of adhesion forces measured by the LDP method for arrays of relatively long fibrils (average height of ~1 μm) with different drag velocities (e.g., 2, 20 and 200 μm/s). Drag distance was set at 1 μm. Arrows indicate the location of the medians within each set of data.**

The average adhesion force decreases in proportion to an inverse in drag velocity in the measurements using longer fibrils. Differences between each of these sets of data were within 1 nN, but the variance in the data, from 2 μm/s to 200 μm/s, was 49.7, 57.0 and 52.7 nN, respectively. These values were higher than the results obtained for the shorter fibrils. The p-value of the Levene's test is 0.845, showing a much higher tendency of equal variance among the datasets obtained for the longer fibrils in comparison to the shorter fibrils. The more equal the calculated variance for the data indicates that the test results were more consistent for the average adhesion force. In particular, the force distributions obtained at shear velocities of 20 μm/s and 200 μm/s had very similar shapes. Despite the significant change in drag speed, the similar results obtained for these two sets of data implied that the interactions between the cantilever and the fibrils were similar, and that the possibility of fibril damage was very limited. The measured adhesion at the median and trimmed mean (both ~8 nN) for LDP measurements at 20 μm/s drag velocity were coincident with the peak adhesion force in the histogram, suggesting a central tendency of the data set that matches the histogram shape. The other datasets in this particular study did not have the same property. The p-values of the Kruskal-Wallis ANOVA for the samples of shorter and longer fibrils were

0.013 and 0.042, respectively. This result indicated that drag velocity did not significantly influence on the adhesion force in contrast to the results of varying the drag distance. The loading and dragging processes of the LDP method have been studied by varying drag distance and drag velocity. These studies revealed further insight into contact formation between the fibrils and the tipless cantilever. Disrupting the points of contact during the subsequent pulling movement was studied by systematically investigating the vertical retraction of the cantilever from these fibrillar surfaces.

6.3.3. Investigation of the retract velocity in LDP experiments

The process of retraction of the cantilever from the fibrillar surfaces contains important information on the release of the established contacts. Adhesion force recorded for each measurement was defined as the minimum force, or maximum attraction force, achieved during the cantilever retraction. The adhesion force though does not represent all aspects of the detachment process. A series of typical measurements obtained using different pull up speeds for the cantilever, representing the portion of the FT curves that correlate with the period of cantilever retraction, were plotted in Figure 6.8. All of these traces have a sharp peak at the period in time when the two contacting surfaces were completely separated. The peak force indicates that the cantilever was significantly bent right before the moment of separation. Significant oscillations were observed when the retract speeds were relatively slow. These oscillations might be the result of re-engaging interactions between the cantilever and the fibrils. After the sudden separation of the two types of surfaces, the thin cantilever itself would oscillate for a few cycles in resemblance to a springboard after unloading an applied force. The cantilever could further interact with the fibrillar surfaces during these cycles depending on the distance of retraction, which was directly proportional to the retract velocity. Some of the observed oscillations might, therefore, be attributed to further interactions between the cantilever and the arrays of fibrils during the retraction step. As the speed of retraction increased, the possibility of this interaction decreased as observed in the data plots (Figure 6.8). These oscillations did not change the adhesion performance of the fibrillar samples.

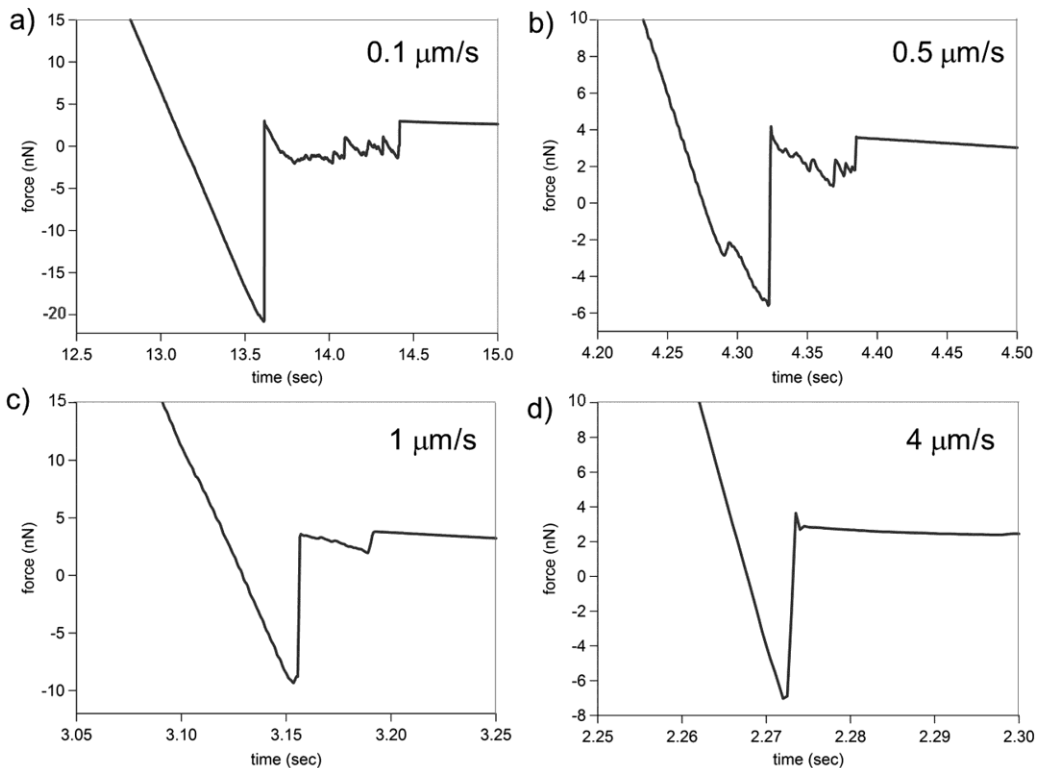

Figure 6.8. Representative force-time curves corresponding to different retract velocities, a) 0.1 μm/s, b) 0.5 μm/s, c) 1μm/s, and d) 4 μm/s, following LDP based measurements when separating the SPM controlled cantilever from an array of fibrils (average heights of ~0.1 μm). The figures depict the portion of the FT curves upon reaching complete detachment of the cantilever from the fibrillar surfaces. Drag distance and velocity were set at 1 μm and 20 μm/s, respectively.

Details of the detachment process were investigated by appropriately scaling the FT curves in Figure 6.8. The slope of the FT curve at the highest retract velocity was actually much steeper than it appears. A rapid retraction of the cantilever may cause perturbation to the established contacts even before a complete detachment. The influence of the retraction velocity can be more clearly observed in a statistical analysis of the adhesion forces for the arrays of shorter and longer fibrils (Figure 6.9 and 6.10, respectively). Both samples had a lower measured adhesion force for LDP measurements with a higher retract velocity.

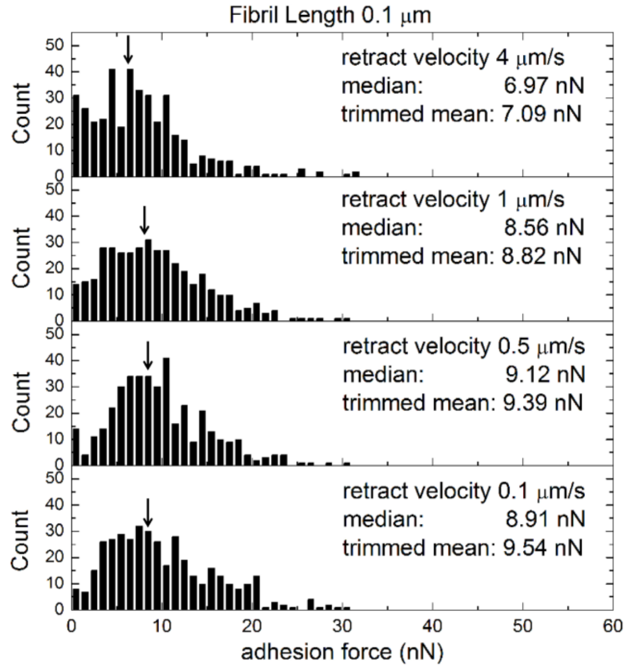

Figure 6.9. **Histograms of adhesion forces acquired using the LDP method for an array of ~0.1 μm tall fibrils for different velocities for retraction of the SPM cantilever from these fibrillar surfaces. Drag distance and velocity were set at 1 μm and 20 μm/s, respectively. Arrows indicate the location of the medians in each set of data.**

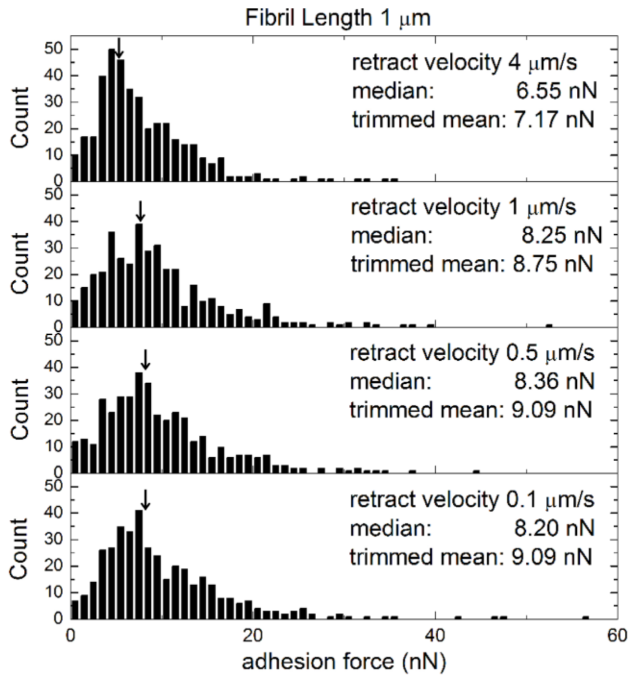

Figure 6.10. Histograms of adhesion forces acquired using the LDP method for arrays of ~1-μm tall fibrils using different retraction velocities of the SPM cantilever. Drag distance and velocity were set at 1 μm and 20 μm/s, respectively. Arrows indicate the location of the medians in each set of data.

In the measurements performed on the arrays of shorter fibrils (Figure 6.9), the shape of the histogram for data obtained using a retract speed of 1 μm/s most closely resembles a normal distribution. This histogram had a flat peak that closely corresponded to the median and trimmed mean. This result suggests a high probability of measuring adhesion forces near the median and trimmed mean. The retract velocity of 0.5 μm/s exhibited the best average adhesion among the four different velocities tested. The variance of adhesion (27.9 nN) measured using a 0.5 μm/s retract velocity was the smallest in all of these measurements. The variance observed in the other sets of data, from lower to higher retract velocities, was 35.9, 31.5 and 45.2 nN. The p-value of Levene's test was 0.376, showing a relatively high possibility for equal variances. A retract velocity of 4 μm/s had the lowest average adhesion and the most symmetric distribution of measured adhesion forces (Figure 6.9) in comparison to the data sets obtained at the other retract velocities. These results indicated instability in the interactions between the cantilever and the fibrillar surfaces caused by the relatively quick withdrawal of the cantilever. It can be also concluded that a less predictable adhesion force can be expected when using a relatively high retract velocity. The overall Kruskal-Wallis p-value was << 0.01, further indicating that retract velocity significantly influences the adhesion force measured by the LDP method.

Similar trends were observed for the average adhesion forces measured for the longer fibrils and the shorter fibrils, but their histograms exhibited a significant difference in overall shape. The highest median and trimmed mean for the adhesion forces were observed for data obtained using a retract velocity of 0.5 μm/s, but these results were similar to those obtained using retract velocities of 0.1 and 1 μm/s (Figure 6.10). The shapes of the histogram for these three sets of data were also a close resemblance of each other. The calculated variances of all four sets of data, from slow to fast retract velocities, were 53.8, 45.8, 57.0 and 30.1 nN, respectively. The p-value of Levene's test was 0.04, indicating a relatively different variance among the datasets. The variance and average adhesion force obtained using a retract velocity of 4 μm/s drastically decreased in comparison to the other tests, suggesting a general degradation in adhesion performance using fast retraction speeds. The Kruskal-Wallis ANOVA p-value is << 0.01, which is a similar result to that obtained for the shorter fibrils. In summary of the measurements using different retract velocities, a fast withdrawal (4 μm/s) of the cantilever decreases the adhesion performance of both the shorter and longer fibrils. A retract velocity of 0.5 μm/s, generally, provides the best adhesion performance for these samples. The retract velocity of the cantilever significantly influences the adhesion force measured using the LDP method.

6.4. Conclusion

Geckos have developed their own way to efficiently climb on different surfaces. Observation on the movement of geckos inspired the development of a Load-Drag-Pull measurement technique using a scanning probe microscope. The utility of the LDP method is to characterize the adhesive properties of materials and to provide further insight into an optimal set of parameters for using materials inspired by the nanosized fibrils on geckos climbing feet. The lateral distance and velocity of the cantilever during the drag step, and the velocity at which the cantilever was pulled away from a surface were studied for their influence on the measured adhesion force of fibrillar samples. In this study, two samples were compared one with shorter (~0.1 μm) fibrils and another with longer (~1 μm) fibrils. A systematic study was performed on each parameter along with a detailed analysis of the information contained within the resulting force-time curves. A further statistical analysis was also performed on the large sets of data collected using the LDP method on a SPM system. The relationship of the tested parameters to the measured adhesion force was not predicted by classical mechanics and friction theories. Observation on the force-time response of the LDP measurements revealed further details into the interactions between the flat cantilever and the fibrillar surfaces. The adhesion force measurements also revealed a difference in response to varying test parameters when comparing the results of samples with different fibril lengths. The drag velocity did not have as significant an influence on the measured adhesion force in comparison to changes in the drag distance and retract velocity. The drag distance had a greater influence on the results obtained for the longer fibrils than for the shorter ones, which was attributed to differences in fibril alignment and overall contact area with the tipless cantilever. Rapid cantilever withdrawal from the fibrillar surfaces generally reduced the measured adhesion forces. A moderate retraction velocity of the cantilever, specifically 0.5 μm/s, provided the highest average adhesion from all the tested velocities in samples of both the longer and shorter fibrils. These results provided insight of the interactions between the cantilever and the fibrillar surfaces, and also guidance for future experiments on the gecko-like fibrillar adhesives. Applications, such as the use of fibrillar adhesives on climbing robots, will benefit from the results obtained from this study.

6.5. Experimental Section

6.5.1. Fabrication of polymeric fibrillar dry adhesives

The fibrillar arrays were fabricated using an epoxy-based photoresist (SU-8 2010, MicroChem) following a recipe detailed in previous work [26]. The polymer was patterned into 1 mm x 1 mm squares on a silicon wafer using photolithographic procedures, and etched in a Reactive Ion Etching (RIE) system (Etchlab 200, Sentech).

The length of this etching process was proportional to the lengths of the resulting fibrils. The samples used in this study were prepared by etching for either 5 or 30 min with nominal fibril lengths of ~0.1 and ~1 μm, respectively, as verified by scanning electron microscopy (Strata DB-235 SEM, FEI). Samples were also further inspected by SEM after the adhesion force measurements to investigate potential destruction of the surfaces. There was, however, no observable sample damage following the adhesion force measurements. Prior to each measurement the samples were also examined for surface defects using an optical microscope (Axio Imager M1m, Zeiss).

6.5.2. Measurement of adhesion forces in fibrillar dry adhesives

The adhesion force measurements were conducted using a scanning probe microscope (MFP-3D-SA AFM, Asylum Research) and a customized script written (with assistance from Jason Bemis, Asylum Research, Santa Barbara, CA) for specific motion control over the manipulations of the AFM probe. Tipless silicon nitride cantilevers with a nominal resonance frequency of 56 kHz and spring constant of 0.24 N/m (specifically the triangle labeled “C” in the NP-O10 probes, Veeco Instruments) were manipulated in order to approach, interact with and withdraw from the fibrillar surfaces with specific control over different parameters. These parameters included the lateral and vertical position of the cantilever, lateral and vertical velocity of the cantilever and the interactive forces. To implement the LDP method for adhesion force measurements described in this study, the cantilever was controlled to follow a trajectory that largely represented a “sewing” type of motion. The cantilever was first brought into contact with the sample’s surfaces in a vertical motion until reaching a preset force (~10 nN). At this preset position, the cantilever was moved in a lateral shear. Our study investigated a combination of different distances and velocities for this lateral shear before pulling the cantilever away from the surfaces in a vertical retraction. The retraction ended after a complete separation of the two surfaces. The cantilever was subsequently moved to another location on the sample to repeat the process for a second measurement, and this process repeated for a total of 400 measurements. The force exerted during the final vertical displacement, (i.e. the pull-off force) was measured as a single data point. Spring constant of the cantilever (~320 nN/μm) and resonance frequency (~60 kHz) were calibrated before each set of measurements, and were used in the adhesion force calculations. For each measurement cycle, a Force-Time (FT) curve was also recorded, which depicted the cantilever response curve with respect to the time elapsed during each cycle. In these measurements the FT curve for each cantilever-sample interaction can be interpreted using a simple beam model.

The three most important parameters for the subsequent set of LDP measurements were the lateral distance and velocity of the contacting surfaces during the applied lateral shear, and the velocity at which the two surfaces were separated. The ranges evaluated for each of these parameters was 0 – 2.5 μm, 2 – 200 μm/s and 0.1 – 4 μm/s, respectively. The extremes in each set of experimental parameters were determined by the current limitations of our instrumentation. The default values for these parameters were set at a 1 μm drag distance, a 20 μm/s drag velocity and a 1 μm/s retraction velocity. During the systematic investigation of one parameter, the other parameters were held constant, set at their default values; only one parameter was tuned at a time for each set of measurements. Each set of measurements consisted of 400 independent data points obtained from different locations on a sample. Further detail of the force measurements obtained using a SPM system using the LDP method can be found in our previous work [5].

6.5.3. Statistical analysis of experimental results

The statistical analysis used herein was performed, in part, using methods demonstrated in our previous studies [5]. Each analysis was performed on 400 data points for each type of measurement. Each data set was plotted as a histogram in order to visualize trends in the population. Two indicators of trends in the population, median and 12.5% trimmed mean, were calculated for each test parameter to help interpret the calculated average adhesion force. The median was calculated from the average of the two central most values for a sorted dataset of 400 individual points. The 12.5% trimmed mean was calculated from the average of 300 data points, which were selected from the original 400 data points by excluding equal portion of outliers from either side of the mean. Determination of the percentage of trimmed data was based on a close examination of a normal probability plot. From observing the shape of the histograms plotted, we observed that the data did not follow a normal distribution. Therefore, without fulfilling the necessary assumptions, a traditional ANOVA analysis would be invalid for this study. A nonparametric test method, Kruskal-Wallis one-way ANOVA [27], was used to indicate if the parameter of interest is significantly influencing the measured adhesion forces between the two surfaces. Levene's test [27] was used to compare the variances between different sets of measurements within each study.

6.6. Acknowledgements

This work was supported in part by the Natural Sciences and Engineering Research Council (NSERC) of Canada, and the Canada Research Chairs Program (B.D. Gates). This work made use of 4D LABS shared facilities supported by the Canada Foundation for Innovation (CFI), British Columbia Knowledge Development Fund (BCKDF), Western Economic Diversification Canada, and Simon Fraser University. We appreciate the assistance of Jason Bemis at Asylum Research for assistance in co-developing the software necessary for measuring adhesion forces resulting from shear induced alignment of fibrils using scanning probe microscopy techniques.

6.7. References

[1] K. Autumn, M. Sitti, Y. A. Liang, A. M. Peattie, W. R. Hansen, S. Sponberg, T. Kenny, R. Fearing, J. N. Israelachvili, R. J. Full, *Proc. Natl. Acad. Sci. U.S.A.* **2002**, *99*, 12252-12256.

[2] K. Autumn, C. Majidi, R. E. Groff, A. Dittmore, R. Fearing, *J. Exp. Biol.* **2006**, *209*, 3558-3568.

[3] Y. Tian, N. Pesika, H. Zeng, K. Rosenberg, B. Zhao, P. McGuiggan, K. Autumn, J. Israelachvili, *Proc. Natl. Acad. Sci. U.S.A.* **2006**, *203*, 19320-19325.

[4] K. Autumn, Y. Liang, T. Hsieh, W. Zesch, W.-P. Chan, T. Kenny, R. Fearing, R. J. Full, *Nature* **2000**, *405*, 681-685.

[5] Y. Li, C. Zhang, J. H.-W. Zhou, C. Menon, B. D. Gates, *Macromol. React. Eng.* **2013**, *7*, 638-645.

[6] K. Autumn, A. Dittmore, D. Santos, M. Spenko, M. Cutkosky, *J. Exp. Biol.* **2006**, *209*, 3569-3579.

[7] K. Autumn, N. Gravish, *Phil. Trans. R. Soc. A* **2008**, *366*, 1575-1590.

[8] N. Gravish, M. Wilkinson, K. Autumn, *J. R. Soc. Interface* **2008**, *5*, 339-348.

[9] M. P. Murphy, B. Aksak, M. Sitti, *J. Adhes. Sci. Technol.* **2007**, *21*, 1281-1296.

[10] B. Schubert, J. Lee, C. Majidi, R. S. Fearing, *J. R. Soc. Interface* **2008**, *5*, 845-853.

[11] M. Piccardo, A. Chateauminois, C. Fretigny, N. M. Pugno, M. Sitti, *J. R. Soc. Interface* **2013**, *10*, 20130182.

[12] K. Autumn, S. T. Hsieh, D. M. Dudek, J. Chen, C. Chitaphan, R. J. Full, *J. Exp. Biol.* **2006**, *209*, 260-272.

[13] J. Lee, B. Bush, R. Maboudian, R. S. Fearing, *Langmuir* **2009**, *25*, 12449-12453.

[14] S. Gorb, M. Varenberg, A. Peressadko, J. Tuma, *J. R. Soc. Interface* **2007**, *4*, 271-275.

[15] H. E. Jeong, J.-K. Lee, H. N. Kim, S. H. Moon, K. Y. Suh, *Proc. Nat. Acad. Sci. U.S.A.* **2009**, *106*, 5639-5644.

[16] Y. Menguc, S. Y. Yang, S. Kim, J. A. Rogers, M. Sitti, *Adv. Funct. Mater.* **2012**, *22*, 1246-1254.

[17] S. Kim, M. Spenko, S. Trujillo, B. Heyneman, D. Santos, M.R. Cutkosky, *IEEE Trans. on Robotics* **2008**, *24*, 65-74.

[18] A. Mahdavi, L. Ferreira L. Feirrara, C. Sundback, J. W. Nichol, E.P. Chan, D.J.D. Carter, C. J. Bettinger, S. Patanavanich, L. Chignozha, E. Ben-Joseph, A. Galakatos, H. Pryor , I. Pomerantseva, P.T. Masiakos, W. Faquin, A. Zumbuehl, S. Hong, J. Borenstein, J. Vacanti, R. Langer, J. M. Karp, *Proc. Nat. Acad. Sci. U.S.A.* **2008**, *105*, 2307-2312.

[19] S.Y. Yang , A. Carlson , H. Cheng , Q. Yu , N. Ahmed , J. Wu , S. Kim , M. Sitti , P. M. Ferreira, Y. Huang , John A. Rogers, *Adv. Mater.* **2012**, *24*, 2117-2122.

[20] Y. Kim, R. K. Claus, F. Limanto, R. S. Fearing, R. Maboudian, *Langmuir* **2013**, *29*, 8395-8401.

[21] H. Izadi, M. Golmakani, A. Penlidis, *Soft Matter* **2013**, *9*, 1985-1996.

[22] S. Hu, Z. Xia, X. Gao, *ACS Appl. Mater. Interfaces* **2012**, *4*, 1972-1980.

[23] N. Gravish, M. Wilkinson, S. Sponberg, A. Parness, N. Esparza, D. Soto, T. Yamaguchi, M. Broide, M. Cutkosky, C. Creton, K. Autumn, *J. R. Soc. Interface* **2009**, *7*, 259-269.

[24] J. B. Puthoff, M. Holbrook, M. J. Wilkinson, K. Jin, N. S. Pesika, K. Autumn, *Soft Matter* **2013**, *9*, 4855-4863.

[25] C. Zhang, J. Zhou, D. Sameoto, X. Zhang, Y. Li, H. W. Ng, C. Menon, and B. D. Gates, *J. Adhes. Sci. Technol.* **2014**, *28*, 320-336.

[26] D. Sameoto, Y. Li, C. Menon, *Advances in Science and Technology* **2008**, *54*, 439-444.

[27] D. C. Montgomery, *Design and Analysis of Experiments*, *8th ed*.; Wiley: Hoboken, NJ, **2013**.

[28] S. Das, S. Chary, J. Yu, J. Tamelier, K. L. Turner, J. N. Israelachvil, *Langmuir* **2013**, *29*, 15006-15012.

Chapter 7.

Improved adhesion and compliancy of hierarchical fibrillar adhesive

A hierarchical fibrillar adhesive containing nano-fibrils and micro-fibrils was eventually investigated in this chapter with all the knowledge obtained in previous chapters. The adhesion forces and structure compliancy were studied to reveal the correlation of these properties. Comparison between single level fibrillar adhesive and dual level fibrillar adhesive uncovered the advantage of hierarchical fibrillar structure. Enhanced adhesion forces of this hierarchical fibrillar adhesive was a result solely contributed by topography change. Compliancy, as another outcome of topography change, was also increased with evidences provided by the techniques introduced in the previous chapters. This chapter demonstrated the realization of the ultimate goal of this thesis (OBJECTIVE 5): prove that hierarchical fibrillar structure can produce an increase adhesion force by providing extra compliancy. The following contents are submitted as a paper: Yasong Li, Byron D. Gates and Carlo Menon, “Improved adhesion and compliancy of hierarchical fibrillar adhesives” to ACS Applied Materials & Interfaces.

7.1. Abstract

Gecko’s remarkable climbing ability relies on van der Waals forces to cling onto surfaces with a variety of topography and composition. The hierarchical fibrillar structures on their climbing feet, ranging from meso-scale to nano-scale, enable these animals to conquer both smooth and rough surfaces. Nanometer-size fibrils can induce molecular attractive force only when they reach an intimate contact with the surfaces they are climbing. The larger scale supporting fibrils that connect the nano-fibrils and the gecko’s feet facilitate the nano-fibrils reaching into the recesses of a substrate. This hierarchical structure can also create a softer contact by providing more space for the

fibrils to move around and adapt to the contacting objects. An artificial hierarchical fibrillar adhesive was prepared herein to further study the influence of the hierarchical structures on the properties of a dry adhesive. The experiments performed highlight the advantages of a hierarchical structure despite a reduction of overall density and aspect ratio of nano-fibrils. In contrast to an adhesive containing only nanometer-size fibrils, the hierarchical fibrillar adhesives exhibited a higher adhesion force and better compliancy when tested on an identical substrate.

Keywords: adhesion forces, hierarchical adhesive, nano-structured fibrils, scanning probe microscopy, compliancy

7.2. Introduction

The mystery of gecko's amazing ability to climb a variety of surfaces has been resolved in the last decade. This ability has been attributed to the hierarchical fibrillar structures on the gecko's feet [1-2]. These fibrils, ranging from micro-scale to nano-scale dimensions, are arranged within the gecko's feet in the shape of branches from a tree [3]. Millions of nano-fibrils, which extend from the top surfaces of micro-fibrils, interact with the climbing surfaces through van der Waals forces. Numerous molecular attractive forces collectively constitute a large enough gripping force for the gecko to defy gravity. Many attempts have been made to prepare artificial fibrillar adhesives that mimic the structure of gecko's feet. In early attempts, adhesives composed by only arrays of micro- or nano-fibrils were prepared using various materials and studied for their adhesion properties [4-10]. Adhesion of these adhesives can be as good as or superior to geckos' when they are tested against very flat surfaces, such as glass slides and silicon wafers. These adhesives containing only one size of fibrils have now probably reached their best possible performance, which has been achieved by reducing fibril size [11], increasing fibril aspect ratio [12] and changing material composition [13].

Adhesives containing fibrils of different sizes appear to be another route to improve their adhesion performance. In an early attempt, one type of hierarchical fibrillar adhesive was prepared with a relatively simple shape that subsequently reduced the surface area of contact; adhesion performance was, therefore, worse than for a nonhierarchical structure [14]. Later, hierarchical fibrillar adhesives were prepared that had further variations in shape and size in attempts to mimic the geometry of the gecko's adhesive. Mushroom cap shape fibrils [15], tilted fibrils with high aspect ratios [16], reduced diameter fibrils [17], and the used of inorganic materials [18] were each explored as alternative methods and materials for hierarchical adhesives. Most of these researchers primarily focused on studying the adhesion response of these materials and structures under an applied shear, or in other words through a measure of the frictional force [16-18]. It should, however, be noted that conditions of a high friction force typically result in irreversible fibril damage [17-18], which is unfavorable to most applications for which dry adhesives seem to be the most suitable, such as pick-and-place automation [16], microchip handling [19] and design of climbing robots [20-21]. In one type of hierarchical adhesive, a demonstrated advantage of having hierarchical structures is the ability to adapt to an increased surface roughness of the test substrate [16]. Based on the size of the fibrils, this increase in friction might indicate that the nano-fibrils induce mechanical interlocking on the rougher surfaces in addition to an increased van der Waals interaction. Another type of hierarchical adhesive, which were characterized for their pull-off force instead of their frictional force, did not yet show any improvement when compared to adhesives that only contain nano-fibrils [22]. Some other hierarchical dry adhesives, which contain larger fibrils that are sandwiched by thin sheets of polymer, are not suitable for a direct comparison to those hierarchical structures having separate micro-fibrils since they have a radically different geometry [23-24].

Two previously reported studies are particularly relevant to the work presented here with implications to both the preparation and testing of gecko-inspired adhesives. Mohrig et al. used a three-dimensional (3D) laser photolithography method to prepare hierarchical fibrils with control over their aspect ratio, cap shape, density and tilt angle with respect to the substrate [25]. The adhesion force of these fibrils was measured using an atomic force microscope (AFM) and a colloidal probe, which combines a flat cantilever with an attached borosilicate sphere that was brought into contact with the array of fibrils. The sphere diameter (~20 μm) was much larger than the diameter of both the nano-fibrils and micro-fibrils. The use of the AFM enabled a correlation between adhesion forces and the physical topography of the hierarchical structures. The adhesion force and topography were represented in two-dimensional plots, which were referred to as adhesion force map and height map. Correlations between the two maps could be determined by matching pixels located at the same coordinate in the adhesion force and height maps. Although the conclusion of this study was that their hierarchical fibrillar adhesive did not demonstrate an improvement of the adhesion properties over those for nano-fibrillar adhesives [25], the massive amount of data acquired on the adhesion response with changing preload provided further insight into the properties of the adhesive. Large standard deviation in the measured adhesion for the hierarchical structure indicated the structure introduce more uncertainty than in the measurements for a single level adhesive. The mushroom cap structure did, however, show a positive effect on the adhesion.

In a second study that is also very relevant to our own studies, Lee et al. used a soft material to demonstrate an enhancement of adhesion in hierarchical fibrillar adhesives [26]. The shape of the fibrils in their hierarchical adhesives was much closer to that in a gecko adhesive than those analyzed in the study described above [25]. Using an AFM with a colloidal probe, the measured adhesion force of the soft hierarchical adhesive was twice as high as that for a single level fibrillar adhesive with an aspect ratio of 5:1, length:diameter. Analysis of the frictional force response versus preloading force was performed in this study, but the results were not relevant to structure compliancy.

These previous studies also demonstrated a few limitations. First, the preparation of hierarchical fibrillar adhesives was generally expensive due to the required instrumentation and/or customized materials. Second, most of these studies demonstrated no improvement on the pull-up force in comparison to that for single layer adhesives. Third, very few studies investigated normal adhesion. And fourth, characterization methods provided limited information on compliancy enhancement from the hierarchical structure.

In this article, a low cost and high yield method to prepare hierarchical fibrillar adhesives is introduced and characterized. Although the topography of the demonstrated adhesive does not show a high resemblance to the gecko adhesive, the adhesion or pull-up forces measured on the hierarchical adhesives were higher than for our fabricated adhesives that only contained a single layer of nano-fibrils. Applying an AFM technique developed in our previous studies [27-28], the fibrillar adhesives were analyzed for the uniformity of their topography and adhesion performance. This technique has the flexibility of implementing a frictional induced adhesion, which applies shear movements before pulling up on the contacting substrate. The AFM was also able to vary the preload force (i.e. the compression force initiating adhesion) to investigate potential compliancy changes of the hierarchical structure. By comparing performances of both a hierarchical fibrillar adhesive and a single level nano-fibrillar adhesive that were composed of the same material, we were able to determine that enhancement of both adhesion and compliancy were solely attributed to changes in topography.

7.3. Sample Preparation and Evaluation Method

7.3.1. Preparation of hierarchical fibrillar arrays

The hierarchical fibrillar arrays were prepared using epoxy (TC-1622, BJB enterprise). An overview of the procedures used in the preparation of the hierarchical fibrillar arrays is illustrated in Figure 7.1. First, microscale fibrillar arrays were fabricated using photolithography. Circular micro-fibrils with a diameter of ~10 μm were fabricated using SU-8 (diluted from SU-8 2050, solid contents 58%, MicroChem) on a polished silicon wafer substrate. The micro-fibrils were arranged in arrays upon the silicon wafer. Spaces in between the micro-fibrils were 5 μm, and the micro-fibrils were ~20 μm in height. The micro-fibrils supported on a silicon wafer were subsequently placed into a desiccator for coating with a release layer. A scintillation vial cap containing 3 mL of a mold release agent (1H, 1H, 2H, 2H – perfluorodecyldimethylchlorosilane, Alfa Aesar, >90%) was placed beside the silicon wafer overnight in the desiccator while vacuum was applied to the chamber. The wafer was subsequently examined for its hydrophobicity by measuring static water contact angles. The silicon wafer originally had a static water contact angle of ~20 degrees. The static water contact angle increased to ~90 degrees after deposition of the silane coating. The silane coated micro-fibrils and silicon wafer were immersed in a precursor to polydimethylsiloxane (PDMS, Sylgard 184, Dow Corning) as depicted in Figure 7.1a. The PDMS negative mold containing arrays of micro-holes was separated from the SU-8 micro-fibrils after completely curing the polymer for 24 h at room temperature. An epoxy precursor was mixed from its two components and poured onto the PDMS negative mold with an excess amount of epoxy precursor to form the substrate that would connect all of the micro-fibrils (Figure 7.1b). To improve the filling of the recesses within the mold, the PDMS mold with liquid epoxy precursor applied to its surfaces were placed in a vacuum chamber for 20 min to remove gases trapped in these recesses. The array of epoxy based micro-fibrils were cured over 24 h at room temperature and removed from the PDMS mold as a single piece (connected to a single substrate of cured epoxy) for further attachment of arrays of nano-pillars (Figure 7.1c).

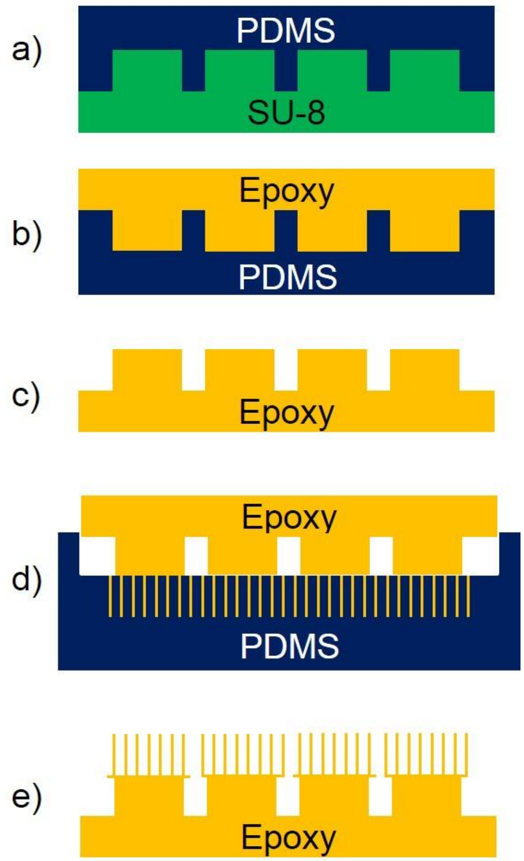

Figure 7.1. Schematic procedure for the preparation of the hierarchical nanostructured adhesives. a) A liquid PDMS precursor was poured over arrays of circular micrometer-size pillars, which were fabricated from SU-8 using photolithographic techniques; b) a liquid epoxy precursor was poured into the circular micrometer-size holes in the PDMS mold prepared following demolding in the previous step; c) the epoxy was cured and separated from the PDMS mold; d) the arrays of epoxy micro-pillars were brought into contact with a PDMS mold containing arrays of nano-holes prefilled with a liquid epoxy; and e) epoxy in the arrays of nano-holes was cured and the entire piece of epoxy peeled from the PDMS mold.

Preparation of arrays of nano-holes in PDMS was introduced in a previous paper [29], which enabled a broader material choice for preparing arrays of nano-fibrillar structures using arrays of nano-holes in PDMS. To attach the epoxy based nano-fibrils onto the ends of the micro-fibrils, freshly mixed epoxy precursor was poured on top of the array of nano-holes in PDMS, and excess liquid precursor was removed from these surfaces. The previously prepared piece of epoxy containing the arrays of micro-fibrils was immediately placed on top of these arrays of nano-holes, with the ends of each of the micro-fibrils in contact with the uncured interface of epoxy precursor within the arrays of nano-holes (Figure 7.1d). This stack of epoxy precursor and PDMS mold were sandwiched by two 1 mm thick glass slides and held in place using binder clips. The entire assembly was placed upon a flat surface to cure the epoxy over 24 h at room temperature. The hierarchical fibrillar structure of epoxy (Figure 7.1e) was removed from the PDMS mold containing the arrays of nano-holes. Scanning electron microscopes (SEM, Explorer and Helios, FEI) were used to examine the appearance of these hierarchical structures. The nano-fibrils were ~200 nm in diameter and ~0.8 µm in height.

7.3.2. Evaluation of adhesion properties in hierarchical fibrillar adhesives

The adhesion force and uniformity of the hierarchical structure was examined using an atomic force microscope (AFM, MFP-3D-SA, Asylum Research) with a customized script written (with assistance from Jason Bemis, Asylum Research, Santa Barbara, CA) for moving the AFM probe in specific directions. AFM cantilevers without sharp tips (specifically cantilever “A” in HQ: NSC36/TIPLESS/CR-AU, MIKROMASCH) were used in the measurements. Spring constant of the cantilever was calibrated every time the cantilever was loaded into the AFM system for a new set of measurements. The spring constant of cantilever “A” was ~1.7 N/m. There were two types of movements that the cantilever used to locate the area of interest and to measure the adhesion forces between the two contacting materials. The first type of cantilever movement is called a Push-Pull (PP) method, which lowers (or pushes) the cantilever vertically towards the surfaces of an adhesive until reaching a certain preload force, and subsequently the cantilever is vertically pulled up from these surfaces until the cantilever is completely separated from the fibrillar surfaces. The second type of cantilever movement is called the Load-Drag-Pull (LDP) method, which has an extra movement in between the “push” and “pull” movements of the cantilever. The additional movement in this method consists of a horizontal displacement of the cantilever with respect to the array of fibrillar structures. The differences between these two types of cantilever movements are described in further detail in our previous work [27-28]. In this article, the PP method was used to locate the area of interest and the LDP method was used to measure the adhesion forces of the fibrillar arrays. The preload force was set to 100 nN.

A force map and height map were obtained using the automatic script running with the AFM. The force map correlated the planar location in both X and Y directions. For example, measuring an area of 20 x 20 μm^2 with 400 individual measurements were executed using the following procedures: the AFM cantilever first finished one measurement, moved 1 μm in the X-direction (horizontal direction in the force map; moving from left to right) and performed another measurement. These procedures were repeated 20 times in the X-direction, which constructed one row of the force map. The cantilever subsequently moved 1 μm in the Y-direction (vertical direction in the force map) and continued the measurements for another row data points comprising the force map. Therefore, in each force map 400 individual measurements were performed, which were represented in a grey scale map as an array of 20 x 20 small squares. The height map represented the distance the cantilever moved toward the substrate, instead of the adhesion force in the force map, during each measurement to maintain the same preload force. The adhesion force and height information were simultaneously recorded in each measurement.

7.3.3. Statistical analysis of experimental results

Since 400 individual measurements were acquired for each sample, a statistical analysis was required to evaluate the adhesion properties of the hierarchical structure. Histograms of the measurements on different samples were plotted in order to better visualize trends in the main population and its distribution. Mean values were calculated as a further indicator of the trends in the main population. Friedman test, a non-parametric ANOVA method specifically for data of non-Gaussian distribution, was performed to detect differences between the series of data collected for each experiment.

7.4. Results and Discussion

Preparation of samples investigated in this work made use of a molding technique reported in our previous work [29], which enabled the selection of different materials for preparing arrays of nano-pillars. This method was extended to the fabrication of micrometer-size arrays of fibrils for the formation of a hierarchical fibrillar structure. Combination of the two levels of fibrillar arrays was achieved by adapting the dip and transfer method reported in the literature [15, 30-31]. Advantage of using the dip and transfer method is that the excess liquid polymer can form a thin film in the shape of a mushroom cap at the interface between the scale levels of structures. Figure 7.2a depicts the mushroom shape of the micrometer-size fibrils arranged in an array upon a substrate. The transferred thin film, which has a diameter slightly larger than the supporting fibril, contains arrays of low aspect ratio nano-fibrils. Figure 7.2b shows a magnified view of this thin film. Both SEM images were taken at a 45-degree stage tilt, which enables the observation of the micro-fibril underneath the thin film cap. Figure 7.2c is an optical microscopy image of the SU-8 micro-fibrils as fabricated using photolithography. The epoxy replica of these micro-fibrils, which served as the supporting fibril in the hierarchical fibrillar structure, has the same shape as its SU-8 master. From examination of the spaces between the micro-fibrils, it was determined that the radius of the mushroom shape thin film was ~2 μm wider than the supporting fibril. Instead of dipping the arrays of micro-fibrils into freshly prepared precursor to the epoxy by the dip and transfer method, epoxy was poured onto the PDMS mold containing arrays of nano-holes and the excess amount of epoxy was scraped off from the mold. This scraping step created a very thin film of excess epoxy, which enabled the micro-fibrils to remain separate in the final hierarchical structure. Although the observable area containing nano-fibrils was reduced due to the vacancies in between each micro-fibril, the thin film or mushroom cap shaped array of micro-fibrils provided improved flexibility and compliancy towards the contacting surfaces. The spaces in between the micro-fibrils provided enough room to sufficiently comply with rough surfaces and potentially to improve the adhesion performance of the dry adhesive.

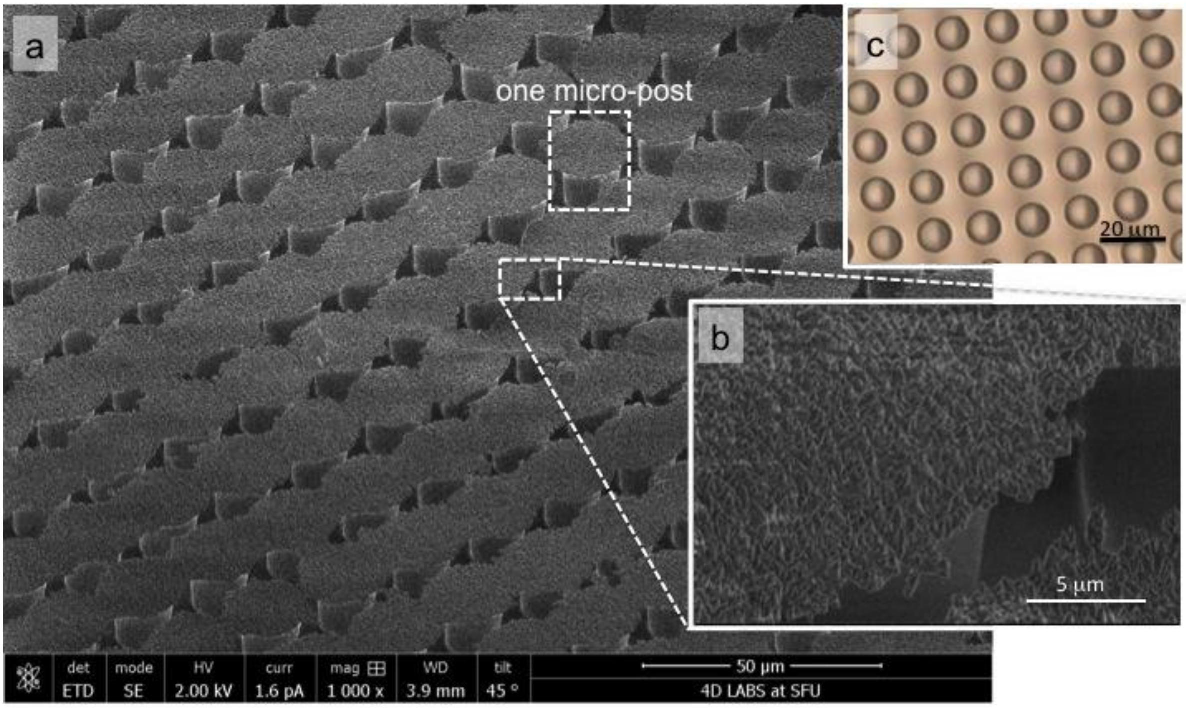

Figure 7.2. The hierarchical fibrillar structure examined using scanning electron microscopy (SEM) and the arrays of micro-posts examined using optical microscopy. a) Arrays of hierarchical epoxy fibrils with a mushroom cap like thin film of nano-fibrils supported on the ends of each micro-post. b) Magnified SEM image corresponding to the dashed box annotated in (a). c) Examination of the arrays of SU-8 micro-posts by optical microscopy. Both a) and b) were obtained by SEM at a 45 degree stage tilt.

To assess the adhesion properties of the hierarchical fibrillar structure, we adapted a technique [27-28] that used an atomic force microscope to characterize surface uniformity and correlate physical locations in the sample with the measured adhesion force between the sample and a flat silicon nitride cantilever. Figure 7.3 depicts a typical set of measurements obtained from the hierarchical fibrillar structures using the PP method. These measurements covered an area of 40 x 40 μm^2, comprising of 20 x 20 independent data points. Both images represent measurements over the same area of the sample, but report complementary information. Figure 7.3a represents the distance traveled by the cantilever before reaching the set value for the preload force, which was 100 nN in this set of measurements. The slightly brighter region of the upper left corner of the image indicates the substrate of the hierarchical array of fibrils was not parallel to the cantilever within the scanning head of the AFM. It is clearly observed from the height map (Figure 7.3a) that the data depicts 3 bright circles, each of which represents a micro-fibril, and several other partial circles also appear in this measured region. However, the adhesion map does not have as distinct a pattern (Figure 7.3b). The colored circle and oval noted on both images represent the empty regions between adjacent micro-fibrils. Specifically, the red solid circle indicates a region where the side of the cantilever was in contact to the edge of a post during the measurements. We believe that in this region of the sample the tip of the cantilever traveled below the surface of the thin film into the space between the mushroom caps. When the preload reached 100 nN, the cantilever was underneath the thin film and got “stuck” when a pulling force was applied to the cantilever. This behavior could explain the relatively high adhesion observed (Figure 7.3b) in the location of the red circle. The adhesion force measured in this location was, therefore, the force required to bend the mushroom caps upwards, such that the cantilever was released from these structures in the sample.

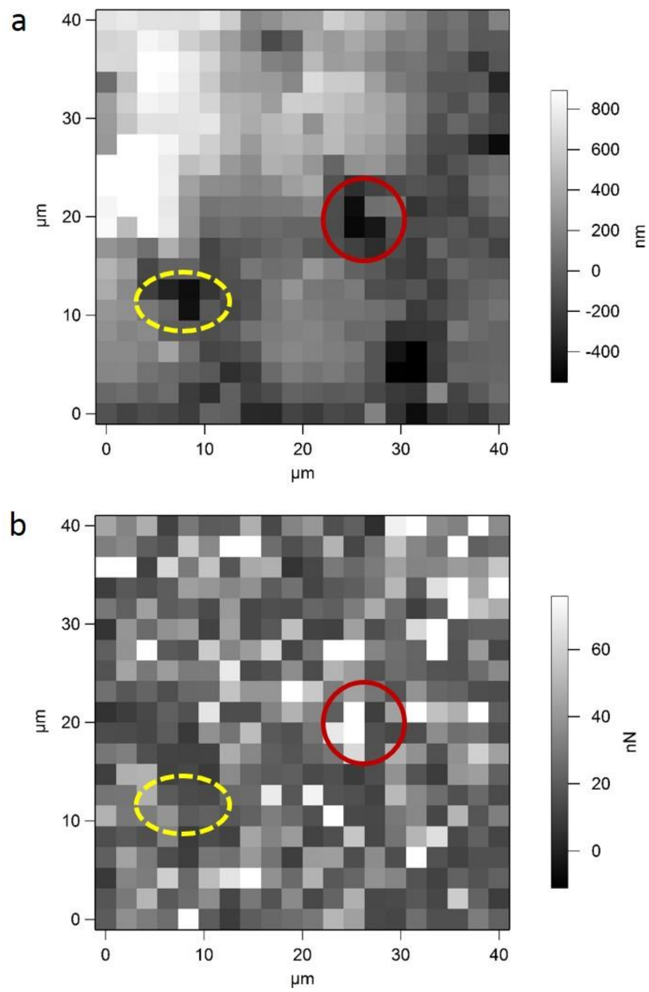

Figure 7.3. **Correlations between height and adhesion force maps. Both sets of data were obtained simultaneously during these measurements. a) Height map for an array of hierarchical fibrillar adhesives, representing the 3D geometry of the measured area. b) Adhesion force map for the same region depicted in the topography map.**

The yellow dashed oval in Figure 7.3a depicts another gap between the mushrooms caps. In this case, we believe that the thin film of the mushroom caps that surrounded the gap was thicker and the displacement of the cantilever was not sufficient to penetrate under this region of the mushroom cap. Interlocking of the mushroom cap and the cantilever was, therefore, not dominating in this case, as observed in the force map (Figure 7.3b).

It should be noted that the adhesion force observed in the force map was randomly distributed for the hierarchical arrays when tested under the same preload conditions. The apparent disadvantage of empty regions between the separated micro-fibrils had a negligible effect on the observed adhesion forces. This result would be particularly important for the situation that the adhesive must comply with rough surfaces, simulated by the normal movements and small dimensions of the cantilever, where interlocking of the two surfaces may occur.

The average adhesion force for the hierarchical structures in Figure 7.3b was ~32 nN, which was higher than the measured average adhesion force (23.2 nN) of a single layer containing only nano-fibrils [29]. To further investigate adhesion strength and uniformity, measurements were also obtained from a small area located on top of a mushroom cap. Measurements using the LDP method were repeated on 10 different, randomly chosen micro-fibrils. The results are plotted in Figure 7.4 with a vertical offset in the y-axis, which represents the total number of measured counts at each force. Each line corresponds to 400 measurements obtained from a force map over a 5 x 5 μm^2 area corresponding to a single mushroom cap. For each of the 10 separate sets of measurements, the corresponding average adhesion force is noted on the right-hand side of each line graph (Figure 7.4). The average force from the total of 4,000 independent measurements was 36.7 nN. The minimum and maximum average adhesion forces were 22.3 nN and 57 nN, respectively. This large variation in the adhesion force suggests a relatively poor uniformity of the hierarchical fibrillar adhesive. The lowest measured value (22.3 nN) was, however, similar to the average adhesion force measured using a single layer of nano-fibrils (23.2 nN reported in [29]), thus indicating the overall improved performance of the hierarchical structure.

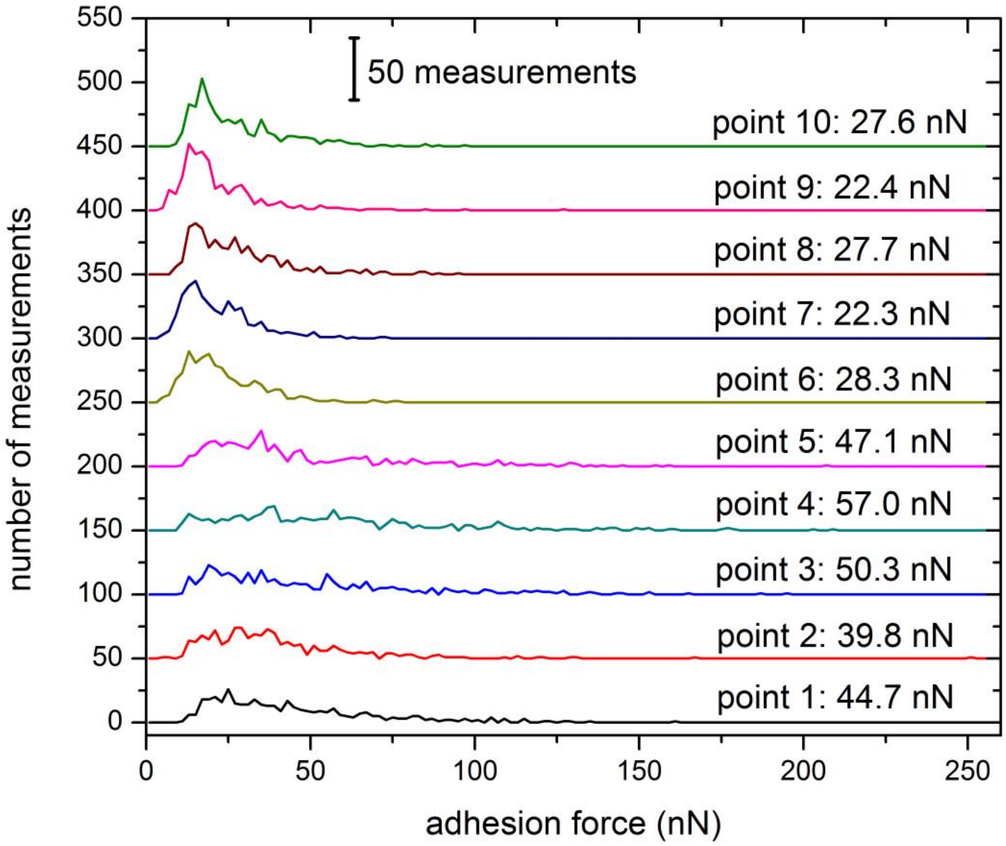

Figure 7.4. Line graphs of measurements obtained from 10 different arrays of nano-fibrils supported on top of micro-fibrils pillars. Each analysis contains 400 measurements, and these trend lines are vertically stacked with an offset of 50 measurements. Annotation above each line indicates the average value of each set of 400 measurements.

In Figure 7.4, these sets of measurements can be grouped into two types: either (1) relatively low or (2) high average adhesion forces. Measurements with average adhesion forces less than 30 nN are plotted in the top most 5 line graphs (marked as points 6 to 10 in the sample). Each of these lines shows a clear peak in their overall counts. The range of measured adhesion forces in these samples is relatively small, typically within 100 nN. For measurements with an average adhesion force greater than 30 nN the corresponding line graphs are plotted in the bottom-most traces in Figure 7.4 (marked as points 1 to 5 in the sample). There was no obvious peak force in the measured counts for these five data sets; the peak was not as sharp as those observed in the other line graphs for points 6 to 10. The range of adhesion forces measured for points 1 to 5 were also much broader with a spread of up to 200 nN. In summary, the hierarchical arrays of fibrils, which overall have a higher average adhesion force than the single layers of fibrils, have broader distribution or more variation in their adhesion performance. The non-uniformity of the handcrafted scraping method to remove excess liquid epoxy precursor from the mold might be the reason for this observed phenomenon. The scraping method, which used a flat spatula, might in fact be squeezing epoxy out of some regions of the mold if the relative scraping pressure is too high. The pressure of the spatula varies since the procedure was performed manually. Furthermore, the binder clips could provide an uneven pressure during the process that combines the epoxy micro- and nano-fibrils into a single hierarchical structure, although the non-uniformities in applied pressure will be partially compensated by the backing glass slides. Variations in the conditions across the molded sample resulting from the preparation method could lead to a non-uniform performance of the hierarchical fibrillar adhesive. Despite the non-uniformity of the hierarchical fibrillar adhesive, the average adhesion forces of these structures outperformed those of the single level fibrillar adhesive. It should be noted that the nano-fibrils of the single level fibrillar adhesive reported in [29] had a higher aspect ratio and a more well-defined shape than the nano-fibrils within the hierarchical fibrillar adhesive presented herein. The observed improvement in adhesion of the hierarchical fibrillar adhesive is attributed solely to the changes in geometry of the fibrils, since the material composition was identical between these two types of samples.

To further investigate the effect of geometry on the fibrillar adhesive, measurements on a freshly prepared single level nano-structured adhesive were compared with those from the hierarchical fibrillar adhesive. A range of different preloading forces was investigated to reveal the compliancy of these structures. The single level nano-structured adhesive contained the similar topography as reported in [29]. Measurements performed in this comparative study were obtained using the LDP method. From this point forward in the discussion, the single level adhesive refers to adhesive that is comprised of arrays of only nano-fibrils; the dual level adhesive refers to the hierarchical fibrillar adhesive that contained arrays of both micro-fibrils and nano-fibrils. Figure 7.5 illustrates the effect of varying the preload force on the measured adhesion forces for both the single and dual level adhesives. The measured area was held constant for each sample. Each data point is the average adhesion force from 400 independent measurements obtained from a single force map. Adhesion forces increased in proportion to the increase in preloading force for both the single and dual level adhesives. The dashed lines represent a linear trend line plotted with the increase of applied preload force. The rate of observed increase in adhesion force for the dual level adhesive is more than two times greater than that for the single level adhesive. Adhesion force differences between the single level adhesive and the dual layer adhesive were also investigated using a statistical method. Suspecting that the data were not from normal distributed populations the Friedman test, a non-parametric statistical test, was performed on the two series of data. The p-value of this test was much smaller than 0.01, which indicated there were substantial differences in adhesion force between the two samples. The slight decrease in adhesion force for the hierarchical structure at a preloading force of 170 nN raised concerns for fibril damage and adhesion force saturation. Measurements were, therefore, performed using a preloading force of 300 nN to further investigate the possibility of either scenario. The 300 nN preloading force was selected because of the maximum deformation this particular cantilever could withstand. Average adhesion forces measured, using a 300 nN preload force, were 31.2 nN on the single level adhesive and 42.3 nN on the dual level adhesive. The enhanced adhesion force measured using a higher preloading force suggested a limited damage to the fibrils, which was further confirmed by SEM analysis of the tested regions of the samples. The high variation from linearity observed in the data points for the dual level adhesive (Figure 7.5) is, therefore, attributed to deformation of the micro-fibrils. Specifically, during adhesion force measurements using the LDP method, the shear movement applied to the sample could cause the micro-fibrils to bend rather than sliding over the nano-fibrils with the AFM cantilever. After overcoming the micro-fibril deformation with a higher compression force, nano-fibrils were severely bent and adjust themselves to conform to a less stressed position. We believe that the tips of the fibrils overcome the initial static friction and release the stress of deformation while the flat cantilever continues compressing them. Once the compression force passes a threshold that causes the deformation of fibrils, which was represented by the observed plateau in the measurements between 10 and 70 nN (Figure 7.5), the advantage of having micro-fibrils becomes more relevant. This advantage is observed in the subsequent increase in measured adhesion force associated with the large increase in the adhesion force measured when changing from a preload force of 70 nN to 90 nN.

The flexibility provided by the arrays of micro-fibrils enhances the process of aligning the nano-fibrils, which subsequently increases the measured adhesion force.

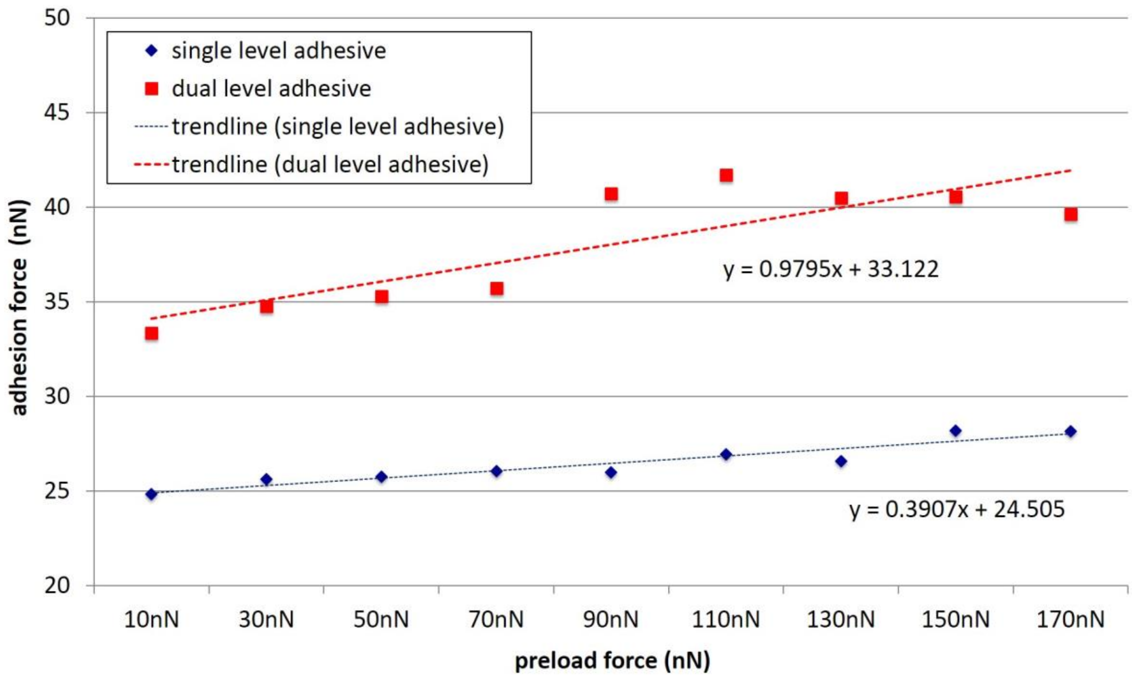

Figure 7.5. Average adhesion forces measured for samples containing either nano-fibrils or hierarchical fibrillar structures as a function of different applied preload forces. Dashed lines are linear trend lines to indicate deviations from linearity within the data. Every data point in the graph, either for the single layer adhesive (only containing the nano-fibrils) or the dual level adhesive (containing both micrometer-size and nanometer-size fibrils), was measured over the same area while changing the preload force.

Enhanced flexibility or compliancy can be assessed from the information provided in the height maps. Histograms of the height measurements for both single level and dual level adhesives using a 100 nN preloading force are plotted in Figure 7.6. Each histogram consists of 400 independent measurements obtained from height maps. In order to plot both histograms on the same scale the mean value of each set of measures were subtracted from each corresponding set of height measurements. The histogram for the single level adhesive has a well-defined peak around a value of 0, which corresponds to the mean value in the original data set. The total number of measurements in the left portion of the histogram was slightly higher than that in the right portion, which could be attributed to a tilt of the sample plane with respect to the cantilever in the AFM scanning head. On the other hand, the histogram for the dual level adhesive was much more evenly distributed and does not contain a well-defined peak. The variance observed in the dual level adhesive was almost two times higher than that in the single level adhesive. Although the range spanned by the measured heights is almost identical between these two types of samples. The wide spread values in the measured heights implies that the dual level adhesive provides a higher compliancy under the same measurement conditions. In the dual level adhesive, there is a higher possibility that the cantilever travels further while in contact with the thin film of the mushroom-like cap. This increased travel corresponds to a higher count of lower values in the histogram of these height measurements. The counts at the right-most portion of the histogram could be attributed to contributions from non-uniformity in the fibrillar surfaces and tilting of the sample. An increase of the variance of the vertical distance traveled by the cantilever implies that the fibrillar surfaces become softer and less uniform when prepared as a dual level adhesive. The observed enhanced compliancy supports the hypothesis that adhesion forces increase through the use of a hierarchical fibrillar structure.

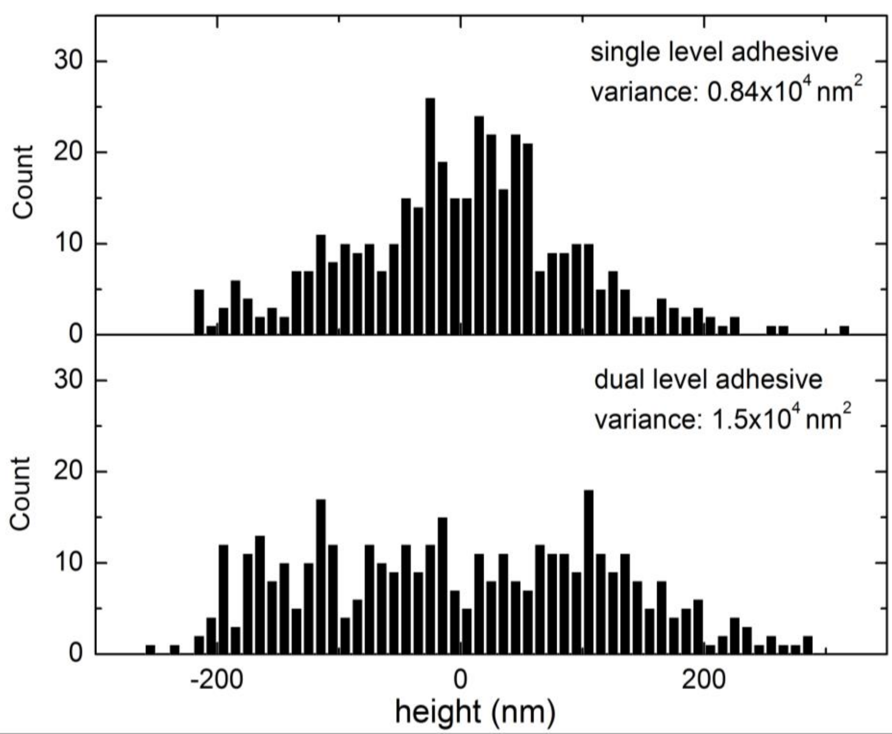

Figure 7.6. Histograms of height measurements on single and dual level adhesives. Preload force for these measurements was 100 nN.

7.5. Conclusion

We presented in this work a hierarchical fibrillar adhesive prepared using epoxy. The hierarchical adhesive comprised of two levels of fibrils consisting of micrometer-size fibrils and nanometer-size fibrils. Adapting the “dip and transfer” method, a thin film of nano-fibrils was prepared on top of the micrometer-size fibrils, which had a mushroom cap shape. This thin film containing nano-fibrils provided extra compliancy to the flexible micro-fibrillar structure. A measurement technique was implemented using an atomic force microscope to characterize the adhesion properties of the hierarchical structures. A thin, flat AFM cantilever was used to repeat Push-Pull or Load-Drag-Pull measurements on different locations within a preset area. These measurements simulated the interactions of the hierarchical adhesive with rough surfaces with a constant applied preload force at each point of the measurements. An interlocking phenomenon between the cantilever and adhesive occurred at the edges of the mushroom-like caps. An investigation into the uniformity of adhesion forces within the dual layer adhesive was performed by obtaining measurements on top of 10 different micro-fibrils. The average adhesion force of the hierarchical fibrillar adhesive was generally greater than that measured for an adhesive only containing a single layer of nano-fibrils. Given that the material composition of both the single and dual layer adhesives was the identical these results suggest that the improvement in measured adhesion force was due to the hierarchical structure of the dual layer. A study was also performed to investigate the influence of the applied preload force on the resulting adhesion forces. By increasing the preload force, the dual layer adhesive demonstrated a further improvement in performance with respect to the single layer adhesive, which was attributed to the higher compliancy of the dual layer adhesive. The vertical distance travelled by the AFM cantilever was also studied for both the single and dual layer adhesives. The broader distribution observed in the vertical distance travelled by the cantilever when contacting the surfaces of the dual layer adhesive highlighted the non-uniform compliancy of this adhesive, as a result of its hierarchical structure. Adhesion forces and compliancy to rough surfaces were both improved for the hierarchical fibrillar adhesive prepared and evaluated in this work.

7.6. Acknowledgements

This work was supported in part by the Natural Sciences and Engineering Research Council (NSERC) of Canada, and the Canada Research Chairs Program (B.D. Gates). This work made use of 4D LABS shared facilities supported by the Canada Foundation for Innovation (CFI), British Columbia Knowledge Development Fund (BCKDF), Western Economic Diversification Canada, and Simon Fraser University. We appreciate the assistance of Jason Bemis at Asylum Research for assistance in co-developing the software necessary for measuring adhesion forces resulting from shear induced alignment of fibrils using scanning probe microscopy techniques.

7.7. References

[1] K. Autumn, Y. Liang, T. Hsieh, W. Zesch, W.-P. Chan, T. Kenny, R. Fearing, R. J. Full, *Nature* **2000**, *405*, 681-685.

[2] K. Autumn, M. Sitti, Y. A. Liang, A. M. Peattie, W. R. Hansen, S. Sponberg, T. Kenny, R. Fearing, J. N. Israelachvili, R. J. Full, *Proc. Natl. Acad. Sci. U.S.A.* **2002**, *99*, 12252-12256.

[3] K. Autumn, *MRS Bull.* **2007**, *32*, 473-478.

[4] A. K. Geim, S. V. Dubonos, I. V. Grigorieva, K. S. Novoselov, A. A. Zhukov, S. Y. Shapoval, *Nat. Mater.* **2003**, *2*, 461-463.

[5] N. J. Glassmaker, A.Jagota, C.-Y.Hui, and J. Kim, *J. R. Soc. Interface* **2004**, *1*, 23-33.

[6] L. Ge, S. Sethi, L. Ci, P.M. Ajayan, and A. Dhinojwala, *Proc. Natl. Acad. Sci. U.S.A.* **2007**, *104*, 10792-10795.

[7] H. E. Jeong, S. H. Lee, P. Kim, K.Y. Suh, *Colloids Surf., A* **2008**, *313-314*, 359-364.

[8] L. Qu, L. Dai, M. Stone, Z. Xia, Z. L. Wang, *Science* **2008**, *322*, 238-242.

[9] D. Sameoto, C. Menon, *J. Micromech. Microeng.* **2009**, *19*, 115026.

[10] J. Tamelier, S. Chary, K. L. Turner, *Langmuir* **2012**, *28*, 8746-8752.

[11] T.-I. Kim, C. Pang, K. Y. Suh, *Langmuir* **2009**, *25*, 8879-8882.

[12] C. Greiner, A.D. Campo, E. Arzt, *Langmuir* **2007**, *23*, 3495-3502.

[13] W.-G. Bae, M. K. Kwak, H. E. Jeong, C. Pang, H. Jeong, K.-Y. Suh, *Soft Matter* **2013**, *9*, 1422-1427.

[14] C. Greiner, E. Arzt, A. del Campo, *Adv. Mater.* **2009**, *21*,479-482.

[15] M. P. Murphy, S. Kim, M. Sitti, *ACS Appl. Mater. Interfaces* **2009**, *4*, 849-855.

[16] H. E. Jeong, J.-K. Lee, H. N. Kim, S. H. Moon, and K. Y. Suh, *Proc. Nat. Acad. Sci.* **2009**, *106*, 5639-5644.

[17] A. Y. Y. Ho, L. P. Yeo, Y. C. Lam, I. Rodriguez, *ACS Nano* **2011**, *5*, 1897-1906.

[18] Z. Rong, Y. Zhou, B. Chen, J. Robertson, W. Federle, S. Hofmann, U. Steiner P. Goldberg-Oppenheimer, *Adv. Mater.* **2014**, *26*, 1456-1461.

[19] M. Zhou, Y. Tian, D. Sameoto, X. Zhang, Y. Meng, S. Wen, *ACS Appl. Mater. Interfaces* **2013**, *5*, 10137-10144.

[20] Y. Li, A. Ahmed, D. Sameoto, C. Menon, *Robotica* **2011**, *30*, 79-89.

[21] M. Henrey, A. Ahmed,P. Boscariol, L. Shannon, C. Menon, *J. Bionic Eng.* **2014**, *11*, 1-17.

[22] H. Lee, B. Bhushan. *J. Colloid Interface Sci.* **2012**, *372*, 231-238.

[23] A. Asbeck, S. Dastoor, A. Parness, L. Fullerton, N. Esparza, D. Soto, B. Heyneman, M. Cutkosky, presented at *IEEE Int. Conf. Robotics and Automation,* Kobe, Japan, May 12-17, **2009**.

[24] H. Izadi, M. Golmakani, A. Penlidis, *Soft Matter* **2013**, *9*, 1985-1996.

[25] M. Roehrig, M. Thiel, M. Worgull, H. Hoelscher, *Small* **2012**, *8*, 3009-3015.

[26] D. Y. Lee, D. H. Lee, S. G. Lee, K. Cho, *Soft Matter* **2012**, *8*, 4905-4910.

[27] C. Zhang, J. Zhou, D. Sameoto, X. Zhang, Y. Li, H. W. Ng, C. Menon, B. D. Gates, *J. Adhes. Sci. Technol.* **2012**, *28*, 320-336.

[28] Y. Li, C. Zhang, J. H.-W. Zhou, C. Menon, B. D. Gates, *Macromol. React. Eng.* **2013**, *7*, 638-645.

[29] Y. Li, H. W. Ng, B. D. Gates, C. Menon, *Nanotechnology* **2014**, *25*, 285303.

[30] A. D. Campo; C. Greiner, I. Alvarez, E. Arzt, *Adv. Mater.* **2007**, *19*, 1973-1977.

[31] M. P. Murphy, B. Aksak, M. Sitti, *J. Adhes. Sci. Technol.* **2007**, *21*, 1281-1296.

Chapter 8.

Conclusion

In this thesis, a systematical study of the fabrication and the characterization of hierarchical fibrillar gecko adhesive were presented. Evidences illustrated the influence of hierarchical fibrillar structures on adhesion force. Correlation between adhesion force and structure compliancy was given to support the rationale for using a hierarchical fibrillar structure in artificial adhesives. The achievement of this ultimate goal went through different milestones with progressing results.

First, a preliminary study on the adhesion forces of the hierarchical fibrillar structures was conducted to support the hypothesis that the hierarchical structures improved the adhesion performance of the adhesive. Micro-size and millimeter size fibrils were combined as the structure resemblance to the gecko adhesive and were tested the adhesion response with different pull up directions. This study not only set up the foundation for the entire study of the hierarchical structure, but also revealed the anisotropic properties, which inspired the development of characterization method to assess adhesion performance of nano-size fibrils.

Second, the ability to prepare nano-fibrillar arrays with desired materials was presented, as a necessary step in preparing the hierarchical fibrillar arrays using nano-size and micro-size fibrils. The high reproducibility of nano-fibrils using this method guaranteed further implantation of such nano-fibrils in a hierarchical structure. The versatility of material choices also eliminated certain difficulties of preparing the hierarchical fibrillar arrays.

Third, a proper technique for characterizing nano-fibrils was developed for assessing both uniformity and adhesion properties. The technique made use of a scanning probe microscope to automatically collect information of interaction between the flat substrate and the fibrillar arrays. Inspired by gecko adhesive, an extra shear movement between attachment and detachment was introduced to optimize fibrils interaction with the counter substrate. Individual measurement was studied to visualize this interaction. Uniformity was also studied with respect to the physical location on the sample. Statistical analysis provided a general description of the large amount of adhesion forces measured on the sample. The relative movement between the two contacting substrates could potentially control the complicated fibril-substrate interaction. This method allowed such a study by varying different parameters used in the measurements.

Fourth, as described in the study of the characterization method using a scanning probe microscope, there is flexibility to change the parameters used in the measurements. The substrate drag velocity, drag distance and retract velocity were studied based on the analysis of the procedures done within one measurement cycle. Identification of such a set of optimal parameters, which resulted in the desired adhesion performance, becomes important for testing hierarchical fibrillar arrays.

Finally, the ultimate goal was realized by applying all the knowledge obtained in the previous studies. Enhanced compliancy and adhesion performance by using hierarchical fibrillar structure were studied using the technique specially tailored for such a structure. The research in this thesis provides valuable information on studying hierarchical fibrillar adhesives, which will lead to future development of artificial fibrillar adhesives.

There were already some noticeable improvement points which could be addressed for future development. As described in Chapter 3, the stiffness of the hierarchical structure depends on both the geometry (cross sectional area and length), and material property (Young's modulus of the material). Hence, future work on developing the hierarchical fibrillar adhesive could be stressed on the following methods. First, the aspect ratio of the micro-fibrils should be increased to provide better compliancy to adapt to rougher surfaces. The aspect ratio of micro-fibrils in the current hierarchical fibrillar arrays was 2, which can only provide limited deformation. Realization of improving the fibril aspect ratio could be possibly made by reducing fibril diameter.

Second, the aspect ratio of the micro-fibrils versus adhesion force is an interesting subject for further investigation. Slender fibrils can provide better compliancy but also raise potential concern about fibril buckling, which potentially leads to the detachment of nano-fibrils from the contacting substrate. The optimal combination of fibril aspect ratio and preloading force can be determined by adhesion force measurements. Third, the shape of nano-fibrils in the current hierarchical fibrillar structure was not optimized. Increasing aspect ratio and shape uniformity could potentially provide a better performance of the adhesive. Fourth, adding mushroom cap structure on the nano-fibrils to optimize the contact area. The thin cap on the micro-fibrils showed the better adhesion performance. This advantage might also be valid in the nano-size fibrils. Last but not least, multiple layers of hierarchical fibrillar structures should provide better performance on a broader surface roughness. Each length scale of fibril should comply with a range of corresponding surface roughness. Multiple layers of the hierarchical fibrillar structure have the potential to adhere to a broader variety of surfaces.

Deeper and deeper understanding of the climbing mechanism used in the animals have inspired better and better design of artificial adhesive over the past decade. Advances of current technology in both preparation and characterization of the fibrillar adhesive will continue propelling the development of smart adhesives which accommodate different purposes in various applications. This thesis served as one of the contributions to the process of developing artificial fibrillar adhesives. The hierarchical structures have been chosen as the focus of the study and are believed to be one of the most promising future directions of developing a reliable, reversible and reusable adhesive.